GEOMAR REPORT

GEOMAR

Helmholtz-Zentrum für Ozeanforschung Kiel

RV POSEIDON Fahrtbericht / Cruise Report POS535

Loki2GrimseyEM: Geophysical and geological investigations of massive sulfides at and in the vicinity of Loki's Castle (Norway) and similar experiments around the Grimsey Hydrothermal Field (Iceland) for the assessment of the geothermal potential and the exploration for potential mineralizations within the seafloor

Akureyri (Iceland) – Bremerhaven (Germany)
09.06 – 03.07.2019

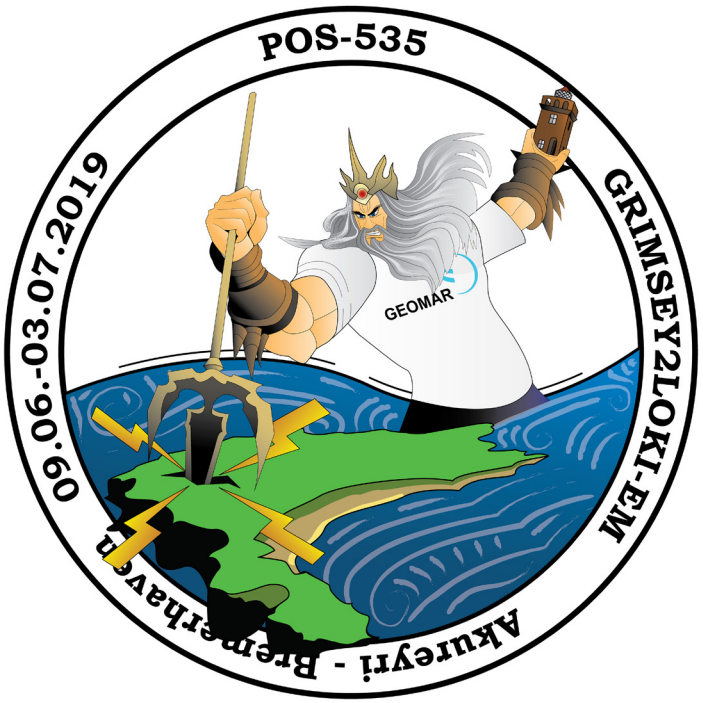

Berichte aus dem GEOMAR
Helmholtz-Zentrum für Ozeanforschung Kiel

Nr. 53 (N. Ser.)

December 2019

GEOMAR

Helmholtz-Zentrum für Ozeanforschung Kiel

RV POSEIDON Fahrtbericht / Cruise Report POS535

Loki2GrimseyEM: Geophysical and geological investigations of massive sulfides at and in the vicinity of Loki's Castle (Norway) and similar experiments around the Grimsey Hydrothermal Field (Iceland) for the assessment of the geothermal potential and the exploration for potential mineralizations within the seafloor

Akureyri (Iceland) – Bremerhaven (Germany)
09.06 – 03.07.2019

Berichte aus dem GEOMAR
Helmholtz-Zentrum für Ozeanforschung Kiel

Nr. 53 (N. Ser.)

December 2019

GEOMAR
Helmholtz-Zentrum für Ozeanforschung Kiel

Das GEOMAR Helmholtz-Zentrum für Ozeanforschung Kiel ist Mitglied der Helmholtz-Gemeinschaft Deutscher Forschungszentren e.V.

The GEOMAR Helmholtz Centre for Ocean Research Kiel is a member of the Helmholtz Association of German Research Centres

Herausgeber / Editors:
Sebastian Hölz, Amir Haroon and Sofia Martins

GEOMAR Report
ISSN Nr.. 2193-8113, DOI 10.3289/GEOMAR_REP_NS_53_2019

Helmholtz-Zentrum für Ozeanforschung Kiel / Helmholtz Centre for Ocean Research Kiel
GEOMAR
Dienstgebäude Westufer / West Shore Building
Düsternbrooker Weg 20
D-24105 Kiel
Germany

Helmholtz-Zentrum für Ozeanforschung Kiel / Helmholtz Centre for Ocean Research Kiel
GEOMAR
Dienstgebäude Ostufer / East Shore Building
Wischhofstr. 1-3
D-24148 Kiel
Germany

Tel.: +49 431 600-0
Fax: +49 431 600-2805
www.geomar.de

Table of Contents

1. Summary – Zusammenfassung

In the marine environment, elevated electrical conductivities may be caused by sulfide mineralizations as well as hot saline pore fluids. In past experiments we used the coil-system MARTEMIS[1] to study mineralizations at hydrothermally inactive sites (Palinuro Seamount, cruises POS483 & POS509; TAG area, cruise JC138) and in June 2018 on the hydrothermally active Grimsey Vent Field (GVF, cruise POS524). Even though the GVF shows high temperature venting of up to approximately 250°C, no relevant occurrences of seafloor massive sulfides (SMS) have been found so far. First interpretations of EM data acquired during the 2018 cruise indicate that such occurrences may exist within the seafloor.

During this year's cruise POS535 (*RV Poseidon*), experiments were carried out in two main working areas:

- Work commenced to the North of Iceland with the following targets and objectives:
  - Investigations were started at the GVF, where first results of last year's cruise POS524 indicate the existence of a large conductive body to the West of the known hydrothermal field. With this years experiment we established a denser network around the anomaly to better delineate its extent. Additionally, we conducted a "4D" experiment by repeating some of the previous measurements in this year's investigations. Seismic swarm activity (1st quarter 2018) indicated that the GVF was potentially in a highly active state in 2018. An experiment in 2019 – with assumed reduced hydrothermal activity – could serve as a proof of concept to determine if EM investigations are capable to distinguish different stages of hydrothermal activity.
  - Subsequently, samples were taken with the gravity corer at two additional sites with potential hydrothermal activity – provided to us by courtesy of Ögmundur Erlendsson and colleagues (ISOR). They showed no sign of hydrothermal activity at the first site (Öxarfjörður) but significant hydrothermal alteration was found in one of the cores taken at the second site (Skjalfandadjup).
- After a transit, work was continued at the known hydrothermal site "Loki's Castle" and the nearby inferred site "Mohn's Treasure", both in Norwegian boundary waters. The EM experiments at Loki's Castle were the first investigations with the MARTEMIS system at a hydrothermally active vent site at an ultra-slow spreading ridge with known mineralization. First results indicate that there seems to be conductive anomalies associated with the active mound structures at Loki's Castle. It seems that these anomalies are restricted to a rather thin layer directly at the surface without a deeper reaching root. Future evaluation will show if this is a stable feature in all acquired data sets or if modifications to these first findings will be necessary.

With these experiments, we have completed all necessary investigations in order to have a "complete" set of EM experiments above active / inactive sites with / without SMS occurrences at the seafloor in different tectonic settings.

1 Marine transient electromagnetic induction system

Im marinen Bereich können sowohl Sulfidmineralisierungen als auch heiße, saline Fluide zu erhöhten elektrischen Leitfähigkeiten führen. In früheren Experimenten haben wir das MARTEMIS Spulensystem verwendet, um Mineralisierungen an hydrothermal inaktiven geologischen Zielen (Palinuro Seamount, Ausfahrten POS483 & POS509; TAG-Field, Ausfahrt JC138) und im Juni 2018 am hydrothermal aktiven Grimsey Vent Field (GVF, Ausfahrt POS524) zu untersuchen. Obwohl am GVF Fluidaustritte von bis zu ~250°C gemessen wurden, konnten bisher keine relevanten Vorkommen von massiven Sulfiden (SMS) am Meeresboden nachgewiesen werden. Erste Interpretationen von EM-Daten, die während der Ausfahrt 2018 gemessen wurden, deuten darauf hin, dass solche Vorkommen möglicherweise in größerer Tiefe im Meeresboden vorkommen.

Im Rahmen der diesjährigen Ausfahrt POS535 (*FS Poseidon*) durchgeführten Experimente wurden in zwei Hauptgebieten durchgeführt:

- Im ersten Teil der Ausfahrt wurden Arbeiten nördlich von Island durchgeführt:
    - Die ersten Untersuchungen wurden am GVF durchgeführt, wo vorläufige Ergebnisse der letztjährigen Ausfahrt POS524 einen Hinweis auf die Existenz eines großen leitfähigen Körpers westlich des bekannten hydrothermalen Feldes geben. Mit dem diesjährigen Experiment haben wir ein dichteres Netzwerk um die Anomalie herum aufgebaut, um ihr Ausmaß besser abgrenzen zu können. Zusätzlich haben wir ein "4D" Experiment durchgeführt, indem wir einige der vorherigen Messungen in den diesjährigen Untersuchungen wiederholt haben. Seismische Schwarmaktivität (1. Quartal 2018) zeigte, dass der GVF im Jahr 2018 möglicherweise in einem hochaktiven Zustand war. Ein Experiment im Jahr 2019 – bei wahrscheinlich geringerer hydrothermalen Aktivität – sollte somit zeigen, ob EM-Untersuchungen in der Lage sind, verschiedene Stadien der hydrothermalen Aktivität zu unterscheiden.
    - Im Anschluss an die Arbeiten am GVF wurden an zwei weiteren Untersuchungszielen, die vor unserer Ausfahrt von Ögmundur Erlendsson und Kollegen vom ISOR also mögliche hydrothermale Ziele identifiziert wurden, Proben mit dem Schwerelot genommen. Während am ersten Untersuchungsziel (Öxarfjörður) keine Anzeichen hydrothermaler Aktivität nachgewiesen werden konnten, zeigte einer der beiden Kerne am zweiten Untersuchungsziel (Skjalfandadjup) signifikante hydrothermale Alterationen.
- Nach einem Transit wurden die Arbeiten am bekannten Hydrothermalfeld „Loki‘s Castle“ und dem nahegelegenen potentiellen Feld „Mohn‘s Treasure“, die sich beide in norwegischen Gewässern befinden, durchgeführt. Die bei Loki‘s Castle durchgeführten EM Messungen mit dem MARTEMIS System sind die ersten Messungen mit diesem System, die an einem hydrothermal aktiven Feld mit nachgewiesener Mineralisierung durchgeführt worden sind. Erste Ergebnisse zeigen, daß die hydrothermalen Hügel von Loki‘s Castle mit leitfähigen Anomalien übereinstimmen, die sich aber anscheinend nur auf eine relativ dünne Schicht direkt am Meeresboden beschränken. Ob sich diese Interpretation auch in der Auswertung der anderen gewonnen Datensätze bestätigen lässt, wird sich in den zukünftigen Auswertungen zeigen.

Mit den während der Ausfahrt POS535 durchgeführten Experimenten haben wir nun einen „kompletten“ Satz von EM Experimenten über aktiven / inaktiven Feldern mit / ohne nachgewiesenen SMS Vorkommen in verschiedenen tektonischen Gebieten.

2. Participants

	Name	Position (Affiliation)	Function on board
1	Sebastian Hölz	Senior Scientist (GEOMAR)	chief scientist, marine EM
2	Sofia Martins	Senior Scientist (GEOMAR)	co-chief scientist, GC, heat flow
3	Amir Haroon	Scientist (GEOMAR)	co-chief scientist, marine EM
4	Konstantin Reeck	PhD-student (GEOMAR)	marine EM
5	Zarah Faghih	Master Student (GEOMAR)	Marine EM
6	Chris Galley	PhD-student (Memorial University, Canada)	marine EM
7	Tristan Sinnecker	Bachelor student (Fachhochschule Kiel)	marine EM
8	Martin Wollatz-Vogt	Technician (GEOMAR)	marine EM
9	Natalia Rodriguez	Bachelor student (GEOMAR)	gravity core, heat flow

3. Working Areas & Research Program

3.1. General

Hydrothermal circulation is driven by heat and occurs mainly at marine plate boundaries such as mid ocean ridges, volcanic arcs and at back arc basins where thermal energy is supplied by increased magmatic activity. In places where hydrothermal circulation of seawater leaches metal bearing ores out of the host rock, mineral enriched fluids can rise towards the seafloor where they are cooled and precipitating metals can form accumulations of seafloor massive sulfides (SMS). Depending on the structure of the seafloor and the overall composition of hydrothermal circulation, the cooling of the fluids occurs either within the seafloor, in which case deposits may form within the seafloor or, alternatively, within the water column, where venting of high-temperature fluids can produce chimney structures, i.e. black smokers.

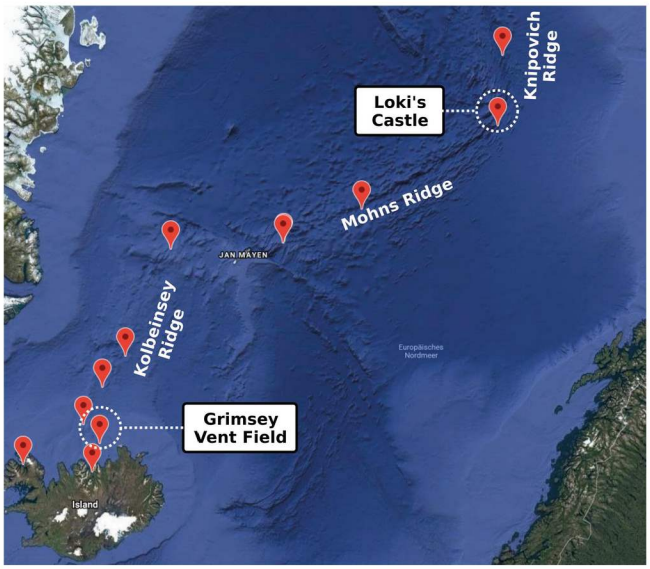

Fig. 1: Arctic Mid-Oceanic Ridge (AMOR) with the two proposed working areas Grimsey Vent Field (GVF) and Loki's Castle as well as additional vent fields (Beaulieu, 2015).

Along oceanic plate boundaries approximately 330 vent sites have been observed. Of these sites, a majority of 237 contain massive sulfide mineralizations (Beaulieu et al., 2015; Monecke et al., 2016). The estimate of the global potential yields a total accumulated volume of 600 million tons of SMS containing 30 million tons of copper and zinc, which are present in the immediate vicinity of the oceanic plate boundaries (Hannington et al., 2010 & 2011). Due to the fact that SMS are compact structures close to the seafloor with potentially high ore grades, the possibility of mining such SMS deposits has gained increased attention on both a national and international level (Boschen et al., 2013).

Along the Arctic Mid-Oceanic Ridge (AMOR), which runs from the northern coast of Iceland along the Kolbeinsey, Mohns and Knipovich Ridges (Fig. 1) and further North, several hydrothermal vent fields have been confirmed (Beaulieu, 2015). The Grimsey Vent Field (GVF) and Loki's Castle are the southern- and northernmost confirmed active vent fields along the AMOR showing high-temperature venting above 250°C (Hannington et al., 2001; Pedersen et al., 2010; Baumberger et al., 2016). With spreading rates of 18.1mm/a at GVF and 15.1mm/a at Loki's Castle (Beaulieu, 2015), both sites are hosted on ultra-slow spreading segments of the ridge (Snow & Edmonds, 2007). German et al. (2016) state that there is an "excess" of high-temperature venting along slow and ultra-slow spreading ridges and conclude that these may have the strongest mineral resource potential for the global ridge crest.

Consequently, studying hydrothermal systems and potential SMS sites along ultra-slow spreading ridges using suitable geophysical instruments such as the electromagnetic (EM) coil-system MARTEMIS will substantially contribute to quantifying the resource potential of SMS through constraining potential sites laterally and vertically, as well as providing information on the electrical conductivity distribution of the

seafloor, which is otherwise only obtainable from costly drilling. Furthermore, the comparison to previous experiments conducted at sites located at slow-spreading ridges (e.g. Shinkai & Double Mound, MIR Zone, cruise JC138, 2016) or in an island-arc setting (e.g. Palinuro, cruises POS483 & POS509) will help understand the composition and evolution of SMS at various hydrothermal systems situated in different geological settings.

3.2. Working Areas – Iceland

3.2.1. Grimsey Vent Field (GVF)

In Iceland, occurrences of high-temperature hydrothermal systems are clearly linked to the neovolcanic zone, which crosses the island from the SW to the NNE (Fig. 2). The neovolcanic zone is an expression of the Mid-Atlantic Ridge system crossing the Iceland hot spot (Hannington et al., 2001). As part of the system, the neovolcanic zone extends into the submarine domain to the SW along the Reykjanes Ridge and to the NNE along the Kolbeinsey Ridge.

In a review of Icelandic geothermal areas, Ármannsson (2016) lists 33 prospective high temperature geothermal systems of which three are submarine. Investigations of geothermal settings on and around Iceland are of special interest, because geothermal energy is presently of major importance for Iceland's economy and infrastructure (Orkustofnun, 2018). The current hydrothermal potential is mainly exploited on the main island, but the potential of offshore reservoirs is investigated e.g. by Atkins & Audunsson (2013). Based mainly on research results gained through *RV Poseidon* cruises POS229, POS253 and POS291 (1997, 1999, 2002, respectively), the authors consider the Grímsey vent field to be the most compelling site for offshore power production offshore Iceland due to the size of the field (comparable to geothermal areas on land), its temperature of at least 250°C (Botz et al., 1999), and its proximity to land (16km from Grímsey island and 50km from mainland Iceland). The GVF is located in the Grimsey Graben, a pull-apart basin within the Tjörnes Fracture Zone (see Fig. 16). It is about 10 km wide, 30–40 km long and filled with glacial sediments from ice-fed rivers draining the north coast of Iceland (Lackschewitz et al., 2006). Seismic and geochemical investigations indicate high permeability in the deep crust which facilitates fluid and gas migration from the crust–mantle boundary to the seafloor (Riedel et al., 2001). During these Poseidon cruises between 1997 and 2002, Hannington et al. (2001) identified 24 mounds and chimneys in JAGO dives, of which 14 are characterized as high-temperature vents (boiling). They also show acoustic scatter-

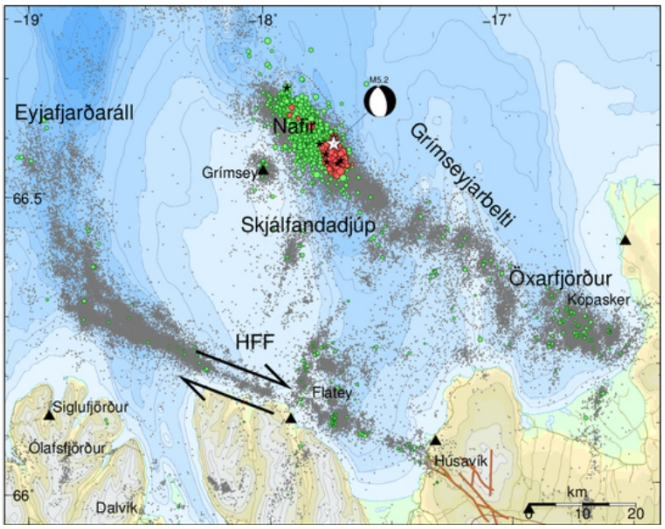

Fig. 2: Seismic activity offshore northern Iceland since 1994 with recent activity indicated by green (January 2018) and red points (since 19th of February). Magnitude larger 4 are shown as black stars, the white star indicates the location of a M5.2 earthquake (IMO, 2018b).

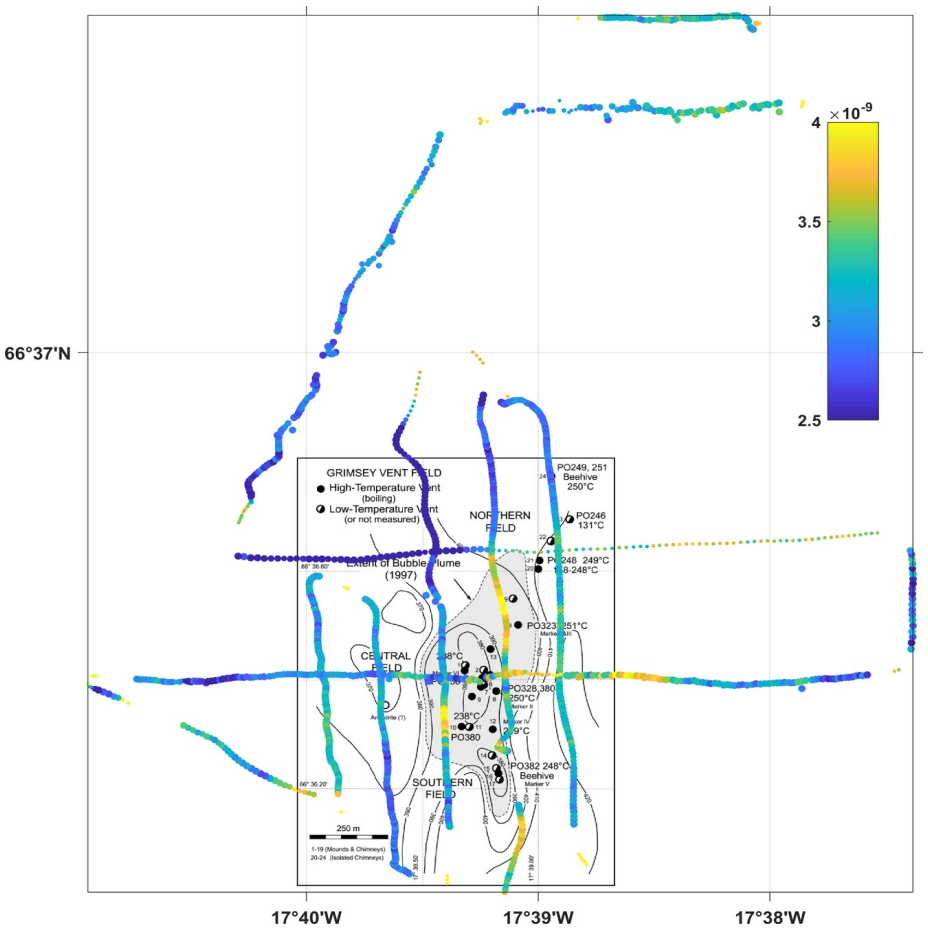

Fig. 3: Preliminary result from TEM measurements with the MARTEMIS system during cruise POS524 (from Hölz & Martins, 2018) showing color coded amplitudes of transients @ 4ms. Stations with increased amplitudes are evident above the GVF. As reference the map of Hannington et al. (2001) marks positions of the vent field and previous investigations.

ing within the water column in echo-sounder profiles (their figure 5), which they used to map out the extent of the hydrothermal field.

Fluid analyses on core samples are reported with end-member chlorinity of 274mM, which is about half of seawater chlorinity (Lackschewitz et al., 2006). Even though sulfur smell was apparent on fresh chimney samples, the lack of smoke in the venting fluids and the only patchy distribution of bacteria mats on the surfaces of mounts suggests that neither sulfur nor metals are abundant at the surface. However, it remains unclear if accumulations of massive sulfides may exist at greater depth (Hannington et al., 2001). Some additional data is presented by Magnúsdóttir et al. (2015) who show an E-W striking section of chirp seismic data, in which the GVF is associated with two separate, cone-shaped acoustic anomalies along a stretch of about 500m. This is a first indication that the vent field is actually larger than depicted in Fig. 2 and could consist of several areas of strong hydrothermal activity. They also present some stratigraphy from the approximately 38m long drill core MD-75, which was taken at a location about 6km SW of the GVF. Additional information about this core can be found in Gudmundsdóttir et al. (2011).

The Grimsey Vent Field was the main target of the recent research cruise POS524 (June 2018), which focused on EM investigations using the MARTEMIS system and a Coil2Dipole experiment to explore the

resistivity structure at shallow to intermediate depths. Fig. 3 shows a preliminary result of the TEM investigations during cruise POS524 (2018) with increased amplitudes above the vent field.

News reports indicated that the area around the GVF was shaken by swarms of earthquakes starting in January 2018 (Fig. 2). The highest activity of about 2000 events was reported mid February[1] (IMO, 2018a). The Icelandic Met Office (IMO, 2018b) reported the highest activity on February 19th with the largest earthquake (M5.2) located 14km ENE of Grímsey together with five smaller earthquakes (M4-4.9). Generally, such pattern of activity occur every few years with similar activity reported in May and September 1969, during the Christmas period in 1980, in September 1988 and April 2013. Thus, the investigations conducted in June 2018 potentially recorded the active state of the hydrothermal field.

Consequently, the research program for this year's cruise POS535 to the GVF was:

- to revisit selected sampling sites and EM profiles during a "dormant" state of hydrothermal activity to map potential time-dependent variations of the electrical conductivity that may reveal fluid flow patterns within the shallow seafloor of the GVF,
- to extend and consolidate previous experiments & sampling, focusing especially on an area to the West of the known active site, where results of the 2018 EM experiments show a good conductor with considerable lateral extent.

3.2.2. Öxarfjörður & Skjalfandadjup

Prior to the cruise, Ögmundur Erlendsson (ISOR, Iceland) pointed us to several promising sites for hydrothermal activity in the vicinity of the GVF. These sites were identified based on structural interpretation of multibeam data and in some cases seismic activity. Based on prominent cone shaped or chimney shaped features along faults, the two structures named Öxarfjörður & Skjalfandadjup were chosen for closer investigation in order to determine, if they are volcanic features or chimney features. Since investigations at these structures was not part of the original proposal, only a very limited amount time (~12h) was set aside for investigations at these structures.

3.3. Working Areas – Norway

3.3.1. Loki's Castle

The active vent site Loki's Castle was discovered during a research cruise in 2008 (*R/V G.O. Sars*) and was further investigated by Norwegian scientific parties in the following years. Currently, it is considered the northernmost confirmed active black smoker site (Beaulieau, 2015). A first detailed description is given by Pedersen et al. (2010): It is located where the Mohn's Ridge passes into the Knipovich Ridge through a sharp northward bend in the direction of the spreading axis (see Fig. 1). The venting occurs near the summit of an ~30km long axial volcanic ridge (AVR) and is associated with a 50–100m deep rift that runs along the crest of the volcano (Fig. 4a). The field is composed of four active black smoker chimneys, up to 13m tall, at the top of a mound of hydrothermal sulfide deposits (Fig. 4b). Venting of 310–320°C hot black smoker fluids occurs at two sites that are around 150m apart and are estimated to be 20–30m high and

1 http://icelandreview.com/news/2018/02/19/magnitude-52-earthquake-near-grimsey

approximately 150–200m across (Baumberger et al., 2016). Pedersen et al. (2010) also report on fluid geochemistry (see also Baumberger et al., 2016) and the vent fauna.

During the recent MarMine cruise (RV Polar King, summer 2016) further investigations – including visual inspections (video / photo / photogrammetry) for geological and biological purposes, underwater hyperspectral imaging, magnetometry, collection of samples (grab and core samples) – were carried out by the Norwegian University of Science and Technology (NTNU, Trondheim, see Ludvigsen et al., 2016). First mineralogical analyses report several samples with concentrations of copper and zinc above 1% with the highest concentration reaching almost 6% (Kowalczuk et al., 2018). Since these samples were most likely collected directly from, or close to the black smokers it remains unclear if such high concentrations can also be found at depth.

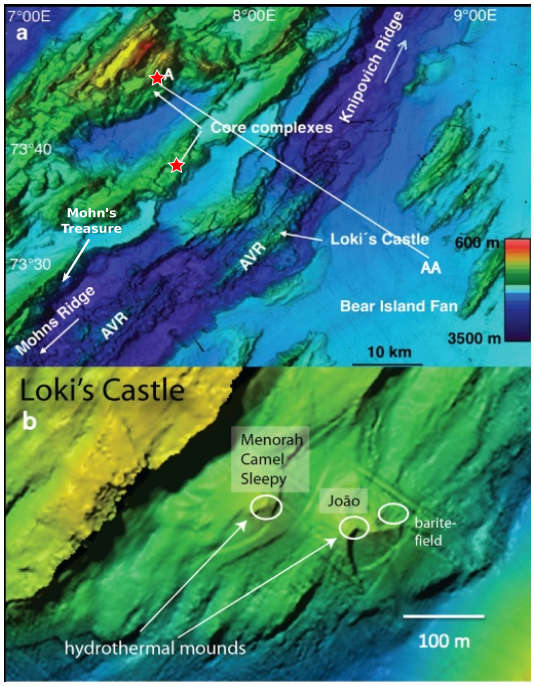

Fig. 4: (a) Bathymetric map of ridge section (compare Fig. 20) with Loki's Castle, Mohn's Treasure, core complexes and location of two mineralized grab samples (red stars). (b) Close up of vent field showing two hydrothermal sulfide mounds with chimneys as well as location of the diffuse, low-temperature hydrothermal barite field (from Baumberger et al., 2016, modified).

Additionally, ultramafics (lower crustal- and mantle rock types) have been recovered from the core complexes located to the NW of Loki's Castle (red stars in Fig. 4a; Pedersen et al. 2010). Generally, oceanic core complexes and the large-offset detachment faults characteristic of the slow-spreading Mid-Atlantic Ridge are crucial for the structural control of large hydrothermal systems, including those forming sub-seafloor polymetallic sulfide mineralization (Pertesev et al., 2012). Petersen et al. (2009) describe a similar geological setting for the ultramafic hosted Logatchev hydrothermal field. Thus, it seems possible that the core complexes NW of Loki's castle host undiscovered SMS sites.

In a recent publication, Johansen et al. (2019) report on a large scale CSEM experiment, which crossed Loki's Castle along a 70km long, NW ↔ SE trending profile (Fig. 5). Their interpretation reaches down to a depth of about 5km beneath the seafloor, which is far beyond the depth of investigation achievable with

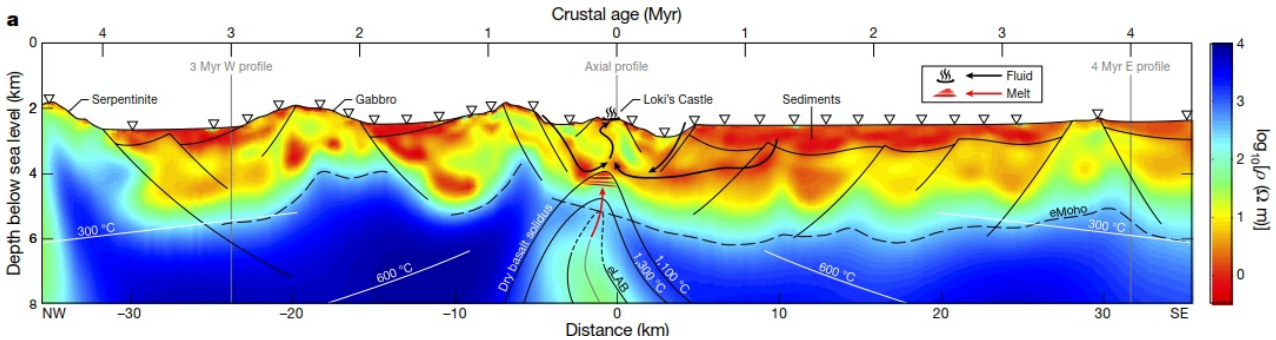

Fig. 5: Inversion result of large scale CSEM experiment crossing Loki's Castle from NW to SE (from Johansen et al., 2019).

our instrumentation. However, their interpretation lacks the fine resolution at shallow depth, which can be obtained with GEOMAR's EM systems.

Based on the previous findings, the research program for this year's cruise POS535 at Loki's Castle was defined as follows:

- Measurement of profile(s) with the MARTEMIS coil system in combination with stationary OBEM receivers (→ Coil2Dipole) across Loki's Castle in order to investigate if high concentrations of minerals can be found at shallow depth,
- measurement with a deeper reaching EM configuration for the same problem, additionally also for the identification of possible fluid migration pathways,
- gravity coring in order to gather sample material as well as pore fluid samples.

Due to the strike direction of the structure and the existence of the previous CSEM measurements of our Norwegian colleagues it was decided to base our experiments along the same profile in order to facilitate potential future comparisons of results from measurements with different depths of penetration.

3.3.2. Mohn's Treasure

About 40km to the WSW of Loki's castle, additional occurrences of SMS (mostly Pyrite) were dredged and brought up from about 2600m water depth from a site named Mohn's Treasure (Pedersen & Bjerkgård, 2016; see Fig. 4a). No seawater anomalies were recorded here, thus the material presumably originates from an extinct field. Further investigations during the MarMine cruise did not find the hydrothermal venting of Mohn's Treasure to be very pronounced (Ludvigsen et al., 2016). A small mineralized area was observed, but only covered a few meters along oxidized basalt outcrops comprising minor pyrites and distinctive features. Since it possibly formed by diffuse discharges, it was concluded that mass-wasting events may have played a major role in displacing and burying the overall massive sulfide deposits and its associated extinct vent field. Even though this pointed to a location somewhere uphill on the ridge (S.L. Ellefmø, personal communication), there were also other results from magnetic measurements giving indications that the main area of mineralizations may indeed be further down the slope (A. Lim, personal communication).

Due to the fact that the length of *RV Poseidon's* winch cable was limited to 2600m during the cruise, it was uncertain if the main site of mineralization could be reached with the EM systems. Therefore, it was decided to dedicate only a limited amount of time for investigations at Mohn's Treasure by running a single profile along the ridge hoping to pass the hidden site of mineralization with the available length of the winch cable.

4. Narrative of Cruise

08.06.2019

Mobilization of the equipment had already been conducted in Bremerhaven before the departure of RV Poseidon towards Iceland. Therefore, after embarkment onto the vessel in Akureyri, the scientific crew of nine persons could start right away with preparing the laboratories, OBEM Loggers, MARTEMIS coil system and with the installation of the Posidonia system. Since the transit from Akureyri to the first survey area around the Grimsey Vent Field (GVF) is only about four hours, it was important that the key components needed during the first days of the cruise were prepared before departure.

09.06.2019

We departed Akureyri mid-day and arrived in the working area at approximately 16:00h. Shortly after arrival, we conducted a pressure test for the releases and acquired a CTD-depth profile. The acquired sound-velocity profile was needed for the calibration of the Posidonia USBL-system, which had to be delayed since one critical component was not operational (see below). The CTD data will also be of used for the calibration and interpretation of EM data.

10.06.2019

The hours from breakfast until lunch were used to sample three gravity cores (GC01-GC03) in the area of the GVF. After lunch, we deployed the first seven OBEM stations (OBEM01 -OBEM07) in a free-fall approach. The devices were assembled and synchronized before they were deployed over the side of the ship and released at the water surface. As the water depth at Grimsey is relatively shallow (~400m), we chose this approach as it is more time efficient compared to lowering each device individually to the seafloor. Precise positions will be determined during post processing of ranging data, which is measured with a ranging system mounted to the MARTEMIS transmitter cage. OBEM07 was re-deployed to a position that was used during the previously conducted experiment last year (POS524, 2018). During the time where the EM team was busy deploying the OBEMs, the geological team analyzed the first gravity cores in the wet lab.

11.06.2019

We started the day with lowering the heat flow sensor to the seafloor and taking measurements at four locations until lunch. In the meantime, the EM crew was still busy with trying to fix the IXSea releases, a job which had actually been started on the first day. Generally, a USBL release is a critical component for our experiments since its transducer is needed for the calibration of the Posidonia USBL-system and is also used for acquiring positioning data from our EM transmitter during experiments. Ultimately, the bug in the hardware was finally found before lunch and we were able to perform the calibration of the USBL system between 13 – 16h. Subsequently, we deployed the five remaining OBEM receiver stations using the same approach as during the previous day. Note that OBEM08-OBEM12 were all deployed to positions that were used during the 2018 cruise (POS524). The last station deployed OBEM12 was also equipped with a CTD probe to get stationary measurements, which are aimed to determine temporal variations in the measured parameters, which could either be caused by oceanic currents or variations in the activity of the hydrothermal field. Also, these stationary CTD measurements should allow to compensate temporal variations in

CTD data, which were later acquired with a second mobile CTD probe attached to the MARTEMIS frame in order to determine lateral variations of the measured parameters.

12.06.2019

Deployment of the MARTEMIS transmitter system was started at 8:00h in the morning and, after conducting a first successful tests of the electronics and lowering to the seafloor, measurements were started along the first profile. Due to wind and ocean currents, we were forced to restrict our measurements to E-W profiles. After the first profile, the equipment was brought to the surface to check its mechanical integrity. After redeployment, the Hydra logger was off and did not record any coincident-loop data from the second profile. At 22:00h the measurement had to be stopped because of a system failure due to a short circuit caused by water in one of the connectors. Up to the point of retrieval, we were able to measure one full profile.

13.06.2019

We started the day by conducting five heat flow measurements between breakfast and lunch. In the meantime, the MARTEMIS system was repaired and was redeployed at 13:00h to continue with measurements along profiles for the rest of the day. Due to the weather conditions, all profiles were recorded in an E-W direction.

14.06.2019

Continued with the MARTEMIS measurements until 1:00h and successfully retrieved the transmitter equipment. A total of five profiles were measured during this deployment. The remainder of the day was used to conduct six heat flow measurements on and around the GVF. In the meantime, a second EM system called “CAGEM” was assembled on the aft deck. The system applies two perpendicular electrical dipoles – similar to GEOMAR’s SPUTNIK system – to the coil frame of the MARTEMIS setup. The advantage of CAGEM is that it allows for continuous measurements and does not require the system to set down on the seafloor before transmitting the current. Therefore, the system should be more time efficient compared to SPUTNIK and enable a higher data density.

15.06.2019

From 8 – 10:00h, two further gravity cores (GC04-GC05) were taken. The remaining time before lunch was used to recover three OBEMs (04, 08, & 12) due to the prognosis of foggy weather conditions on the following day, which was feared to prevent us from retrieving all 12 stations on one day. After lunch, the CAGEM system was hoisted into the water. A seemingly critical failure of the system forced us to bring MARTEMIS system back on deck. After the cause of the failure of the system was recognized to be simply a faulty calibration of the pressure sensor in the battery tube, which lead to wrong readings of the sensor, the system was redeployed after a re-start and measurements were continued on until the morning hours of the following day.

16.06.2019

After recovery of the transmitter in the morning, the remainder of the day was used to recover the nine remaining OBEM stations. Aside from OBEM12, which was recovered on the previous day, we were able to synchronize the clocks of all loggers to GPS signal to determine the clock drift. Upon retrieving

OBEM01, we noticed that the blue electrode cable of Channel 1 was ripped off, which could however have happened during the station recovery. After successfully retrieving all OBEM stations, we departed for an overnight transit to a new working area to the SE called Öxarfjörður.

17.06.2019

Between 7:00 – 8:30h, two gravity cores were retrieved from the new working area (GC06-GC07). We were then forced to transit to Grimsey Island to wait for a technician to come aboard the ship at approximately 14:00h to fix the ship's gyro compass. After the repair of the compass, we headed back to the site Öxarfjörður overnight to continue with the scientific program in the morning of the following day.

18.06.2019

Between 7:00 – 10:00h, three further gravity cores were sampled, one at Öxarfjörður and two more at an additional potential hydrothermal site (Skjalfandadjup). The cores were immediately opened and briefly analyzed to discuss the further work plan. Shortly after 10:00h, it was decided to finish work in the Icelandic working areas and to start the transit to the northern working areas in Norwegian boundary waters. The ship made its way on a 3.5 day journey.

19. - 21.06.2019

Transit days to Loki's Castle. No scientific program was conducted.

22.06.2019

We arrived in the survey area in the morning and attempted to position the ship to take a first gravity core. However, this was not feasible due to the poor weather conditions and high waves and, thus, the scientific program was postponed to the next day.

23.06.2019

Over night the weather calmed down and we were able to start our scientific work plan at Loki's Castle. It was decided to make up time by beginning work before breakfast by deploying a first OBEM station at 7:00h. Due to the large water depths at Loki's Castle (>2000m) and the lack of time, it was decided to deploy stations free falling, which takes approximately 1h to sink to the seafloor. In the meantime two gravity cores (GC) were taken near the central mounds of Loki's Castle. In between GC stations, ranging data was acquired to estimate the horizontal drift of the deployed OBEM station on its way to the seafloor. After lunch, five further OBEM stations were dropped at coordinates updated to account for the horizontal drift determined during the deployment of the first station. At approximately 16:00h, we finished deploying the stations and immediately started with MARTEMIS measurements. These measurements went on until noon the next day. In total we measured 3 profiles, 2 of which were measured from NNW – SSE and one from SSE – NNW.

24.06.2019

The time before lunch was used to finish the MARTEMIS measurements and recover the system. After lunch two further gravity cores were taken. In the meantime, the EM team reassembled the CAGEM transmitter which was then deployed at midnight to measure one concurrent profile aligned with the first profile measured with the MARTEMIS system during the previous night.

25.06.2019

The CAGEM measurements were conducted from midnight to approximately 7:00h. Subsequently, we successfully recovered all six OBEM stations and continued the journey to the last survey area called Mohn's Treasure. We arrived at around 14:00h and started gravity coring, which however yielded no recovery except for a few grains in the core catcher. In the meantime, the EM team was busy on the aft deck disassembling CAGEM and reassembling MARTEMIS for one last deployment.

26.06.2019

At 7:00h, the final MARTEMIS experiments started at Mohn's Treasure. Along one profile – running from SW to NE along a ridge – a region which was previously identified as a magnetic high by Norwegian colleagues was crossed. With the successful recovery of the MARTEMIS system (scarred with some some bumps and bruises) the scientific work was finished in the early afternoon and we began our journey south towards our final port: Bremerhaven (Germany).

27.06 – 03.07.2019

After 6.5 days of transit we arrived at our final destination port in Bremerhaven, Germany.

5. Applied Methods

5.1. Electric and Electromagnetics

In land-based exploration it has been common practice for several decades to use electromagnetic methods to detect and characterize massive sulfide deposits (i.e. Palacky, 1987). Investigations on marine samples indicate that conductive anomalies may also be expected in the marine environment (e.g. Iturrino et al., 2000). Consequently, both active and passive EM methods are general suitable for the investigation of SMS and the associated hydrothermal systems:

1. active experiments rely on the fact that the generated electromagnetic field couples to the conductive ore body as well as hot and saline hydrothermal fluids and is distorted by the coupled current systems, which are channeled into the conductive medium,
2. passive self-potential (SP) measurements detects naturally occurring anomalies in electrical potential (or electrical field) which can arise from buried conductive bodies (e.g., massive sulfides, graphite shear zones) or from streaming potentials caused by fluid flow (e.g. hydrothermal fluids).

During previous year's cruise POS524, both passive electric (i.e. SP measurements) as well as active electromagnetic experiments had been carried out. Since the SP measurements had not revealed any significant anomaly, it was decided to skip these measurements during cruise POS535 to solely focus on active measurements instead.

Active measurements were carried out with three different systems / configurations, which different depths of investigation:

- The transient electromagnetic coincident loop system MARTEMIS, with a shallow investigation depth of several 10s of meters and a relatively localized footprint (see chapter 5.1.1),
- the Coil2Dipole configuration, which uses the MARTEMIS transmitter coil as source and stationary ocean bottom electromagnetic (OBEM) stations as receivers, which yields an investigation depth of about 100m (see chapter 5.1.2),
- and finally a new dual dipole transmitter system named CAGEM, which in combination with the OBEM receivers offers an investigation depth of about 250m (see chapter 5.1.3).

5.1.1. MARTEMIS Coil System – TEM Measurements

In 2012, our working group suggested to use a transient electromagnetic (TEM) coil system for the detection of conductive features (Swidinsky et al., 2012). In 2015, during cruise POS483, we for the first time used the self developed MARTEMIS system to perform investigations on the inactive target with known mineralization (Palinuro Seamount in the Tyrrhenian Sea, also investigated during cruise POS515 in 2017). Inactive mounds were also investigated in the vicinity of the TAG hydrothermal field at the Mid-Atlantic Ridge (2016). In last years cruise POS525 we for the first time investigated an active target without known mineralization (GVF) to turn to an active target with known mineralization in this years investigations (Loki's Castle).

Fig. 6 shows a sketch of the MARTEMIS system, which consists of two frames connected by a rigging. The lower square frame holds cables of the coincident transmitter (TX) and the receiver (RX) coils. The frame is constructed from glass fiber reinforced tubes. In the first experiments (2015 – 17) we had used corner connectors made of stainless steel, which were identified as one cause of distortions in test measurements in late 2017. Therefore, we had used a new set of custom made corner connectors made from glass fiber reinforced plastic during last years cruise. In addition, all metal parts (weights, shackles, …) had been removed from the lower frame, which finally resulted in a practically distortion free calibration measurement during last years cruise (Hölz & Martins, 2018).

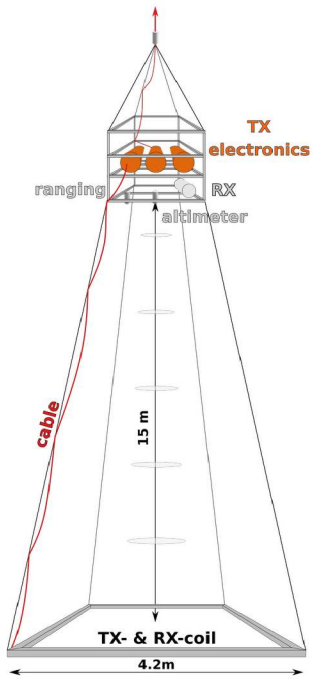

Fig. 6: MARTEMIS coil system used for TEM measurements and as transmitter for the Coil2Dipole experiment.

Generally, the robust connector system allows for flexible loop sizes by simply using tubes with different lengths, which of course also requires a coil cable with a matching length. Thus, the system may be adjusted to the available deck space and the size of the ship's A-frame by up- or downsizing. For measurements on *R/V Poseidon* we used a $4.2 \times 4.2\text{m}^2$ coil. Additionally, barite weights, a metal free attitude sensor and a small altitude sensor – the only metal part on the lower frame – were mounted to the coil frame.

The upper frame holds several pressure tubes with the receiver and transmitter electronics, the power supply, and a self-built acoustic ranging system, which is used to measure the distance between the MARTEMIS system and the remote OBEM receivers (see chapter 5.1.2). The corners of the upper and lower frame are connected via a rigging. Cables, which are attached to the rigging connect the transmitter and receiver coils as well as a downward looking attitude sensor to the associated counter parts within the pressure tubes in the upper frame. The reason for separating the two frames by a distance of about 15m is simply that all metal parts (e.g. pressure tubes, etc.) and components, which create EM noise (e.g. transmitter electronics) should be kept as far away from the sensor (i.e. the receiver coil) as possible.

The receiver unit has three input channels with 24bit resolution, which are sampled at a frequency of 10kHz and have a storage capacity to acquire about 48h of continuous data. For this years TEM experiments we used all available channels connected to the receiver coil to record the transient responses at different gain settings. Contrary to last year, no selfpotential measurements were performed. In principle, a DSL link can be used to download data from the receiver units directly from the laboratory during the experiment. However, due to the low data rates over the coaxial link, the data transfer is too slow to constantly monitor the data in real-time and we only downloaded data every other hour to check, if receiver, transmitter, and ranging system were still operational and recording reasonable data.

The transmitter unit generates a bipolar square waveform with a 50% duty cycle. Repetition frequencies may be switched to 0.25Hz for CSEM measurements (see chapter 5.1.3) or 2.5Hz for TEM measurements or Coil2Dipole measurements (next chapter). Current amplitudes can be selected to be 19A, 38A or 57A. The transmitter current is supplied and regulated through DC/DC converters, buffer batteries and a micro-

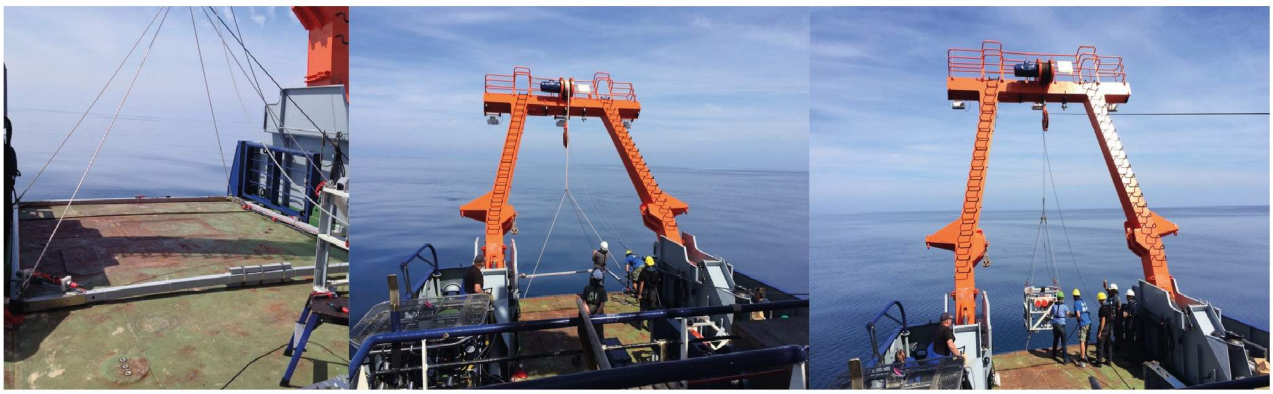

Fig. 7: Deployment of the MARTEMIS system on R/V Poseidon (pictures taken during cruise POS483).

processor controller unit. These units are housed in titanium cylinders, which are mounted to the upper frame.

For experiments, the MARTEMIS system is assembled on the aft of the ship (Fig. 7, left). After assembly, the coil frame is lowered into the water (Fig. 7, middle) and attached at a vertical distance of 15m beneath the upper frame (Fig. 7, right). After deployment the whole system is lowered towards the seafloor using the ship's winch cable and "flown" across the seafloor by moving the ship at a slow speed of approximately 0.5kn. By monitoring the altimeter, the position of the loop is kept at a close distance of about 5m above the seafloor by constantly adjusting the length of the winch cable.

Generally, an automated cycle for TEM measurements was performed as follows:

- ranging measurement,
- TX activation for 8s (50% duty-cycle, I = 19A, repetition frequency 2.5Hz),
- ranging measurement,
- TX activation for 16s (50% duty-cycle, I = 38A, repetition frequency 2.5Hz),

Ranging measurements are needed to determine distance between the transmitter system and the remote OBEM receivers for the evaluation of data acquired in the Coil2Dipole experiment (chapter 5.1.2). After each measurement, a short pause in the order of 5 – 10s was included to give the batteries time to recharge to avoid a creeping decay of the power supply for the experiment.

5.1.2. Coil2Dipole

By using remote receivers, which are placed stationary onto the seafloor, in combination with the transmitter coil of the MARTEMIS system, it is possible to perform an additional EM experiment with increased depth of investigation, thus, adding valuable information about the deeper structure of the hydrothermal system. Since the MARTEMIS transmitter coil is used to transmit the signals which are picked up by the electric dipoles of the OBEM receivers, we call this experiment "Coil2Dipole". Previously, we have conducted such an experiment at the Palinuro Seamount. Theoretical considerations for this type of experiment and first results from Palinuro can be found in Safipour et al. (2017, 2018). A first evaluation of Coil2Dipole data acquired during last year's experiment at GVF has just been evaluated as part of a Bachelor Thesis by Kim Carolin Barnscheidt to be submitted by December 2019.

Stationary OBEM (ocean bottom electromagnetic) receiver nodes (Fig. 8) are equipped with a three component fluxgate magnetometer, and can measure two components of the horizontal electric field. The components of the electric field are measured using Ag/AgCl - electrodes, which are attached at the end of four flexible arms. The total length of each receiver dipole is 11.2m. Additional sensors allow measurements of the attitude (pitch, roll) and the temperature.

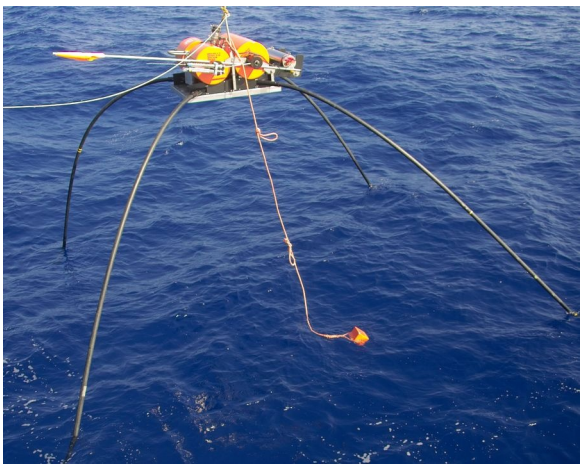

Fig. 8: OBEM receiver during deployment.

We used two different versions of OBEM loggers, the original version (V2008, 10 loggers) and a new version (V2018, two loggers), which received some updates to the logger electronics and sensors. Generally, both versions may be operated in two modes, which can be changed actively by an acoustic signal or by using a predefined timetable.

1. In MT (magnetotelluric) mode, which is usually used to record the natural variations of the Earth's electromagnetic field, three components of the magnetic field and two horizontal components of the electrical field are recorded at a frequency of up to 10Hz (V2008) or up to 100Hz (V2018). Generally, the new version would also allow to measure the z-component of the electrical field, which would however still need mechanical implementation on the frame and new connector cables.

2. In CSEM mode, which is used to record the Earth's response to an active source signal generated by a transmitter, electrical field components are recorded at a frequency of 10kHz. For the old logger, magnetic fields as well as additional environmental data (pitch, roll, temperature) are not recorded during CSEM mode. For the updated V2018 loggers, these parameters may be continuously measured while the CSEM mode is active, i.e. CSEM and MT mode may be operated simultaneously.

For experiments like the Coil2Dipole experiment, it is important to know the exact distance between the transmitter antenna and the remote receivers. While the Posidonia USBL positioning system can provide locations with an accuracy of about ±5m at the given water depth of about 400m (value taken from the calibration measurements), a higher accuracy is needed in the evaluation of data, especially for short transmitter-receiver offsets. Such improved distance measurements can be achieved with the on-board ranging system, which is mounted to the upper frame of the MARTEMIS system. There, a modified release is used to transmit an 11kHz interrogation ping, to which the releases mounted on the OBEM stations can reply with a reply ping with a preset, fixed fre-

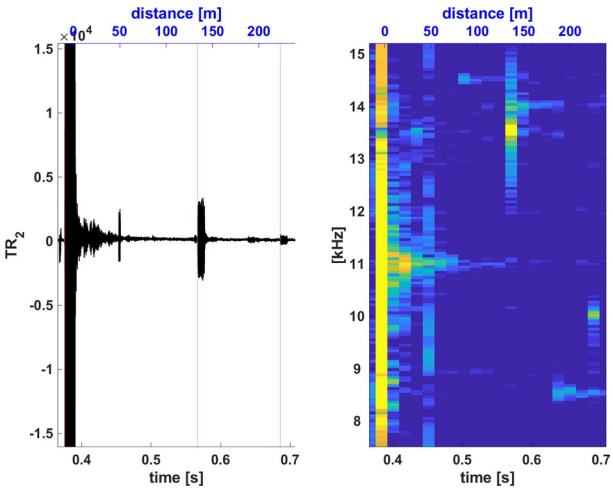

Fig. 9: Example of ranging data with hydrophone track (left) and associated spectrogram (right).

quency between 8 – 15kHz. Hence, these transducer on the OBEM station in combination with the acoustic system attached to the transmitter system are used to determine the range between the transmitter system and OBEM receivers. For the experiment at the GVF we used individual reply frequencies for each OBEM, which allows for a simple and unique identification of OBEMs by the frequencies of received signal. Fig. 9 shows an example of the acquired ranging data with the large amplitude interrogation ping (11kHz, @ ~0.39s) send out from the transducer attached to the upper frame of the MARTEMIS system and answers of OBEM receives (13.5kHz and 10kHz at distances of approximately 134m and 223m, respectively).

Past experiments have shown that measurements with the ranging system are repeatable with ranges varying by at maximum of a a few centimeters, even for large offsets. Thus, the accuracy of the ranging system is mainly determined by the knowledge of the sound velocity at the seafloor, which is measured with the external CTD, and we expect it to be better than 1m for the ranges relevant in this experiment (<300m), possibly even in the order of around 10cm.

For previous projects, the evaluation of ranging data – a prerequisite for the correct interpretation of the Coil2Dipole data – was done by manually picking arrival times of pings. Since there are usually several thousands of ranging measurements in the course of an experiment, e.g. around 2000 for the coil experiment at the GVF, this processing step is too time consuming when performed manually. Therefore, an automated picking algorithm has been implemented, which allows for an automated determination of first arrival times. This picking algorithm was first applied to the ranging data sets acquired in the course of this cruise and we are currently assessing the quality of the algorithm. While first results look promising, the stability of the algorithm still needs to be worked on.

5.1.3. Dual Polarization CSEM – CAGEM

In addition to the MARTEMIS coil experiment, we carried out a “Dual Polarization” CSEM experiment, similar to the one carried out last year. In contrast to last years experiment, where we had simply threaded spherical metal electrodes to the lower parts of the rigging of the MARTEMIS coil frame (see Fig. 19 in Hölz & Martins, 2018), we used a completely new antenna design for this year’s cruise.

The new CAGEM frame uses the small upper frame of the MARTEMIS system and a modified version of the lower frame (Fig. 10). Contrary to the rigging of the MARTEMIS system, which separates the two frames by about 15m, the ropes used for the CAGEM system are much shorter, leading to a vertical distance of about 3 – 4m between the two frames. This is possible because for the Dual Polarization experiment there is no receiver unit attached to the CAGEM system and, thus, electromagnetic noise is of no concern. The shorter rigging greatly simplifies the deployment of the system.

Similar to the MARTEMIS system, the lower frame is modular and may be adjusted to the space available on the aft deck of the ship and the width of the A-frame. On each corner of the lower frame metal gratings are used as electrodes. Cables running along the rigging connect the electrodes on the corners of the lower frame to the transmitter in the upper frame, thus, allowing for the transmission of TX signals into two horizontal, oblique dipoles. Due to the limited space available on *RV Poseidon* during the cruise, we had to settle for a 4.06m × 3.05m large rectangular frame resulting in 5.07m long dipoles intersecting at an angle of approximately 73.8° in the center.

In addition to the electrodes, acoustic transducers are also placed in each corner of the lower frame. They are used to register reply pings, which are send out from the OBEM stations. Together with the interrogation pinger on the upper frame, this forms a USBL ranging system, which allows for a precise measurement of the distance and direction between the CAGEM transmitter system and the remote stationary OBEM receivers, which is an important prerequisite for a correct interpretation of the acquired data.

In comparison to the previously used SPUTNIK system, the new CAGEM setup offers the benefit of not needing to be placed onto the seafloor for measurements, since the two dipoles are permanently in position. The system is operated by lowering it to the seafloor and then drifting along at a slow speed of ~0.3 – 0.5kn with an altimeter controlled elevation of 3 – 5m above the seafloor controlled by constantly adjusting the length of the winch cable. Thus, measurements can be taken quasi continuously, which allows for a much denser spacing of data points. As a drawback, the achievable dipole moment of the CAGEM system is smaller due to the reduced length of the transmitter dipoles (~5m as compared to 10m for the SPUTNIK system). Also, the fact that the CAGEM system is moving during measurements, thus, leading to changing offsets and relative orientations between TX and RX during the acquisition time, will potentially lead to larger error bars / uncertainties in the evaluation of data. However, some of these problems may be solved by using a special waveform as will be explained later.

As this experiment is novel and was conducted for the first time during last years cruise, we are still in the process of changing and adjusting previously established processing routines for the “regular” CSEM data acquired with the Sputnik system. Once these changes have been implemented, the established imaging (Swidinsky et al., 2015) and inversion routines (Hölz et al., 2015) should then be applicable without any further adjustments.

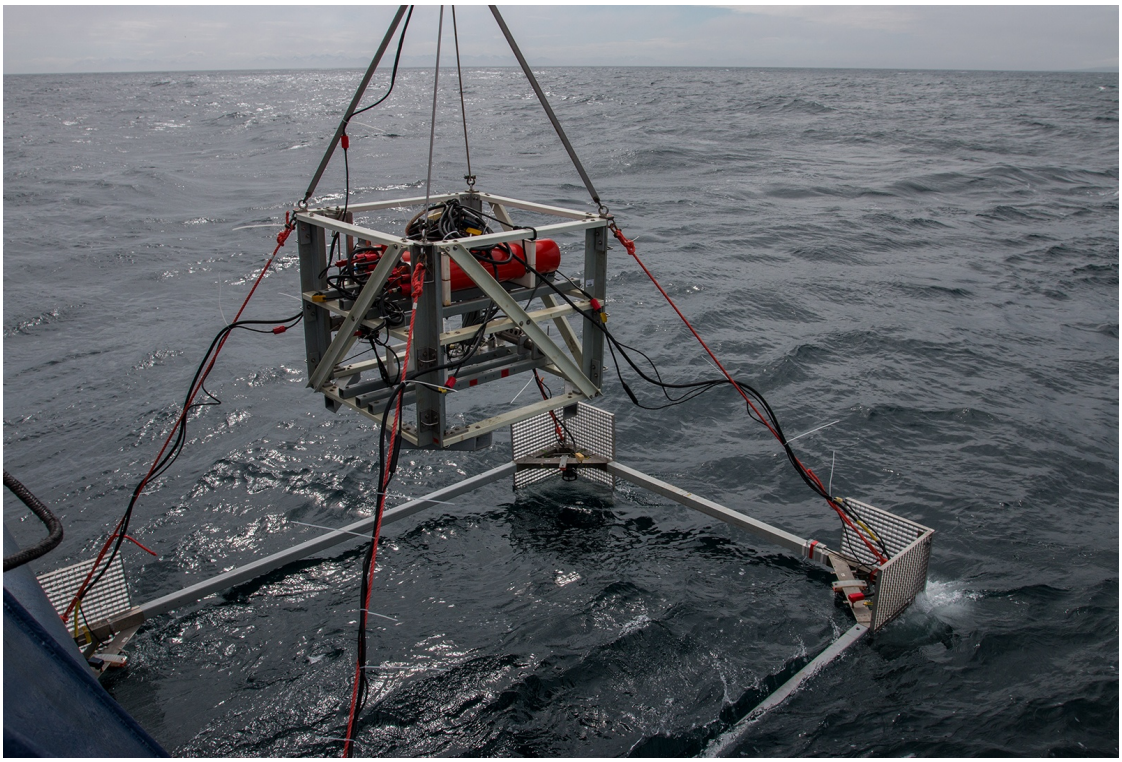

Fig. 10: Dual polarization transmitter system CAGEM during deployment. This system was used for the CSEM experiment carried out during the INSIGHT cruise.

5.2. Heat Flow

Sofia Martins & Natalia Rodriguez

Heat flow measurements were performed only at the GVF, complementing the measurements taken during cruise POS524 (2018). Measurements were performed using GEOMAR's short violin-bow type heat flow probe (Model FIELAX GmbH, Bremerhaven) which allows for data acquisition in seafloor sediments down to a penetration depth of 3m (Hyndman et al., 1979, Lister, 1979).

The sensors for temperature measurements (22 thermistors, NTC1 – NTC22) are located in a sensor string that is attached to the stainless-steel probe. This sensor string also contains a heating wire, from which a heat pulse is released into the sediment.

The in-situ measurements of temperature and thermal conductivity follow the pulse needle probe method (Lister, 1979). Upon sediment penetration the heat friction created between the sensor tube and sediment result in a temperature rise. The temperature decay is measured at a sample rate of 10s, during an established length time (in POS535, 7 minutes), after which a calibrated heat pulse of $1kJm^{-1}$ is generated for 10s. For 7min the heat pulse decay is recorded until the probe is removed from the sediment (Hartmann & Villinger, 2002). The complete sampling event lasted around 15min. In between stations, the probe was heaved 150 – 200m above seafloor. Due to the expected high temperature of the sediment around the GVF, the probe used the calibration file Mem21260.prb which can be used in temperatures between -2°C and 60°C. Villinger & Davis (1987) give a detailed description about the data processing leading to the in-situ temperatures and thermal conductivity values.

The probe was deployed on the ship's port-side and lowered to the seafloor at 1.1m/s winch speed, penetrating the sediment by its own weight. The acquired data was stored in the data logger and later recovered on board, since the operation in real-time mode was not possible.

5.3. Gravity Coring

Sofia Martins & Natalia Rodriguez

Core Handling, Sampling & Description

The gravity coring done during POS535 covered several distinct working areas at GVF, Öxarfjörður, Skjálfandadjúp, Loki's Castle and Mohn's Treasure. A total of 15 gravity core stations were performed (3m, 125mm diameter, 900kg weight on top) with a total of about 19.5m of sediment collected. Three cores only recovered scarce gravely material within the core catcher.

When the gravity corer arrived on deck, the core catcher was checked for the presence of sample material. Provided sediment was found and sufficiently fine grained, several parameters (pH, Eh, electric conductivity and temperature) were measured using two separate probes (Hach Multimeter MM110DL and Hach Multimeter MM150DL).

Still on deck, the core catcher was removed and the core liner was cut into 1m long sections, the measurement of the parameters being repeated on the bottom of each core section and on the top of the shallowest one. Sections were then labeled, sealed with end caps and moved to the lab for further work.

In the lab, core sections were opened lengthwise using a power disc-saw (Fein-Multimaster), special care being taken so that the disturbance to the sediment was kept to a minimum. Both halves (working and archive) were photographed and described (see Appendix 10.3, pp. 55ff). The description contain a drawn graphic representation of the core and a short explanation about the lithology, grain size, structures and color (Munsell Color System – HVC). Sampling was only performed on the working half for sediment and pore fluid (see below for details). Both working and archive halves were then stored in plastic sleeves within labeled D-tubes, which will be deposited at the core repository at GEOMAR, Kiel.

Sediment Sampling

A cut-off, tip-less syringe (20 ml), was used to recover severalcm^3 for subsequent geochemical studies, coarser material was sampled with a small spatula. Sampling was done at the center of the working half at the thickest section to avoid core edges, where contamination and disturbance may occur. The sediment samples were then stored in properly labeled zip-lock plastic bags. The sampling locations were then analyzed for pH, Eh, temperature and electric conductivity with the above-mentioned probes. A total of 79 samples, encompassing sediment and rock/chimney fragments were recovered.

Porefluid Sampling

Whenever possible, pore fluid samples were recovered within the same depth interval as the sediment samples. Pore fluids were collected on the working half using Rhizon CSS (Core Solution Samplers).

Before being used, all the Rhizons CSS were soaked for at least 24h in artificial seawater of approximately Atlantic salinity. These rhizons consists of a 4cm porous polymer tube (0.15µm) with a flat tip and a diameter of 2.5mm, supported by a glass fiber strengthener and connected with a PEC/PVC tubing of 12cm and female luer lock. The syringes (20ml) were screwed directly on the luer and the piston was kept in place with a retainer (wooden piece) that enabled vacuum to be created (Rhizosphere Research Products, 2018).

The pore fluids were stored in 20ml, acid-cleaned, HDPE mini vials. For ICP analyses preparation, 3ml of each of the collected pore fluid was transferred into an acid-cleaned 3ml HDPE mini vial and acidified by adding 30µl of ultra-pure HNO_3. A total of 64 pore fluid samples were collected, including method blanks (every 8 sample), see Appendix 10.4 (p. 79) for detailed information.

5.4. CTD

Chris Galley, Tristan Sinnecker & Sebastian Hölz

CTD measurements were carried out using autonomous Microcat CTD sensors from Seabird. Similar to last years experiment, one CTD was mounted to the hovering MARTEMIS system in order to detect local variations in temperature and / or salinity caused by hydrothermal activity. In order to minimize the influence of the CTD on the electromagnetic measurements, it was decided to move the CTD probe to the upper frame of the MARTEMIS system. Thus, most measurements of this sensor were taken at elevations of about 20m above the seafloor.

Based on experience gained during the previous cruise to the Grimsey Vent Field during cruise POS524 (Hölz & Martins, 2018) it was decided to also mount a second CTD sensor to one of stationary OBEMs

during experiments. Generally, a stationary CTD can facilitate the detection “regional” temporal variations in the measured parameters, which could be caused by large scale temporal variability of hydrothermal systems or alternatively by dynamic oceanic currents near the sea bottom. In both cases, the stationary data can be useful to quantify such temporal drifts and correct for them in the data of the hovering system.

6. Experiments & Preliminary Results

6.1. Grimsey Vent Field

6.1.1. MARTEMIS – TEM Experiment

Measurements with the MARTEMIS coil system were conducted during two deployments on June 12th and 13th along five profiles with a combined length of about 15.5km and along a short profile with a length of about 1300m (Fig. 12). Due to an unfavorable combination of wind, waves and ocean currents, it was only possible to operate the system along W → E profiles and not along a continuous snake line profile, which significantly slowed down operations since the device had to be towed to the W without taking any measurements during the transit. In total, the transmitter cycle (see chap. 5.1.1) was activated at a total of 1185 stations along the profiles (white dots in Fig. 12).

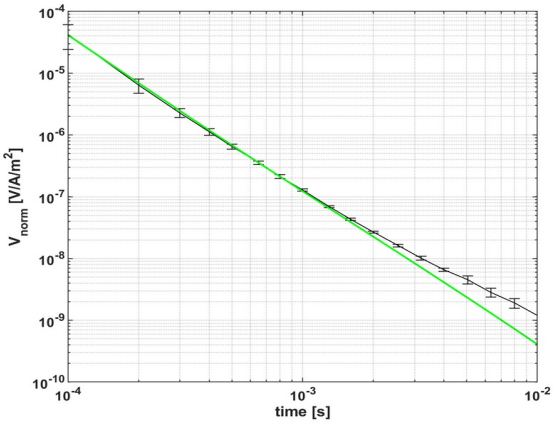

Fig. 11: TEM calibration measurement in water column.

Fig. 11 shows a first result of data processing of a calibration measurement (black line), which was taken within the water column far away from the seafloor and the air-water interface. In such a setting, the mea-

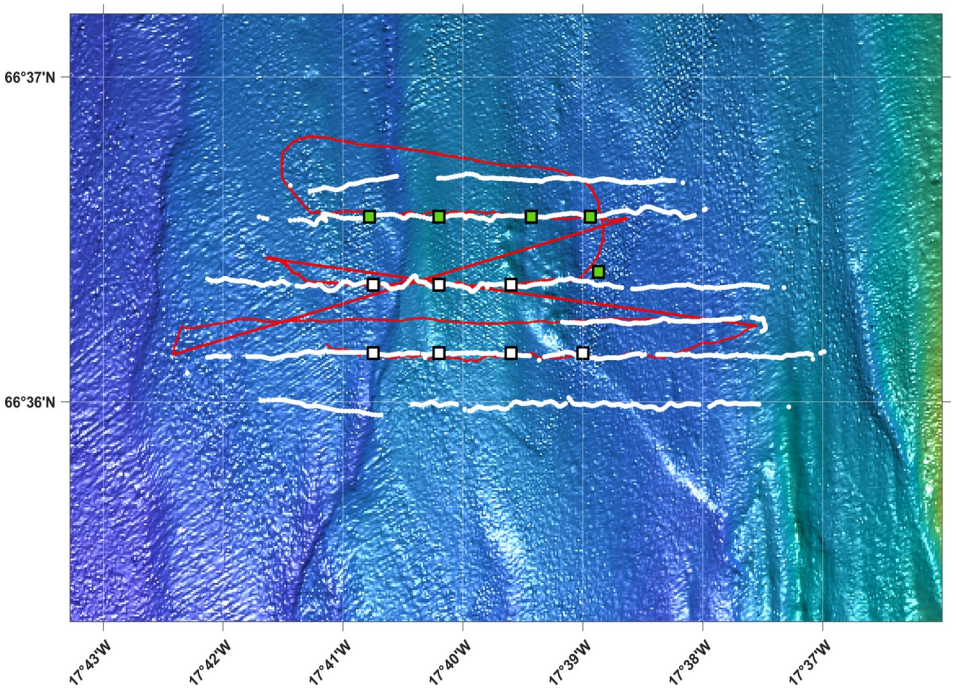

Fig. 12: Transmitter stations of MARTEMIS system during TEM experiments at the GVF (white dots) and track of CAGEM system during Dual Dipole experiment (red line). Squares mark the drop positions of the OBEM receivers with green markers showing receivers, which were deployed to locations which had already been used during the previous experiment in 2018.

surement can be considered to be taken within in a homogeneous full-space, for which a theoretical solution can be calculated (green line). As can be seen in Fig. 11, there is a good agreement between the curves at early times, but increasing distortions at later times. At the time of writing of this report, the reason for this is not yet know. However, theoretical considerations show that such distortions can be accounted for, as long as they are constant and can be quantified with a suitable calibration. Since both requisites are met for our experiment, we will take the observed distortion into account in the future interpretation of data and will further investigate its cause.

6.1.2. Coil2Dipole

For the Coil2Dipole experiment, twelve OBEM receivers were deployed along three profile lines on June 10th and 11th (Fig. 12). All receivers were synchronized to GPS time prior to deployment and also after recovery to determine the time drift of the clocks. Contrary to last years experiment, it was decided to deploy the receivers free falling in order to meet the tight time schedule. Five receivers were deployed onto positions which had already been used during the 2018 experiment (green squares in Fig. 12). This was done in order to acquire time-lapse data which will be investigated to see if different stages of activity in the hydrothermal system may be distinguished in EM data.

As the processing of acquired raw data involves several time consuming steps (e.g. establishing time-synchronization between transmitter and receivers, processing of ranging data in order to establish distances between transmitter and receivers), we cannot yet include any processed data of this year's cruise into this cruise report. Instead, we show a data example in from last year's cruise POS524 Fig. 13, which was just submitted as part of the Bachelor's thesis (Barnscheidt, 2019). The result shows the interpretation of station OBEM04, which in 2018 was deployed to a position located in the SW corner of this year's receiver grid. The interpretation result shows a conductive anomaly at greater depth, roughly coinciding with a conductive anomaly picked up in the interpretation of TEM data acquired during the 2018 cruise.

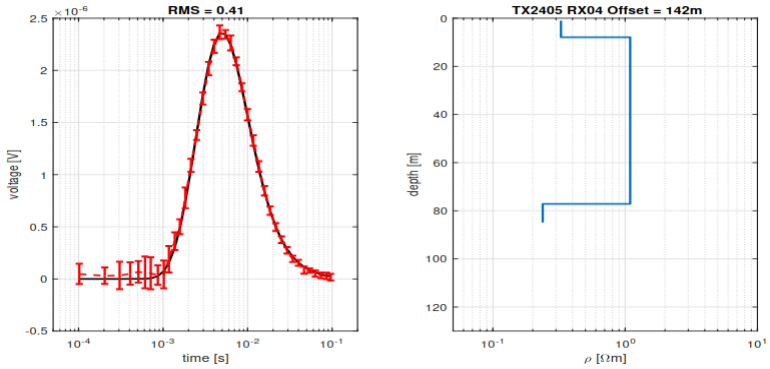

Fig. 13: Data example for processed Coil2Dipole data (red line) taken from Barnscheidt (2019). The interpretation in terms of a 1D model (right) shows that the associated response (black line, left) closely matches the processed data.

The resulting 1D model shows a good conductor at greater depth in the same area where the TEM measurements also picked up a conductive anomaly.

6.1.3. Dual Polarization – CAGEM

Measurements with the CAGEM dual polarization system were conducted during a single deployments on June 15th – 16th along four profiles with a combined length of about 10km (red line in Fig. 12). Just as during the coil experiment, unfavorable combination of wind, waves and ocean currents forced us to solely operate the system along W → E profiles. In total, the transmitter cycle (see chap. 5.1.1) was activated at a total of 331 stations. The transmitter cycle was adjusted to use 38A for both transmissions in the cycle and a longer duration of 64s instead of 16s for the longer switching cycle. Transmitted signals were recorded by twelve stationary OBEM receivers deployed along three profiles (squares in Fig. 12).

Fig. 14 shows a data example in which the signal transmitted in the two transmitter polarizations at location TX10 is shown in panels in the two lower rows and the horizontal components measured at receiver RX01 (left) and RX02 (right) is shown in panels in the upper two rows. It can be seen that first one full cycle (= 0.4s) is transmitted into first polarization direction (→ TX Ch_1) and after that one full cycle is transmitted into second polarization direction (→ TX Ch_2). This alternate style of transmitting into the two polarization directions was implemented to facilitate the later data processing in terms of rotational invariants. The time of receiver RX02 was shifted by 2s in order to ensure a correct time synchronization. A comparison of the received amplitudes shows the effect attenuation with distance for EM signals.

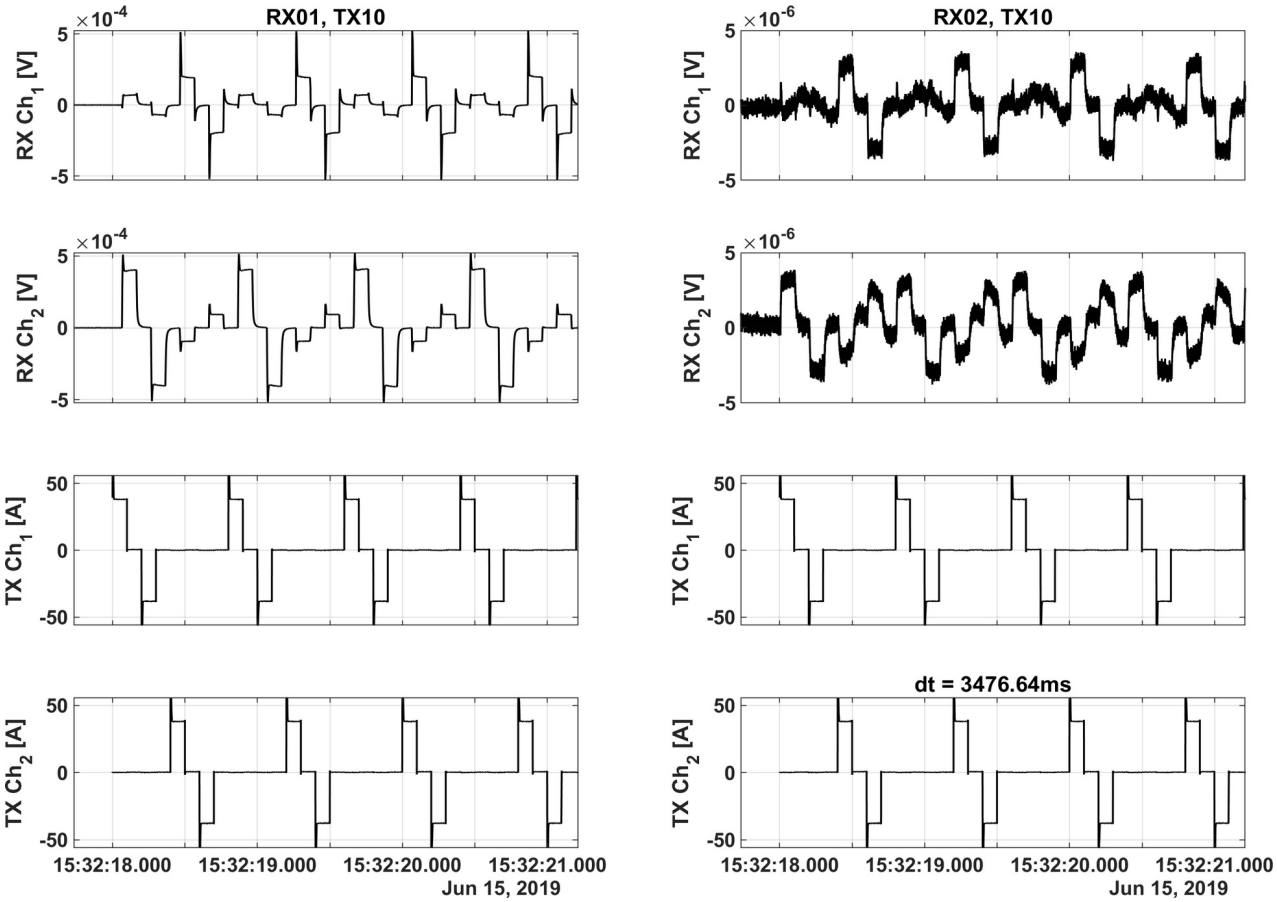

Fig. 14: Example for Dual Polarization data measured with transmitter activation at location TX10 for the OBEM receivers OBEM01 (left) and OBEM02 (right). The top two rows horizontal components measured with the receivers, the bottom two rows show the current fed into the two transmitter polarizations (note: for the the transmitter data each row shows identical data).

6.1.4. Gravity Coring

Due to the abundant coverage of gravity coring during previous cruises to the GVF (Stoffers et al., 1997; Scholten et al., 2000; Devey et al., 2002; Hölz and Martins, 2018), the five cores targeted specific predefined areas of interest (Fig. 15). Cores 01GC and 04GC, recovered 800m west of the main hydrothermal mound where the presence of conductive layers has been inferred by EM studies, do not show strong evidence for hydrothermal alteration (Fig. 16, left). Both cores show strong signs of volcanic influence, with grayish clay/silt with frequent volcanic sand lenses/pockets and pebble size volcanic clasts. The occurrence of centimeter thick layers, in both cores, of dehydrated grayish clay with scarce anhydrite/barite needles is the only indicator of possible hydrothermal events. The maximum temperature recorded in the core catcher was 5.4°C, which is still above the local deep-sea water temperature of 2°C.

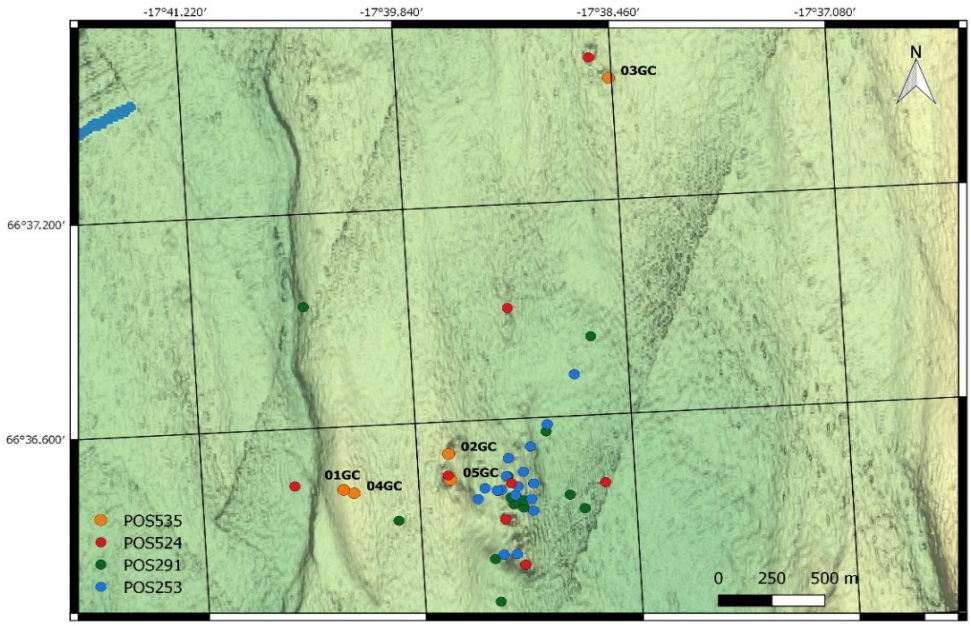

Fig. 15: Locations of sediment cores collected during cruise POS535 (2019) and during previous RV Poseidon cruises, POS524 (2018), POS291 (2001) and POS253 (1999).

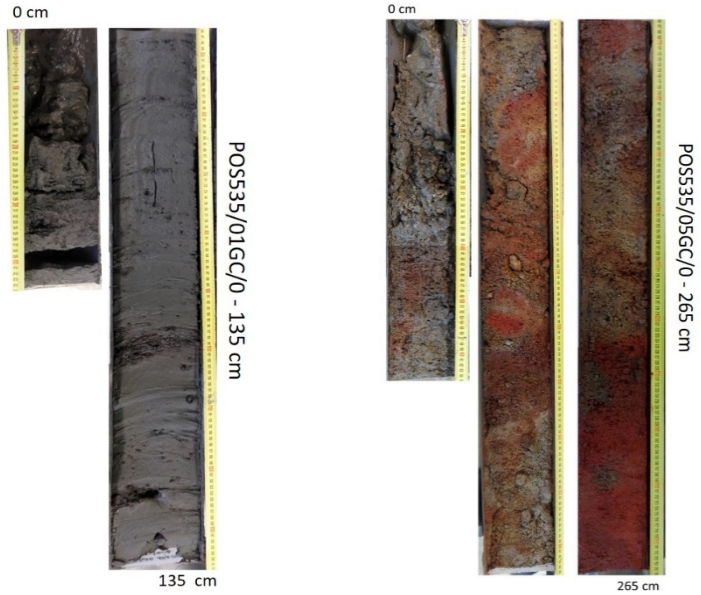

Fig. 16: Example of sediment cores from the Grimsey Hydrothermal Field.

POS535/01GC (left) contains grayish clay with frequent intercalations of sand size volcanic material. POS535/05GC (right) shows anhydrite sand debris flow sequences with frequent Fe oxidation staining.

Core 03GC was recovered 2km NNE of the main hydrothermal mound, in an attempt to find hydrothermal evidence, since high temperature gradient and high heat flow values point to the occurrence of a thermal anomaly. However, 3m of homogeneous dark greenish gray clay were recovered, with no apparent hydrothermal signal. A very similar core was already recovered in 2018 in POS524 (05GC). However, both cores show relative high temperature compared to the background (8°C in 03GC of POS535 and 7.8°C in 05GC in POS524), suggesting the presence of diffuse hydrothermal flow.

Even though the GVF has been extensively sampled, the focus in the past had been the main hydrothermal mound, leaving the bathymetric high, 250m to the W, under sampled. Therefore, two more cores were taken on this mound structure to the W (Fig. 15). Previously, this location had been surveyed shortly during a JAGO dive (station 256) on POS229 (Stoffers et al., 1997). The dive log describes a rugged topography with numerous large boulders (possibly old corroded anhydrite) which suggest that it could be a cooler or older anhydrite ridge. Core 02GC had a recovery of 233cm and is mainly homogeneous greenish clay/silt with frequent intercalations of volcanic sand and volcanic pebbles (rounded and vesicular), however at 90cm depth the clay shows signs of baking and faint channels filled with a yellowish green clay are visible. Core 05G (Fig. 16, right) is very different, being composed of anhydrite debris flows intermixed with volcanic material and clay. The anhydrite material has different grain sizes across the 300cm recovered core, as well as stained patches of yellowish, orange, brown and reddish tints. The staining is most likely related to iron oxidation and formation of Fe-(oxy)hydroxides (limonite, goethite, lepidocrocite, hematite, etc.), derived from Fe rich material such as Fe-sulfides. From 223 – 265cm depth the anhydrite debris is characterized by a strong bright to dark red stain indicating the most likely occurrence of hematite.

Station POS535	Lat Long	Water Depth	Recovery	Description
Grimsey Vent Field				
01GC	66°36.42'N 17°40.32'W	368m	135cm	Greenish grey silt with frequent sand to pebble size volcanic material. Small irregular layer of dehydrated silt with anhydrite/barite. T_{max} = 5.4°C
02GC	66°36.51'N 17°39.64'W	378m	233cm	Homogeneous dark gray clay with frequent intercalations of volcanic sand (pockets/layers) and pebbles (round & vesicular). Fragments of baked clay mixed with volcanic material. Yellowish green clay forming a channel. T_{max} = 10.2°C
03GC	66°37.54'N 17°38.48'W	383m	300cm	Homogeneous dark greenish gray clay with shell fragments. Black patches occur dispersed along the core. T_{max} = 8°C
04GC	66°36.41'N 17°40.25'W	370m	115cm	Greenish grey clay with centimetric intercalations of volcanic fragments, occasional isolated volcanic pebbles. T_{max} = 5.0°C
05GC	66°36.43'N 17°39.63'W	384m	265cm	Heterogeneous layer of anhydrite debris of diverse grain size in a clay matrix with various tones (orange, red, brown). Frequent areas of volcanic material. The deepest 20cm show an intense red color. T_{max} = 21.9°C

6.1.5. Heat Flow Probe

Heat flow measurements were taken at a total of 15 stations during three separate deployments (Fig. 17). From those, three did not have any sediment penetration and at one station no heat pulse was transmitted. A detailed compilation of the acquired data is available in Appendix 10.2 (pp. 54ff). The area of the main active hydrothermal mound, where the bubble plume can be detected in the water column (Stoffers et al., 1997), was avoided since the heat flow probe is not able to measure temperatures above 60°C.

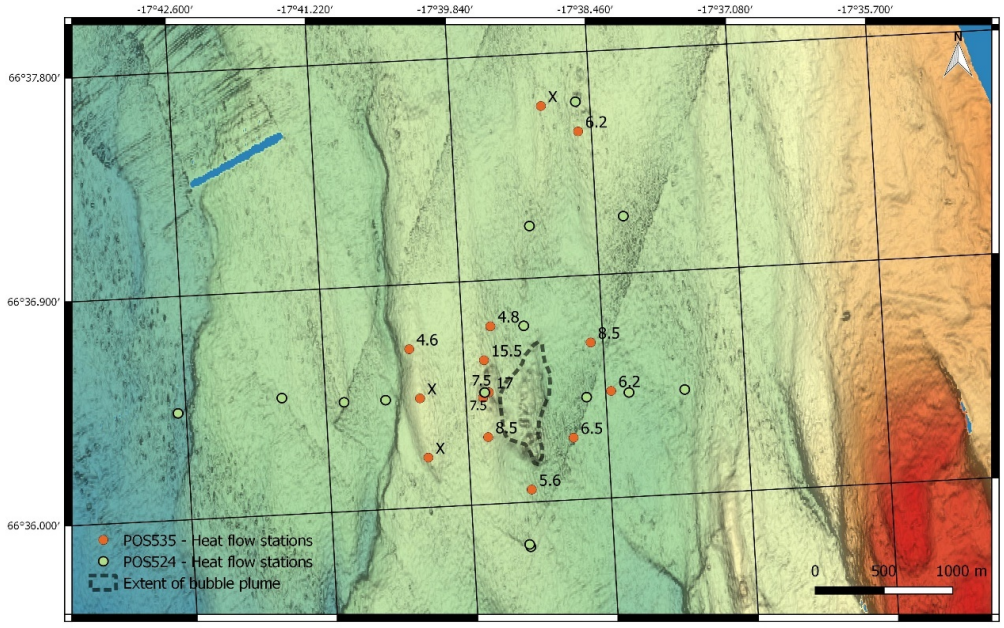

Fig. 17: Heat flow stations with maximum temperature at deepest sensor (orange dots). Crosses indicate stations with no sediment penetration. For reference purposes, heat flow stations of cruise POS524 (green dots) and the extent of the bubble plume mapped out during cruise POS229 (Stoffers et al., 1997) are also included.

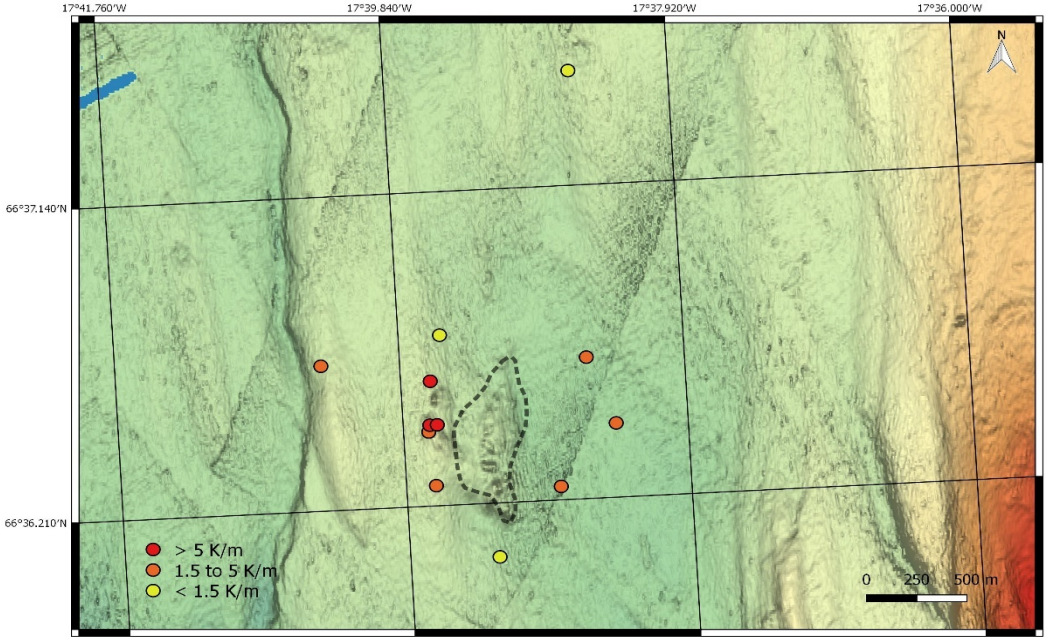

Fig. 18: Thermal gradients at GVF with extent of the bubble plume over main mound (from Stoffers et al., 1997).

The maximum temperatures (15.5°C and 17°C), which due to different sediment penetration do not necessarily relate to the same depth, are observed in the westerly mound. There, a significant temperature change from 17°C to 7.5°C is observed within a relative short distance of about 35m. A measurement of 6.2°C in the N, confirmed by temperature data collected during cruise POS524 in this area, suggests the presence of a separate thermal anomaly to the North. This separation from the main anomaly at the GVF is inferred from the fact that measurements done in between the two areas show lower temperatures (4.3°C and 3.1°C). Fig. 18 shows the thermal gradient with the highest values centered in the west mound. In the north extremity, the values decrease away from the mounds. The northernmost measurement, even though lower than the values close to the mounds, can still be considered elevated (1.32 K/m) since the normal earth geothermal gradient is 0.3K/m, reinforcing once more the presence of a thermal anomaly to the North.

Fig. 19 shows two examples for the collected heat flow data at stations with deep sediment penetration. Station HF04 (top), located in the west mound, recovered a maximum temperature of 15.5°C at a depth of 210cm, giving rise to a high thermal gradient of 5.06 K/m, since the average bottom seawater temperature is 2°C. Thermal conductivities are on average 0.82 W/mK. Station HF15 (bottom) collected data 100m east of the main hydrothermal mound and registered a maximum temperature of 6.5°C at 190cm depth. The thermal gradient is 1.75 K/m, not as high as the previous example but still significantly above the normal average geothermal gradient of 0.3 K/m. Thermal conductivity are on average 0.69 W/mK.

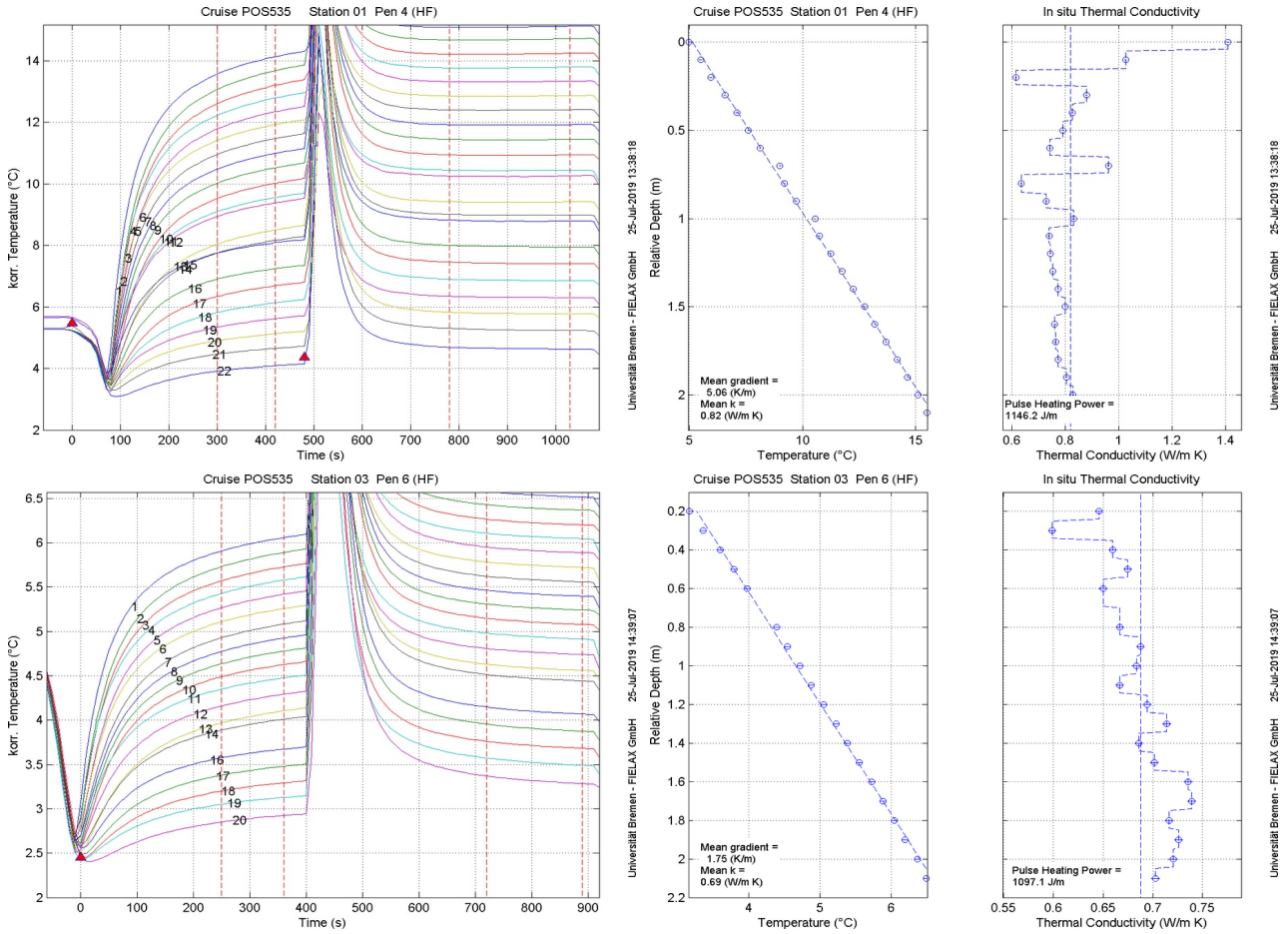

Fig. 19: Measurements at stations HF04 (top) and HF15 (bottom) with temperature data recovered from 22 and 19 sensors, respectively. Plots show transient temperatures measured with sensors at various depth (left), the near steady state temperatures shortly before transmission of the heat pulse (middle), and the derived thermal conductivity (right).

6.1.6. CTD

For the experiment at the Grimsey Vent Field (GVF) receiver OBEM12, which is located in the NW corner of the receiver array, was equipped with the stationary CTD. It was deployed on 11/06/2019 at 17:43 to the NW corner of the receiver array and collected data during the 87.5 hours that it remained on the seafloor.

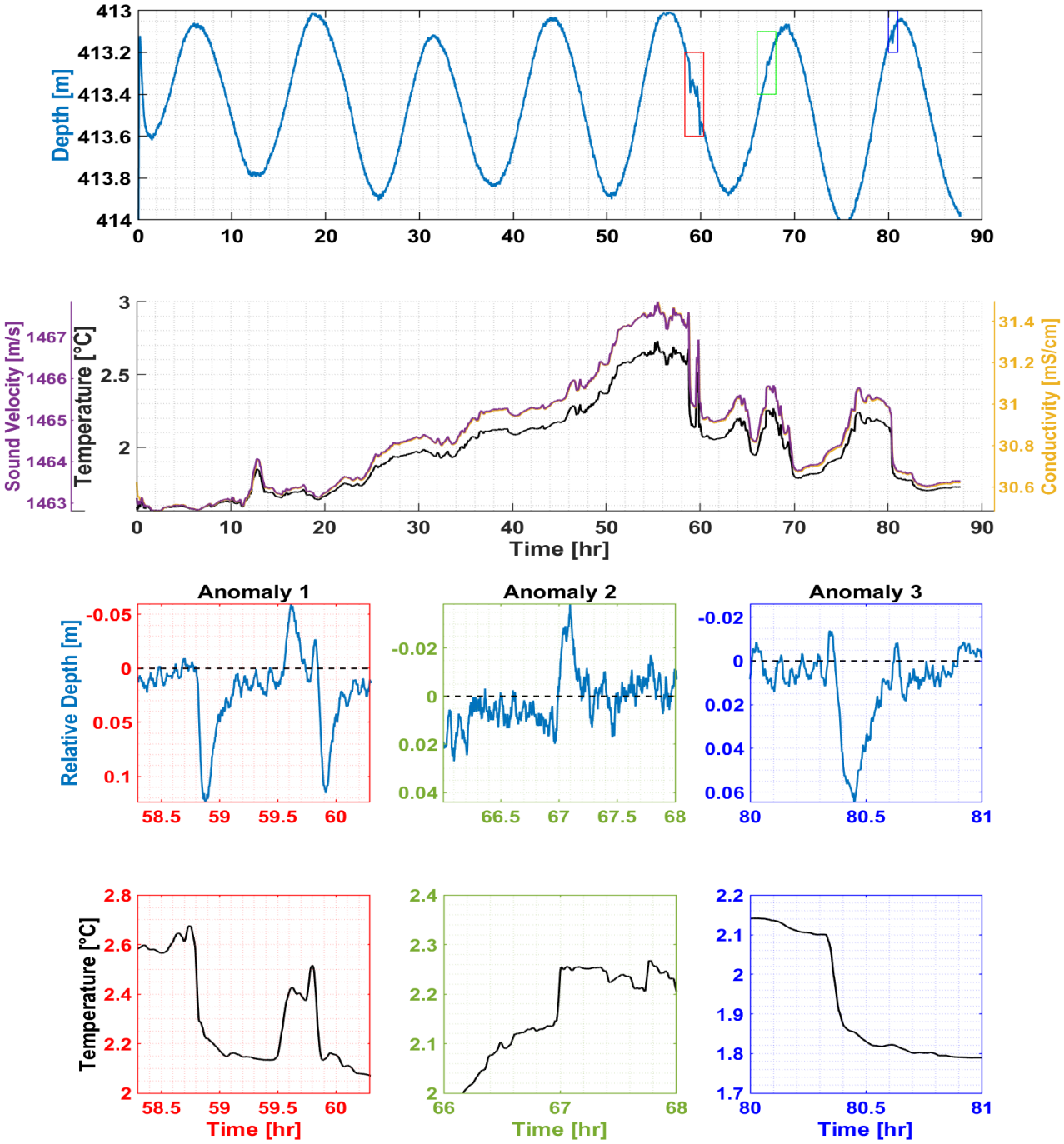

Fig. 20: CTD data from device mounted to OBEM12 at GVF, with depth (top row, converted from pressure) conductivity, temperature and sound velocity (2nd row: yellow, blue and purple line, respectively). After removal of the tidal trend in the pressure signal, three main time ranges with anomalies are observed in the pressure data, which mark significant fast vertical movements of the station (3rd row). These movements strongly correlate with significant changes in the other parameters, exemplarily depicted for the temperature in the bottom row.

The display of collected data in Fig. 20 shows strong tidal variations in pressure (converted to depth in top row) with some small anomalies (colored boxes). For temperature, conductivity and sound velocity (2nd row) the measured variations greatly exceed the levels one would normally expect for the given time scale. Temperature increases of more than 1.0°C within less than 48h and sudden drops of temperature of around 0.5°C within minutes (@60h) are quite remarkable. Similar temperature variations were also recorded by the internal temperature sensors of all deployed OBEMs, thus, confirming the stationary CTD data. After removal of the sinusoidal tidal trend in the pressure signal (3rd row), rapid changes are evident at 58.8hr, 59.5hr, 59.8hr, 67hr, and 80.4hr, which coincide with rapid changes in temperature (bottom row), conductivity, and sound velocity. Each of these anomalies last 2-7min with the depth changing by up to 12cm, temperatures by approximately 0.1-0.4°C, conductivity by approximately 0.3mS/cm, and the sound velocity by 1-2 m/s. A flow of cooler water from above, or heated water from below the OBEM would not have the force to translate the device by that distance.

The observed variability poses the question, if it is due to changes in the activity of the hydrothermal field or rather due to regional ocean bottom currents.

In addition to the stationary CTD attached to OBEM12, one probe was put onto the mobile MARTEMIS system, allowing a sampling of the sea water about the entire survey site. The measured properties (no figure) show a strong dependency on the depth of the probe within the water column. This in combination with the strong temporal drift at the GVF (compare Fig. 20) precludes the identification of anomalies due to hydrothermal activity before further data processing.

6.2. Öxarfjörður & Skjálfandadjúp

6.2.1. Gravity Coring

Two new potential hydrothermal locations, Öxarfjörður and Skjálfandadjúp, where cone shaped or chimney shaped features were detected on multi-beam surveys were sampled with five gravity cores.

At Öxarfjörður (Fig. 21, top), 4 to 5 features, 15 – 20m high and about 400m long with an NNE trend, seemed the most likely target for hydrothermal systems due to its similarity to the GVF (left). However, the three recovered cores 06GC, 07GC and 08G (right), all with less than 1m recovery, show no evidence of hydrothermal activity, but instead strong volcanic influence with grayish clay intermixed with ubiquitous volcanic sand size debris and pebbles. Temperatures collected in the core catcher varied from 8.2 – 9.7°C.

At Skjálfandadjúp (Fig. 21, bottom), two possible chimneys with an NNE-SSW trend, 15 – 20m high, at a depth of 190 – 200m were detected by multibeam data (left). Two cores 09GC and 10GC had a recovery of 80 and 61cm, respectively (right). Core 09GC is entirely volcanic, with the first 50cm showing coarse volcanic material intermixed with grayish clay. A boulder (8×4cm) was identified as a tuff. The deepest part of the core is very homogeneous and finer grained with scarce volcanic sand patches and shell fragments. The first 25cm of core 10GC are composed of very coarse and angular volcanic material with a reddish/orange tint (pyroclastic material?), however the last 35cm show evidence of hydrothermal events. Grayish clay/silt is intermixed with sand size anhydrite domains. Some areas of the clay layers are dehydrated and show rounded alteration zones with distinct colors (light gray halo surrounding a yellowish center). Temperatures in the core catcher were measured at 9.1°C after both recoveries of the gravity core.

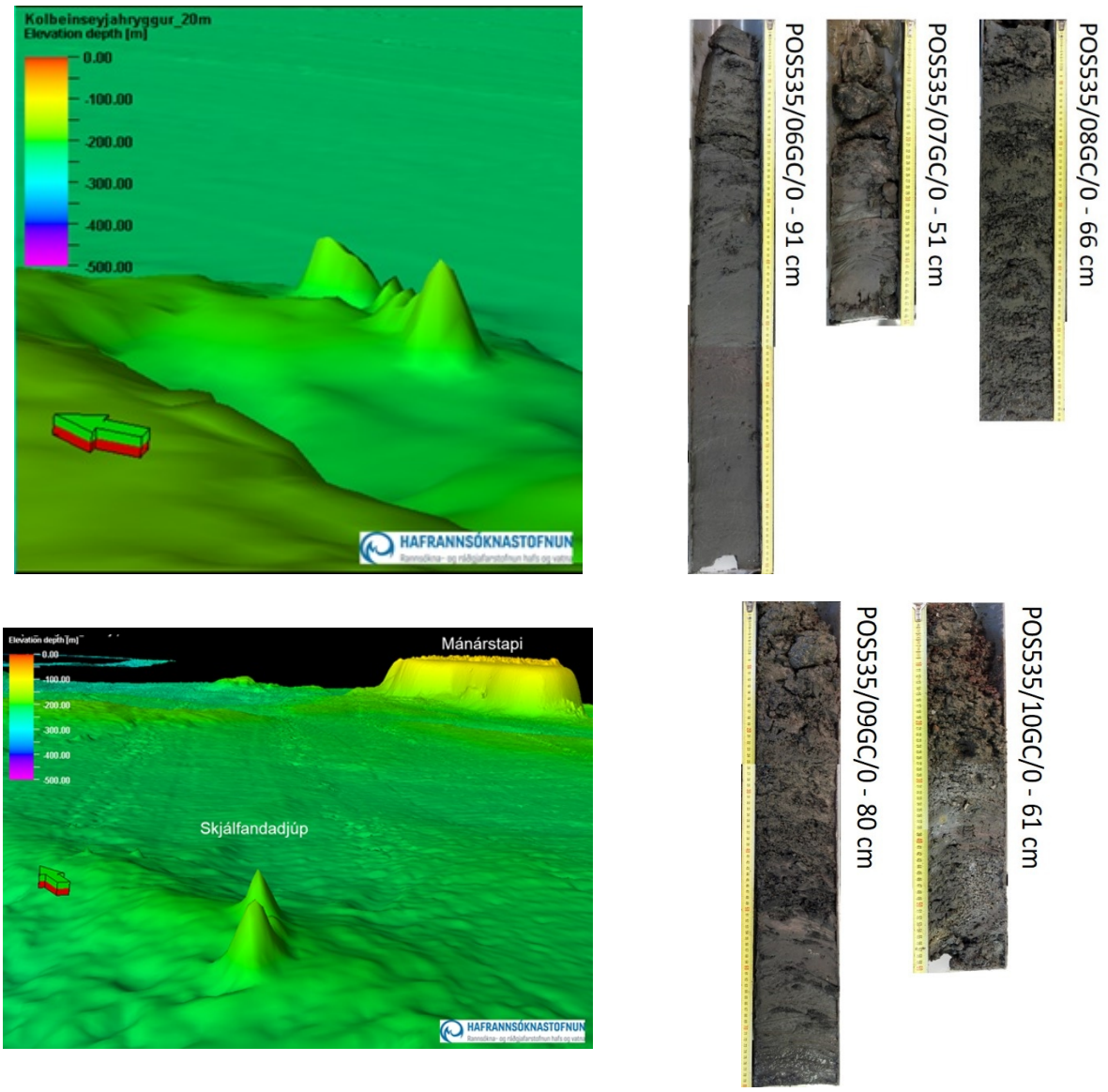

Fig. 21: Gravity coring results from Öxarfjörður (top) and Skjálfandadjúp (bottom) showing the mound features (left) and the collected cores (right). Bathymetry was provided courtesy of Ögmundur Erlendsson and colleagues from ISOR.

Station	Location	Water Depth	Recov-ery	Description
Öxarfjörður				
POS535/06GC	66°21.53'N 16°55.45'W	189m	91cm	Homogeneous greyish clay/silt with intercalations of volcanic sand lenses and volcanic pebbles. T_{max} = 9.7°C
POS535/07GC	66°21.42'N 16°55.43'W	209m	51cm	Volcanic sand size debris sometimes intermixed with greyish silt. Occasional volcanic cobbles. T_{max} = 8.2°C
POS535/08GC	66°21.53'N 16°55.42'W	188m	66cm	Heterogeneous mixture of greyish clay with frequent layers/ lenses of coarse volcanic material.
Skjálfandadjúp				
POS535/09GC	66°26.48'N 17°24.16'W	202m	80cm	Coarse volcanic debris intermixed with clay/silt. The pebbles are angular in shape, dark and reddish in colour. T_{max} = 9.1°C
POS535/10GC	66°26.54'N 17°24.13'W	185m	61cm	Coarse and angular volcanic debris on top, with anhydrite sand and greyish layer and altered clay. T_{max} = 9.1°C

6.3. Loki's Castle

The second site that was visited during the cruise was Loki's Castle, a much deeper hydrothermal system located at approximately 2335m below sea level.

6.3.1. MARTEMIS Coil

Measurements with the MARTEMIS coil system were conducted during a single deployment from June 23rd to 24th along three profiles with a combined length of about 6.3km (Fig. 22). Due to an unfavorable combination of wind, waves and ocean currents, it was only possible to operate the system along NW → SE profiles and not along a continuous snake line profile, which significantly slowed down operations since the device had to be transferred to the NW without taking any measurements during the transit. In total, the transmitter cycle (see chap. 5.1.1) was activated at a total of 600 stations along the profiles (white dots in Fig. 22).

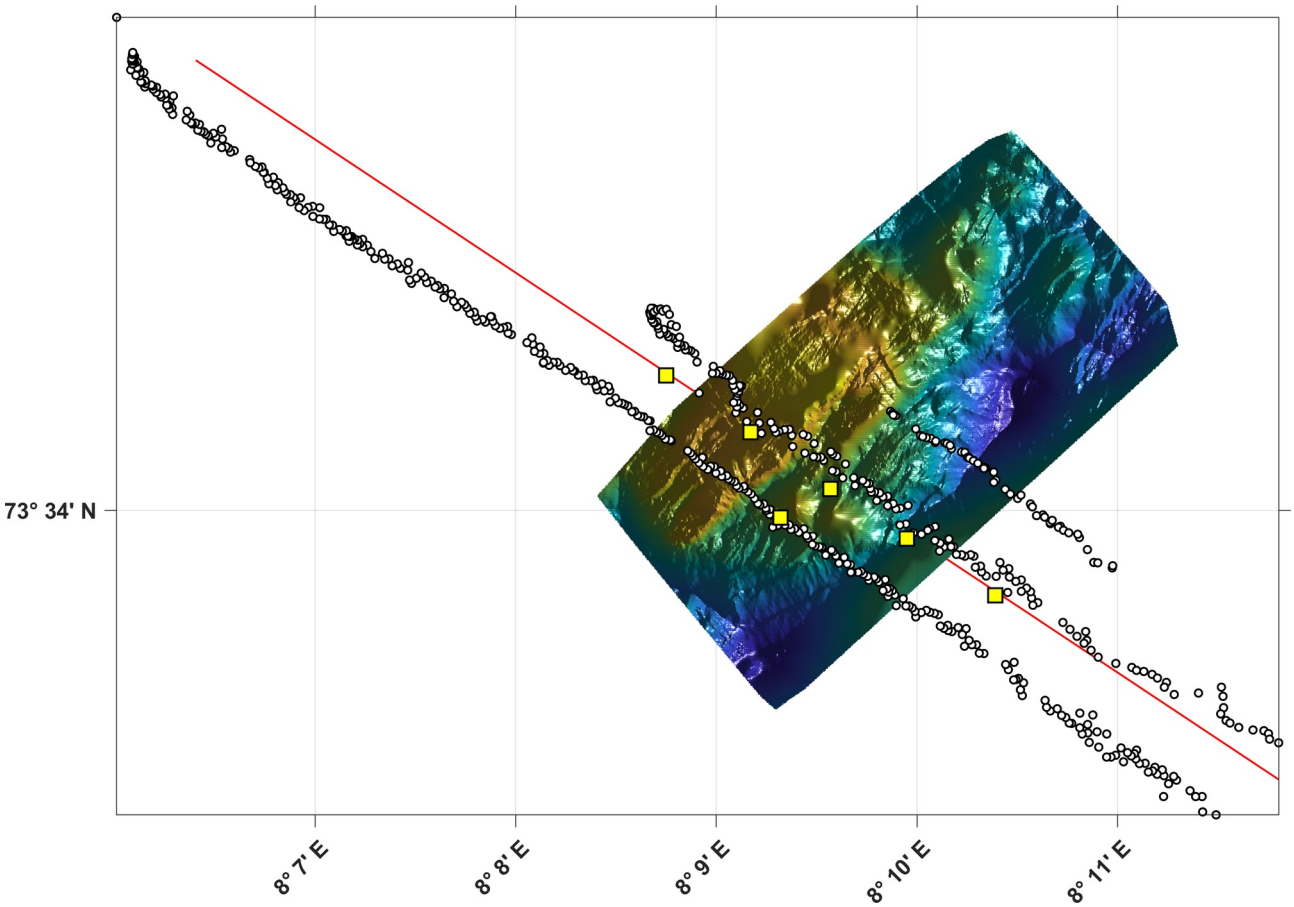

Fig. 22: Transmitter stations of MARTEMIS system along three profiles during TEM experiments at the Loki's Castle (white dots). Drop positions of the OBEM receivers are marked with yellow squares. Final positions on the seafloor will most likely be shifted to the NNW. The red line marks the profile line of the CSEM experiment by Johansen et. Al (2019, see also Fig. 5), which was also used for the Dual Dipole experiment (s. chap. 6.1.3). Please note that the displayed high resolution bathymetry – provided by courtesy of Anna Lim (NTNU) – might be shifted by a few 10s of meters due to a problem with the map projection which still needs to be fixed.

For a recent informal workshop held at the University of Bergen (Norway), we have produced a first interpretation of the TEM data along the main profile line in terms of stitched 1D models. Models shows conductive anomalies in the vicinity of the two hydrothermal mounds at Loki's Castle, which coincide with temperature anomalies evident in the CTD data (see chapter 6.3.4). The interpretation seems to indicate that the conductive features are directly at the surface and rather thin. However, it should be stressed that this interpretation is very preliminary.

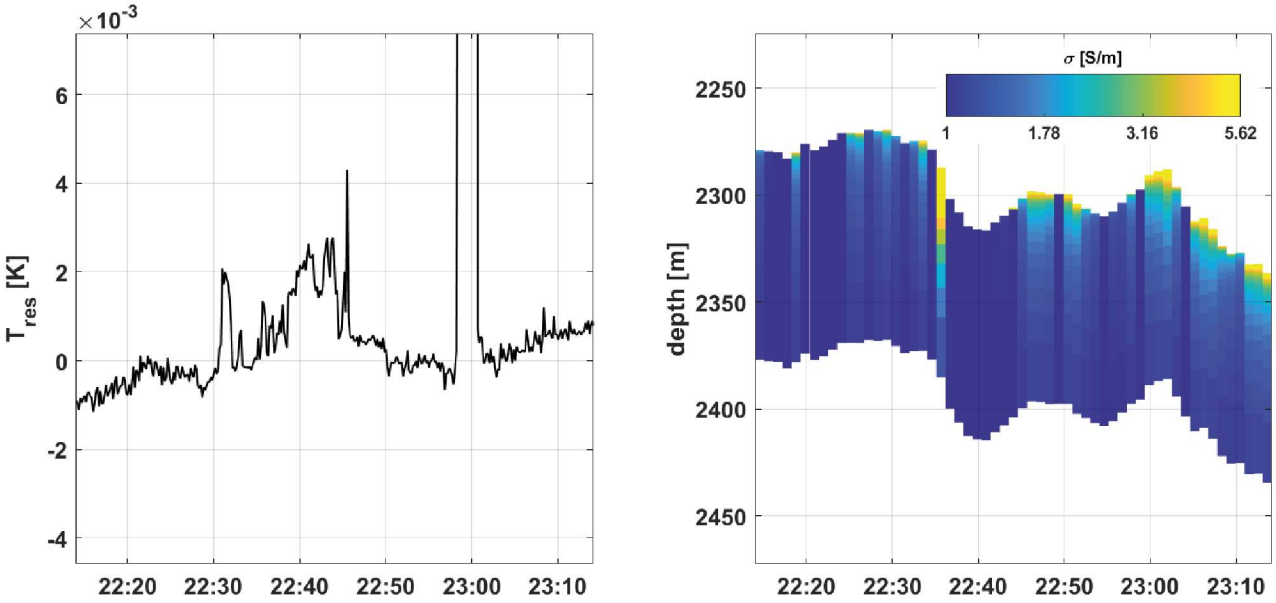

Fig. 23: Drift corrected temperature from CTD measurements (left) and stitched 1D models from TEM interpretation (right). The two active mound at Loki's Castle were passed at approximately 22:28h and 23:02h.

6.3.2. Dual Polarization – CAGEM

Measurements with the CAGEM dual polarization system were conducted during a deployment on June 24th along a single profiles with a length of about 2km (Fig. 22). The transmitter cycle (see chap. 5.1.1) was activated at a total of 91 stations along the profile.

6.3.3. Gravity Coring

At Loki's Castle (Fig. 24), the gravity corer was deployed four times with recovery in two cores 11GC (270cm) & 14GC (300cm) taken within the depression between the mounds. These cores contain heterogeneous debris sequences made up of fragments of fibrous anhydrite, clumps of botryoidal talc, abundant small chimney fragments with altered outer part and inner channels covered by sulfides as well as disseminated sulfides in a black clay matrix (Fig. 25C). The average temperature measured in the core catcher was 4.5°C.

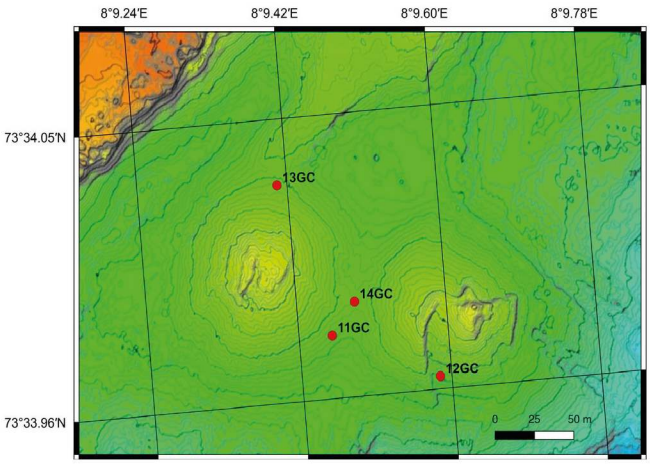

Fig. 24: Location of sediment cores collected at Loki's Castle. Geo-referenced bathymetry image from Brekke (2012).

In core 11GC, there is a 40cm layer (at 125cm depth) of heterogeneous greenish clay layer showing a gradation in color from greenish yellow to greenish dark brown with talc/anhydrite clasts. At the deepest part of the core, chimney fragments were collected with oxidized surface where dispersed native copper crystal occurs with dendritic growth (Fig. 25, left). The occurrence of native cooper is not very common in hydrothermal settings, however, it was already identified as small grains in sediment up to 300µm in length (Devok et al., 1999) and as irregular grains up to 50µm inside amorphous silica (Hannington et al., 1988) at the TAG hydrothermal field and in one hand specimen collected by TV-grab at Logatchev hydrothermal field (Kuhn, 2004). Its origin can be related to supergene alteration of primary Cu-Fe-sulfides and subsequent deposition in adjacent sediments or rocks (Hannington et al., 1988; Dekov et al., 1999). Cores 12GC and 13GC deployed at the mounds flanks only collected scarce gravel material in the core catcher.

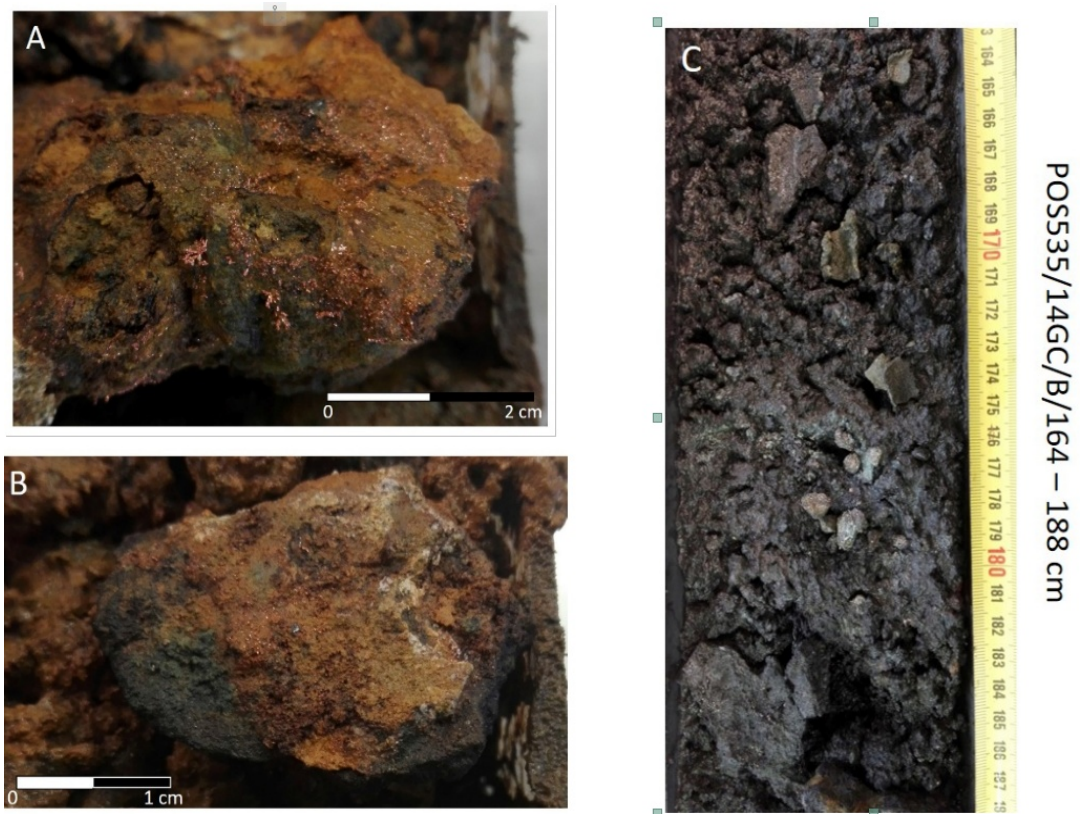

Fig. 25: Detail photos of cores recovered at the hydrothermal field Loki's Castle. Altered chimney fragments with dispersed native cooper crystals, recovered on core 11GC at 265cm depth (A and B). Detailed section of core 14GC, where fragments of massive sulfide chimneys can be identified along the core (C).

Station	Location	Water Depth	Recovery	Description
Loki's Castle				
POS535/11GC	73°33.98'N 8°09.46'E	2200m	267cm	Heterogeneous sediment with black clay, clumps of talc, anhydrite, disseminated sulfides and chimney fragments. T_{max} = 4.7°C
POS535/12GC	73°33.96'N 8°09.58'E	2431m	0cm	Empty core, with scarce anhydrite and clay clumps and oxidized chimney fragments in the core catcher.
POS535/13GC	73°34.03'N 8°09.41'E	2410m	0cm	Empty core, with large oxidized chimney fragments mixed with smaller anhydrite clumps and volcanic material in the core catcher.
POS535/14GC	73°33.99'N 8°09.49'E	2401m	300cm	Heterogeneous debris sequence made up of fibrous anhydrite clumps, botryoidal talc, disseminated sulfides and abundant small chimney fragments. T_{max} = 4.5°C

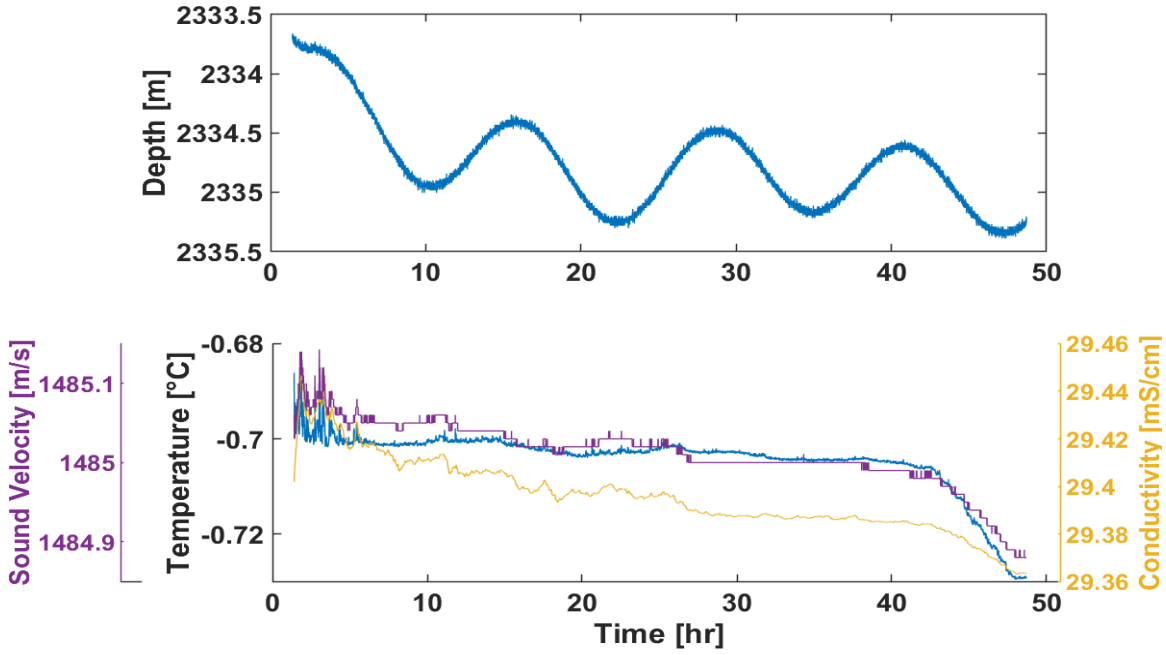

Fig. 26: Measurements of stationary CTD attached to OBEM01 at Loki's Castle (time relative to deployment). Please note the much smaller scale values when comparing to measurements at the GVF (Fig. 20).

6.3.4. CTD

The stationary CTD was attached to receiver OBEM01, which after being deployed free falling from the ship, reached the seafloor on June 23rd around 7:57h and remained on the seafloor for about 50h. Measurements in Fig. 26 show minimal changes in all parameters, as could be expected at such a water depth at some distance from the coast.

The mobile CTD attached to the MARTEMIS system collected data during the two EM surveys. These spanned from 18:30h on June 23rd to 11:20h on June 24th (TEM measurements), and 21:59h on June 24th to 03:11h on the 25th, (CAGEM experiment). A full display of the data acquired during the two experiments can be found in the appendix.

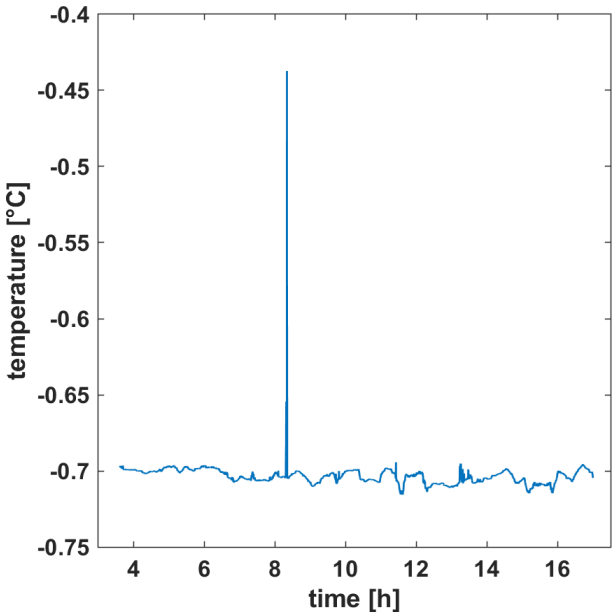

Fig. 27: Temperature of mobile CTD probe during MARTEMIS experiment at Loki's Castle.

Significant changes which are not related to the elevation of the system above the seafloor but which rather seem to be related to hydrothermal activity are only evident in the CTD data acquired during the MARTEMIS experiment. Fig. 27 shows a sudden increase in temperature, which spanned 30 seconds at 8.3 hours since 18:30 on June 23rd. Much smaller peaks are also evident at 11.4h and several times between 13.2 – 13.5h. Especially for the first spike at 8h it is evident that the active site was passed, for the other spikes the further analysis of the data still needs to be carried out.

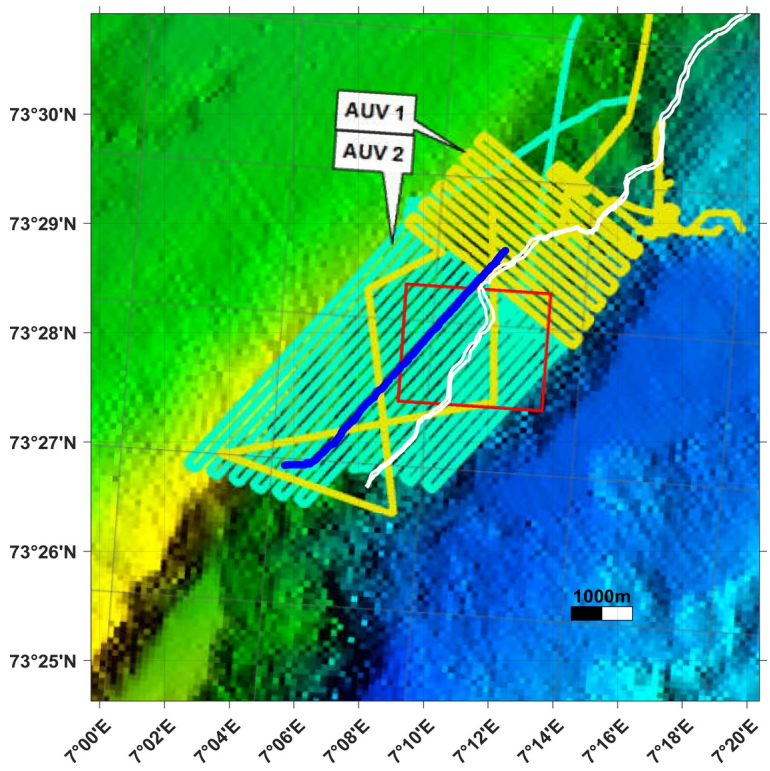

Fig. 28: Transmitter profile (blue line) of MARTEMIS system during TEM experiment. Since the USBL positions are scattered significantly we display actually display the profile line by using the ship track during the experiment duration of the experiment. White lines show the 2600m and the 2620m contour lines marking the maximum depth which could be reached with RV Poseidon's winch cable.

For reference purposes we display Fig. 23 from the MarMine Cruise report (Ludvigsen et al., 2016; changed), which shows AUV tracks where magnetic data was collected (compare Fig. 29; red rectangle shows approximate outline of Fig. 28 in that report).

6.4. Mohn's Treasure

6.4.1. MARTEMIS Coil

Measurements with the MARTEMIS coil system were conducted during a single deployment on June 26th as final experiment of the cruise along a single profile with a length of about 5km (blue line in Fig. 28). In total, the transmitter cycle (see chap. 5.1.1) was activated at a total of 586 stations along the profile. Isohypses of 2600m and 2620m (white lines) show the maximum depth that could be reached with the available cable length of RV Poseidon's winch cable. A comparison with the magnetic data collected during the MarMine cruise (Ludvigsen et al., 2016; here shown in Fig. 28 & Fig. 29) shows that the magnetic anomaly, which potentially marks the hitherto unknown site, is further down the slope at a depth of approximately 2700 – 2800m, thus, out of reach for the MARTEMIS system. Therefore, it is possible that the TEM experiment will not have picked up any potential conductivity anomaly of the covered site at Mohn's Treasure.

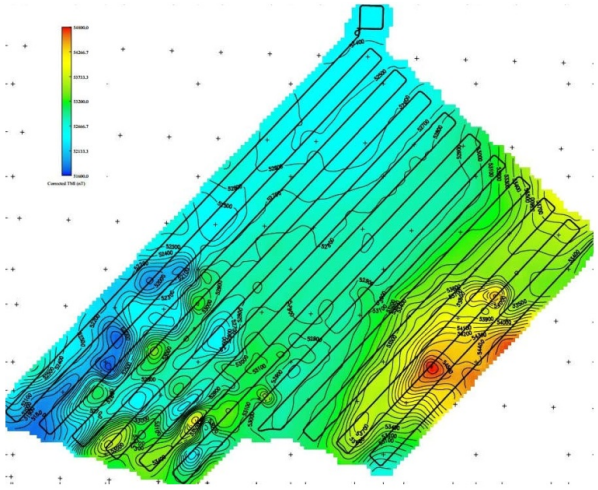

Fig. 29: Magnetic field intensity (Fig.44 from MarMine cruise report; Ludvigsen et al., 2016). Track lines shown here are the same as turquoise track lines in Fig. 28.

6.4.2. Gravity Coring

At Mohn's Treasure a gravity core was attempted where a positive magnetic anomaly high was detected during the MarMine research cruise (Ludvigsen et al., 2016). The recovery was restricted to anhydrite and small sulfide chimney fragments found in the core catcher.

Station	Location	Water Depth	Recovery	Description
Mohn's Treasure				
POS535/15GC	73°27.15'N 7°11.37'E	2835m	0cm	Empty core, with diverse chimney fragments (altered, oxidized, sometimes with sulfides and anhydrite) in the core catcher.

6.4.3. CTD

CTD measurements were acquired along a single profile with the MARTEMIS system. No stationary CTD was used since no OBEMs were deployed. Observed variations in the measured CTD parameters are very small and mostly seem to be related to the hoisting of the system.

7. Data and Sample Storage and Availability

In Kiel a joint data management team of GEOMAR and Kiel University organizes and supervises data storage and publication by marine science projects in a web-based multi-user system. The geophysical data that has been acquired will be for use of GEOMAR scientists and collaborators only for the first phase and can be made available to other researcher by request to Dr. Sebastian Hölz (shoelz@GEOMAR.de) or Dr. Sofia Martins (smartins@geomar.de). All metadata are immediately available publicly via the GEOMAR portal (https://portal.GEOMAR.de/metadata/leg/show/348615).

In addition the portal provides a single downloadable KML formatted file (portal.GEOMAR.de/metadata/leg/kmlexport/348615) which retrieves and combines up-to-date cruise related information, links to restricted data and to published data for visualization e.g. in Google Earth.

8. Acknowledgments

We would like to thank the crew of *R/V Poseidon* for their excellent support during cruise POS535, especially Captain M. Günther and the bridge for patient help in all organizational matters and excellent ship handling, Bosun Frank Schrage and his deck crew for helping us to optimize the deployment procedure of the MARTEMIS system and handling of our gear, and finally the crew down in the engine for their support. We would also like thank the directorate of GEOMAR, who granted substantial financial support for the cruise.

The permission to work in Icelandic boundary waters was generously granted by the Icelandic Ministry for Foreign Affairs (Ref.: UTN18120075/34.R.423). We would also like to thank Geir Hagalínsson from NTE for granting us access to the working area, for which NTE hold an exclusive license for the exploration of hydrothermal energy. Bjarne Richter from ISOR is acknowledged for sharing information on marine hydrothermal systems around Iceland, which were really helpful in planing the current cruise as well as applying for future cruises. Also, Pall Bergmann Reynisson provided us with bathymetric data, which are an essential part in the operation of our systems close to the seafloor. The provided ship-based multibeam bathymetry was collected by the Marine Research Institute (MRI) in Reykjavik, now the Marine & Freshwater Research Institute (MFRI) (https://www.hafogvatn.is/) and University of Iceland (https://www.hi.is/) on board R/V Árni Friðriksson during cruises in summer 2002 and 2004 using the onboard Kongsberg EM300 multibeam echosounder. Information about two new sites with potential hydrothermal activity (Öxarfjörður & Skjálfandadjúp) was provided to us by courtesy of Ögmundur Erlendsson and colleagues from ISOR.

The permission to work in Norwegian boundary waters was generously granted by the Norwegian Petroleum Directorate (NPD, Licence no.: 709/2019) in consent with the Norwegian Directorate of Fisheries. In the preparation of our research at Loki' Castle we have received numerous support by Norwegian colleagues, which we also would like to acknowledge. Steinar Ellefmø and Anna Lim (both NTNU Trondheim) provided us with bathymetric data from the area, which was useful in planing and carrying out our experiments. Jan Stenløkk, Andreas Bjørnestad, Dag Bering and other colleagues from the NPD provided us with bathymetric data and additional information to an additional working area and also granted permission to work in Norwegian boundary waters. Finally, Thibaut Barreyre, Steffen Leth Jørgensen and other

colleagues from the University Bergen adjusted and coordinated their cruise schedule with ours to avoid simultaneously working in the same area. This greatly helped us to meet our tight cruise schedule.

9. References

Ármannsson, H., 2016: The fluid geochemistry of Icelandic high temperature geothermal areas. Applied Geochemistry, 66, 14 – 64.

Atkins, D. & Audunsson, H., 2013: Exploration Techniques for Locating Offshore Geothermal Energy Near Iceland. Proceedings of the 38. Workshop on Geothermal Reservoir Engineering, Stanford University, 11-13.2.2013, SGP-TR-198.

Barnscheidt, K.C. (2019): Qualitative und quantitative Auswertung eines neuartigen marinen elektromagnetischen ”Coil2Dipole” Experiments. Bachelor thesis submitted to the Christian-Albrechts-Universität zu Kiel, 71pp.

Baumberger, T., Früh-Green, G.L., Thorseth, I.H., Lilley, M.D., Hamelin, C., Bernasconi, S.M., Okland, I.E. & Pedersen, R.B. (2016): Fluid composition of the sediment-influenced Loki's castle vent field at the ultra-slow spreading Arctic Mid-Ocean ridge. Geochimica et Cosmochimica Acta, 187, 156-178.

Beaulieu, S.E., Baker, E.T., German, C.R., 2015: Where are the undiscovered hydrothermal vents on oceanic spreading ridges? Deep Sea Research Part II,121, 202–212.

Boschen, R.E., Rowden, A.A., Clark, M.R. & Gardner, J.P.A., 2013: Mining of deep-sea seafloor massive sulfides: A review of the deposits, their benthic communities, impacts from mining, regulatory frameworks and management strategies. Ocean and Coastal Management, 84, 54–67.

Botz, R., Winckler, G., Bayer, R., Schmitt, M., Schmidt, M., Garbe-Schönberg, D., Stoffers, P. & Kristjansson, J.K., 1999: Origin of trace gases in submarine hydrothermal vents of the Kolbeinsey Ridge, north Iceland. EPSL, 171, 83 – 93.

Brekke, H. 2012. International Seabed Authority Workshop. Non-living Resources of the OCS. [Accessed April 2019]. https://ran-s3.s3.amazonaws.com/isa.org.jm/s3fs-public/documents/EN/Workshops/2012/HBrekke-1.pdf

Devey, C.W., shipboard scientific party, 2002. Hydrothermal studies of Grimsey Field, volcanic studies of Kolbeinsey Ridge. Cruise Report POS 291 of R/V Poseidon, University of Bremen. 42 pp.

Devok, V.,Damyanov, Z., Kamenov, G., Bonev, I. & Bogdanov, K. 1999. Native copper and a-copper–zinc in sediments from the TAG hydrothermal field (Mid-Atlantic Ridge, 26°N): nature and origin. Marine Geology, 161, 229 – 245.

German, C.R., Petersen, S. & Hannington, M.D. (2016): Hydrothermal exploration of mid-ocean ridges: where might the largest sulfide deposits be forming? Chemical Geology, 420, 114-126.

Gudmundsdóttir, E.R., Eiríksson, J. & Larsen, G., 2011: Identification and definition of primary and reworked tephra in Late glacial and Holocene marine shelf sediments off North Iceland. J. Quat. Sci., 26, 589–602.

Hannington, M., Herzig, P., Stoffers, P., Scholten J., Botz, R. Garbe-Schönberg, D., Jonasson, I.R., Roest, W. & Shipboard Scientific Party, 2001: First observatons of high-termparature submarine hydrothermal vents and massive anhydrite deposits off the north coast of Iceland. Marine Geology, 177, 199 – 220.

Hannington, M.D., Jamieson, J., Monecke, T. & Petersen, S., 2010: Modern Sea-Floor Massive Sulfides and Base Metal Resources: Toward an Estimate of Global Sea-Floor Massive Sulfide Potential. Economic Geology Special Publication, 15, 317–338.

Hannington M., Jamieson, J., Monecke, T., Petersen, S. & Beaulieu, S., 2011: The abundance of seafloor massive sulfide deposits. Geology, 39, 1155-1158.

Hannington, M., Thompson, G., Rona, P., Scott, S. 1988. Gold and copper in supergene sulphides from the Mid-Atlantic Ridge. Nature, 333, 64-66.

Hartmann, A. & Villinger, H. 2002. Inversion of marine heat flow measurements by expansion at the temperature decay function. Geophys. J. Int., 148, 628 – 636.

Hölz, S., Swidinsky, A., Jegen, M. & Bialas, J., 2015: The use of rotational invariants for the interpretation of marine CSEM data with a case study from the North Alex mud volcano, West Nile Delta. Geophysical Journal International, 1, 224-245.

Hölz, S. & Martins, S., 2018. RV POSEIDON Fahrtbericht / Cruise Report POS524 - GrimseyEM: Geophysical and geological investigations in the vicinity of the Grimsey Hydrothermal Field offshore Northern Iceland for the assessment of the geothermal potential and the exploration for potential mineralizations within the seafloor, Reykjavik (Iceland) – Bergen (Norway), 7.6 - 26.6.2018. GEOMAR Report, N. Ser. 044. GEOMAR Helmholtz-Zentrum für Ozeanforschung, Kiel, Germany, 69 pp.

Hyndman, R.D., Davis, E.E., and Wright, J.A., 1979. The measurement of marine geothermal heat flow by a multipenetration probe with digital acoustic telemetry and in situ thermal conductivity, Marine Geophysical Res., 4, 181–205.

IMO (2018a): Icelandic Met Office - 400 earthquakes detected at Grímsey island in last 12 hours. WWW electronic publication, ice-landmonitor.mbl.is/news/nature_and_travel/2018/02/15/400_earthquakes_detected_at_grimsey_island_in_last_, accessed 26.3.18.

IMO (2018b): Icelandic Met Office - Seismic swarm near Grímsey: update 15:00, 19 February. WWW electronic publication, accessed 26.3.2018, http://en.vedur.is/about-imo/news/seismic-swarm-near-grimsey-update-15-00-19-february.

Iturrino, G.J., Davis, E., Johnson, J., Groeschel-Becker, H., Lewis, T., Chapman, D. & Cermak, V., 2000: Permeability, electrical and thermal properties of sulfide, sedimentary and basaltic units from the Bent Hill area of Middle Valley, Juan de Fuca ridge. Proceedings of the ODP, Scientific Res., Vol. 169.

Johansen, S.E., Panzner, M., Mittet, R., Amundsen, H.E.F, Lim, A., Vik, E. Landrø M. & Arntsen, B.: Deep electrical imaging of the ultraslow-spreading Mohns Ridge. Nature Research Letter, vol. 567, pp. 379 – 383, 2019.

Kowalczuk, P.B., Snook, B., Kleiv, R.A. & Aasly, K. (2018): Efficient extraction of copper and zinc from seafloor massive sulphide rock samples from the Loki's Castle area at the Arctic Mid-Ocean Ridge. Minerals Engineering, 115, 106-116.

Kuhn, T., 2004. Cruise report RV Meteor M060/3 - HYDROMR I - Mineralogical, geochemical, and biological investigations of hydrothermal systems on the Mid-Atlantic Ridge between 14°45'N and 15°05'N (No. 03-04). Leitstelle Meteor, Hamburg.

Lackschewitz, K.S., Botz, R., Garbe-Schönberg, D., Scholten, J. & Stoffers, P., 2006: Mineralogy and geochemistry of clay samples from active hydrothermal vents off the north coast of Iceland. Marine Geology, 225, 177 – 190.

Lister, C.R.B., 1979. The pulse-probe method of conductivity measurement. Geophys. J. R. Astr. Soc., 57, 451–461.

Ludvigsen, M., Aasly, K., Ellefmø, S., Hilário, A., Ramirez-Llodra, E., Søreide, F., Falcon-Suarez, I., Juliani, C., Kieswetter, A., Lim, A., Malmquist, C., Nornes, S., Paulsen, E., Reimers, H., Sture, Ø. . 2016. NTNU Cruise reports 2016 no 1 - MarMine cruise report Arctic Mid-Ocean Ridge 15.08.2016 - 05.09.2016.

Magnúsdóttir, S., Brandsdóttir, B. Driscoll, N. & Detrick, R., 2015: Postglacial tectonic activity within the Skjálfandadjúp Basin, Tjörnes Fracture Zone, offshore Northern Iceland, based on high resolution seismic stratigraphy. Marine Geology, 367, 159 – 170.

Monecke, T., Petersen, S., Hannington, M.D., Grant, H. & Samson, I., 2016: The Minor Element Endowment of Modern Sea-Floor Massive Sulfides and Comparison with Deposits Hosted in Ancient Volcanic Successions. *In:* Rare Earth and Critical Elements in Ore Deposits, Society of Economic Geologists, 2016.

Orkustofnun, 2018: Geothermal. http://www.nea.is/geothermal/. Orkustofnun – National Engergy Authority of Iceland, accessed 30.3.2018.

Palacky, G.V., 1987: Resistivity characteristics of geologic targets, in Electromagnetic Methods in Applied Geophysics, Vol. 1, Theory, pp 1351, SEG.

Pedersen, R.B., Thorseth, I.H., Bygård, T.E. (2010): Hydrothermal activity along the Arctic mid-ocean ridge. In: Diversity of Hydrothermal, Systems on Slow-Spreading Ocean Ridges, Geophys. Monogr. 188, edited by P. Rona et al., AGU, Washington, D. C., 2010.

Pedersen, R.B. & Bjerkgård, T. (2016): Seafloor Massive Sulphides In Arctic Waters. In B. Rognvald, T. Bjerkgård, B. Nordahl, & H. Schiellerup (Eds.), Mineral Resources In The Arctic (1st ed., pp. 209–216). Geological Survey Of Norway.

Petersen, S., Kuhn, K., Kuhn, T., Augustin, N., Hékinian, R., Franz, L. & Borowski, C., 2009: The geological setting of the ultramafic-hosted Logatchev hydrothermal field (14°45'N, Mid-Atlantic Ridge) and its influence on massive sulfide formation. Lithos, 112, 40–56.

Pertsev, A., Bortnikov, N., Vlasov, E., Beltenev, V., Dobretsova, I. & Ageeva, O. (2012): Recent massive sulfide deposits of the Semenov ore district, Mid-Atlantic Ridge, 13° 31' N: Associated rocks of the oceanic core complex and their hydrothermal alteration. Geology of Ore Deposits, 54, 334-346.

Riedel, C., Schmidt, M., Botz, R. & Theilen F., 2001: The Grimsey hydrothermal field offshore North Iceland: Crustal structure, faulting and related gas venting. Earth and Planetary Science Letters, 193(3-4), 409-421.

Rizosphere Research Products, Rhizons 2.5 mm, the standard Rhizons for pore water sampling. 2018 [Accessed July 2018]. http://rhizosphere.com

Safipour, R., Hölz, S., Jegen, M., Swidinsky, A. 2017: On electric fields produced by inductive sources on the seafloor, Geophysics, 82, E297-E313.

Safipour, R., Hölz, S., Jegen, M., Swidinsky, A., 2018: A first application of a marine inductive source EM configuration with remote electric dipole receivers: Palinuro Seamount, Tyrrhenian Sea. Geophysical Prospecting, 2018, 66, 1415-1432.

Scholten, J., Blaschek, H., Becker, K.-P., Hannington, M., Herzig, P., Hißmann, K., Jonasson, I., Krüger, O., Marteinsson, V., Preißler, H., Schauer, J., Schmidt, M., Solveig, P., Theißen, O., 2000. Hydrothermalism at the Kolbeinsey Ridge, Iceland. Technical Cruise Report PO 253, University of Kiel, pp. 22–43.

Snow, J.E. & Edmonds, H.N., 2007: Ultraslow-spreading ridges rapid paradigm changes. Oceanography, 20, 90-101.

Stoffers, P., Shipboard Scientific Party, 1997. Cruise Report of R/V Poseidon 229 Institute of Geosciences, Departments of Geophysics and Geology–Paleontology, University of Kiel, 58 pp.

Swidinsky, A., Hölz, S. & Jegen, M.: On mapping seafloor mineral deposits with central loop transient electromagnetics. Geophysics, 2012, 77, E171-E184.

Swidinsky, A., Hölz, S. & Jegen, M., 2015: Rapid resistivity imaging for marine CSEM surveys with two transmitter polarizations: An application to the North Alex mud volcano. Geophysics, 80, E97-E110.

Villinger, H. & Davis, E.E., 1987. A new reduction algorithm for marine heat-flow measurements. Journal of Geophysical Research, 92(B12), 12846-12856.

10. Appendix

10.1. Station Log

Activity	Timestamp	Device	Action	Latitude	Longitude	Depth (m)	Speed (kn)	Course	Wind Dir	Wind Velocity	Comment
POS535_64-1	26.06.2019 15:12	Martemis	on deck	73° 28,174' N	7° 09,382' E	2296	1,0	205	343	12,7	Completion of research operations
POS535_64-1	26.06.2019 13:26	Martemis	profile end	73° 28,699' N	7° 12,373' E	2581	0,0	46	330	13,1	
POS535_64-1	26.06.2019 06:38	Martemis	profile start	73° 26,835' N	7° 06,670' E	2285	0,0	56	70	6,2	
POS535_64-1	26.06.2019 06:27	Martemis	max depth/on ground	73° 26,812' N	7° 06,539' E	2259	0,0	48	71	6,0	SL_{max} = 2119 m
POS535_64-1	26.06.2019 05:04	Martemis	in the water	73° 26,781' N	7° 06,144' E	2231	0,0	260	96	5,2	
POS535_63-1	25.06.2019 15:25	Gravity corer	on deck	73° 27,163' N	7° 10,713' E	2721	0,0	231	266	3,6	
POS535_63-1	25.06.2019 14:46	Gravity corer	max depth/on ground	73° 27,157' N	7° 11,375' E	2849	0,0	194	241	4,6	SL_{max} = 2767 m
POS535_63-1	25.06.2019 14:15	Gravity corer	in the water	73° 27,170' N	7° 11,461' E	2792	0,0	258	259	4,1	
POS535_62-1	25.06.2019 11:11	OBEM	on deck	73° 34,037' N	8° 08,269' E	2551	0,0	279	299	7,5	
POS535_62-1	25.06.2019 11:03	OBEM	at surface	73° 34,026' N	8° 08,123' E	2551	0,0	195	289	8,3	
POS535_62-1	25.06.2019 10:24	OBEM	information	73° 34,149' N	8° 08,119' E	2551	0,0	140	287	7,7	released
POS535_61-1	25.06.2019 09:26	OBEM	on deck	73° 33,947' N	8° 08,656' E	2551	0,0	126	286	9,8	
POS535_61-1	25.06.2019 09:18	OBEM	at surface	73° 34,000' N	8° 08,980' E	2551	0,0	83	288	9,4	
POS535_61-1	25.06.2019 08:35	OBEM	information	73° 33,920' N	8° 09,726' E	2551	0,0	183	290	9,5	released
POS535_60-1	25.06.2019 08:47	OBEM	on deck	73° 33,929' N	8° 08,146' E	2551	0,0	236	283	9,7	
POS535_60-1	25.06.2019 08:20	OBEM	at surface	73° 34,012' N	8° 09,959' E	2551	0,0	199	291	11,5	
POS535_60-1	25.06.2019 07:36	OBEM	information	73° 34,132' N	8° 08,244' E	2551	1,0	208	290	10,0	released
POS535_59-1	25.06.2019 07:44	OBEM	on deck	73° 34,037' N	8° 07,734' E	2551	0,0	273	262	8,4	
POS535_59-1	25.06.2019 07:29	OBEM	at surface	73° 34,193' N	8° 08,209' E	2551	0,0	181	278	9,1	
POS535_59-1	25.06.2019 06:43	OBEM	information	73° 34,356' N	8° 08,009' E	2551	0,0	121	259	9,4	released
POS535_58-1	25.06.2019 06:58	OBEM	on deck	73° 34,095' N	8° 07,506' E	2551	1,0	247	264	6,5	
POS535_58-1	25.06.2019 06:40	OBEM	at surface	73° 34,351' N	8° 07,948' E	2551	0,0	49	262	8,6	
POS535_58-1	25.06.2019 05:55	OBEM	information	73° 34,274' N	8° 06,607' E	2551	0,0	79	264	9,3	released

Activity	Timestamp	Device	Action	Latitude	Longitude	Depth (m)	Speed (kn)	Course	Wind Dir	Wind Velocity	Comment
POS535_57-1	25.06.2019 05:53	OBEM	on deck	73° 34,263' N	8° 06,505' E	2542	0,0	32	267	8,6	
POS535_57-1	25.06.2019 05:18	OBEM	at surface	73° 34,213' N	8° 09,179' E	2346	0,0	181	275	10,6	
POS535_57-1	25.06.2019 04:07	OBEM	information	73° 34,321' N	8° 09,254' E	2354	0,0	188	249	11,6	released
POS535_56-1	25.06.2019 03:13	CSEM	on deck	73° 33,159' N	8° 11,512' E	2615	0,0	117	255	10,6	
POS535_56-1	25.06.2019 01:46	CSEM	profile end	73° 33,564' N	8° 12,192' E	2601	0,0	144	247	11,0	
POS535_56-1	24.06.2019 23:35	CSEM	profile start	73° 34,242' N	8° 08,630' E	2317	0,0	95	240	9,8	
POS535_56-1	24.06.2019 23:33	CSEM	max depth/on ground	73° 34,237' N	8° 08,565' E	2376	0,0	64	246	8,6	SL_{max} = 2445 m
POS535_56-1	24.06.2019 22:03	CSEM	in the water	73° 34,422' N	8° 07,269' E	2515	0,0	164	225	10,4	
POS535_55-1	24.06.2019 12:55	Gravity corer	on deck	73° 33,997' N	8° 09,522' E	2407	0,0	104	210	4,4	
POS535_55-1	24.06.2019 12:26	Gravity corer	max depth/on ground	73° 33,997' N	8° 09,493' E	2398	0,0	247	209	3,3	SL_{max} = 2306 m
POS535_55-1	24.06.2019 12:02	Gravity corer	in the water	73° 33,993' N	8° 09,496' E	2402	0,0	132	239	3,1	
POS535_54-1	24.06.2019 11:50	Gravity corer	on deck	73° 34,027' N	8° 09,411' E	2405	0,0	56	236	3,6	
POS535_54-1	24.06.2019 11:23	Gravity corer	max depth/on ground	73° 34,028' N	8° 09,407' E	2409	0,0	86	232	4,4	SL_{max} = 2319 m
POS535_54-1	24.06.2019 10:58	Gravity corer	in the water	73° 34,031' N	8° 09,400' E	2547	0,0	289	233	5,0	
POS535_53-1	24.06.2019 09:21	Martemis	on deck	73° 35,656' N	8° 09,463' E	2547	0,0	339	239	4,0	
POS535_53-1	24.06.2019 07:37	Martemis	profile end	73° 34,205' N	8° 09,783' E	2547	0,0	307	252	4,9	
POS535_53-1	23.06.2019 18:24	Martemis	profile start	73° 34,628' N	8° 06,387' E	2547	0,0	103	124	3,3	
POS535_53-1	23.06.2019 18:06	Martemis	max depth/on ground	73° 34,644' N	8° 06,239' E	2547	0,0	250	127	3,8	SL_{max} = 2371 m
POS535_53-1	23.06.2019 16:25	Martemis	in the water	73° 34,666' N	8° 06,076' E	2547	0,0	195	127	4,6	
POS535_53-1	23.06.2019 15:49	Martemis	on deck	73° 34,664' N	8° 06,022' E	2547	0,0	112	135	4,4	
POS535_53-1	23.06.2019 14:49	Martemis	in the water	73° 34,710' N	8° 05,586' E	2519	0,0	73	133	5,9	
POS535_52-1	23.06.2019 13:31	OBEM	deployed	73° 33,877' N	8° 10,587' E	2418	0,0	43	127	5,8	
POS535_51-1	23.06.2019 13:08	OBEM	deployed	73° 33,955' N	8° 10,163' E	2397	0,0	75	125	6,4	
POS535_50-1	23.06.2019 12:44	OBEM	deployed	73° 34,034' N	8° 09,761' E	2410	0,0	18	122	5,9	
POS535_49-1	23.06.2019 12:15	OBEM	deployed	73° 34,110' N	8° 09,363' E	2374	0,0	153	129	6,2	
POS535_48-1	23.06.2019 11:43	OBEM	deployed	73° 34,189' N	8° 08,941' E	2351	0,0	7	125	5,4	
POS535_47-1	23.06.2019 09:00	Gravity corer	on deck	73° 33,957' N	8° 09,596' E	2426	0,0	62	115	6,1	

Activity	Timestamp	Device	Action	Latitude	Longitude	Depth (m)	Speed (kn)	Course	Wind Dir	Wind Velocity	Comment
POS535_47-1	23.06.2019 08:25	Gravity corer	max depth/on ground	73° 33,964' N	8° 09,585' E	2402	0,0	254	113	6,8	2318m max
POS535_47-1	23.06.2019 07:58	Gravity corer	in the water	73° 33,958' N	8° 09,647' E	2357	0,0	217	113	6,2	
POS535_46-1	23.06.2019 07:15	Gravity corer	on deck	73° 33,988' N	8° 09,469' E	2404	0,0	48	115	6,1	
POS535_46-1	23.06.2019 06:41	Gravity corer	max depth/on ground	73° 33,988' N	8° 09,466' E	2429	0,0	157	106	6,4	2309m max
POS535_46-1	23.06.2019 06:15	Gravity corer	in the water	73° 33,981' N	8° 09,495' E	2609	0,0	200	106	6,3	
POS535_45-1	23.06.2019 06:03	OBEM	deployed	73° 33,993' N	8° 09,513' E	135	0,0	242	111	6,5	
POS535_44-1	18.06.2019 09:31	Gravity corer	on deck	66° 26,556' N	17° 24,155' W	228	0,0	349	357	6,8	
POS535_44-1	18.06.2019 09:26	Gravity corer	max depth/on ground	66° 26,549' N	17° 24,139' W	188	0,0	31	0	7,3	202m max
POS535_44-1	18.06.2019 09:22	Gravity corer	in the water	66° 26,538' N	17° 24,153' W	200	0,0	6	341	5,1	
POS535_43-1	18.06.2019 09:09	Gravity corer	on deck	66° 26,486' N	17° 24,145' W	200	0,0	319	5	8,3	
POS535_43-1	18.06.2019 09:04	Gravity corer	max depth/on ground	66° 26,489' N	17° 24,167' W	201	0,0	134	330	7,2	203m max
POS535_43-1	18.06.2019 09:00	Gravity corer	in the water	66° 26,497' N	17° 24,186' W	201	0,0	187	349	6,5	
POS535_42-1	18.06.2019 07:08	Gravity corer	on deck	66° 21,519' N	16° 55,408' W	186	0,0	285	7	8,9	
POS535_42-1	18.06.2019 07:04	Gravity corer	hoisting	66° 21,529' N	16° 55,422' W	188	0,0	138	2	7,4	SZ_{max} = 20,8kN
POS535_42-1	18.06.2019 07:04	Gravity corer	max depth/on ground	66° 21,530' N	16° 55,424' W	188	0,0	20	8	8,2	SL_{max} = 207m
POS535_42-1	18.06.2019 07:00	Gravity corer	in the water	66° 21,520' N	16° 55,390' W	188	0,0	264	9	8,2	Resume research operations POS535
POS535_41-1	17.06.2019 07:38	Gravity corer	on deck	66° 21,441' N	16° 55,429' W	209	0,0	340	0	0,0	Cease of research operations POS535
POS535_41-1	17.06.2019 07:34	Gravity corer	hoisting	66° 21,422' N	16° 55,442' W	208	0,0	252	0	0,0	SZ_{max} = 30,5kN
POS535_41-1	17.06.2019 07:33	Gravity corer	max depth/on ground	66° 21,423' N	16° 55,431' W	209	0,0	273	0	0,0	SL_{max} = 205m
POS535_41-1	17.06.2019 07:30	Gravity corer	in the water	66° 21,411' N	16° 55,438' W	208	0,0	337	0	0,0	
POS535_40-1	17.06.2019 07:08	Gravity corer	on deck	66° 21,531' N	16° 55,435' W	190	0,0	107	0	0,0	
POS535_40-1	17.06.2019 07:05	Gravity corer	hoisting	66° 21,530' N	16° 55,441' W	189	0,0	107	0	0,0	SZ_{max} = 30kN
POS535_40-1	17.06.2019 07:04	Gravity corer	information	66° 21,530' N	16° 55,448' W	187	0,0	6	0	0,0	SL_{max} = 209m
POS535_40-1	17.06.2019 07:01	Gravity corer	in the water	66° 21,522' N	16° 55,451' W	192	0,0	358	0	0,0	
POS535_39-1	16.06.2019 14:35	OBEM	on deck	66° 36,559' N	17° 39,630' W	411	0,0	272	0	0,0	
POS535_39-1	16.06.2019 14:27	OBEM	at surface	66° 36,526' N	17° 39,684' W	411	0,0	247	0	0,0	
POS535_39-1	16.06.2019 14:21	OBEM	information	66° 36,525' N	17° 39,653' W	411	0,0	321	0	0,0	released

Activity	Timestamp	Device	Action	Latitude	Longitude	Depth (m)	Speed (kn)	Course	Wind Dir	Wind Velocity	Comment
POS535_38-1	16.06.2019 14:06	OBEM	on deck	66° 36,311' N	17° 39,655' W	411	0,0	284	0	0,0	
POS535_38-1	16.06.2019 13:59	OBEM	at surface	66° 36,317' N	17° 39,912' W	411	0,0	286	0	0,0	
POS535_38-1	16.06.2019 13:51	OBEM	information	66° 36,305' N	17° 39,913' W	411	0,0	69	0	0,0	released
POS535_37-1	16.06.2019 13:35	OBEM	on deck	66° 36,169' N	17° 39,863' W	411	0,0	2	0	0,0	
POS535_37-1	16.06.2019 13:28	OBEM	at surface	66° 36,118' N	17° 39,765' W	411	0,0	330	0	0,0	
POS535_37-1	16.06.2019 13:20	OBEM	information	66° 36,091' N	17° 39,853' W	411	0,0	49	0	0,0	released
POS535_36-1	16.06.2019 11:28	OBEM	on deck	66° 36,161' N	17° 40,323' W	411	0,0	334	0	0,0	
POS535_36-1	16.06.2019 11:18	OBEM	at surface	66° 36,183' N	17° 40,363' W	411	0,0	357	0	0,0	
POS535_36-1	16.06.2019 11:10	OBEM	information	66° 36,171' N	17° 40,376' W	411	0,0	50	0	0,0	released
POS535_35-1	16.06.2019 10:54	OBEM	on deck	66° 36,447' N	17° 40,053' W	411	0,0	32	0	0,0	
POS535_35-1	16.06.2019 10:46	OBEM	at surface	66° 36,409' N	17° 40,309' W	411	0,0	40	0	0,0	
POS535_35-1	16.06.2019 10:40	OBEM	information	66° 36,406' N	17° 40,334' W	411	0,0	53	0	0,0	released
POS535_34-1	16.06.2019 10:23	OBEM	on deck	66° 36,617' N	17° 40,211' W	411	0,0	20	0	0,0	
POS535_34-1	16.06.2019 10:14	OBEM	at surface	66° 36,631' N	17° 40,494' W	411	0,0	55	0	0,0	
POS535_34-1	16.06.2019 10:04	OBEM	information	66° 36,615' N	17° 40,455' W	411	0,0	332	0	0,0	released
POS535_33-1	16.06.2019 09:44	OBEM	on deck	66° 36,706' N	17° 40,724' W	411	0,0	35	0	0,0	
POS535_33-1	16.06.2019 09:36	OBEM	at surface	66° 36,641' N	17° 41,082' W	411	0,0	69	0	0,0	
POS535_33-1	16.06.2019 09:30	OBEM	information	66° 36,616' N	17° 41,074' W	411	0,0	291	0	0,0	released
POS535_32-1	16.06.2019 09:11	OBEM	on deck	66° 36,405' N	17° 40,816' W	411	0,0	347	0	0,0	
POS535_32-1	16.06.2019 09:02	OBEM	at surface	66° 36,360' N	17° 41,159' W	411	0,0	51	0	0,0	
POS535_32-1	16.06.2019 08:54	OBEM	information	66° 36,361' N	17° 41,146' W	411	0,0	272	0	0,0	released
POS535_31-1	16.06.2019 08:36	OBEM	on deck	66° 36,219' N	17° 40,794' W	411	0,0	2	0	0,0	
POS535_31-1	16.06.2019 08:28	OBEM	at surface	66° 36,176' N	17° 41,184' W	411	1,0	105	0	0,0	
POS535_31-1	16.06.2019 08:17	OBEM	information	66° 36,177' N	17° 41,129' W	411	0,0	262	0	0,0	released
POS535_30-1	16.06.2019 07:35	CSEM	on deck	66° 36,301' N	17° 37,943' W	411	0,0	51	0	0,0	
POS535_30-1	16.06.2019 07:18	CSEM	profile end	66° 36,254' N	17° 38,162' W	411	0,0	78	0	0,0	
POS535_30-1	15.06.2019 21:10	CSEM	profile start	66° 36,371' N	17° 41,190' W	411	0,0	69	0	0,0	

Activity	Timestamp	Device	Action	Latitude	Longitude	Depth (m)	Speed (kn)	Course	Wind Dir	Wind Velocity	Comment
POS535_30-1	15.06.2019 20:57	CSEM	max depth/on ground	66° 36,412' N	17° 41,402' W	411	0,0	156	0	0,0	387m max
POS535_30-1	15.06.2019 20:32	CSEM	in the water	66° 36,442' N	17° 41,680' W	411	0,0	65	0	0,0	
POS535_29-1	15.06.2019 18:33	CSEM	on deck	66° 36,257' N	17° 37,537' W	411	0,0	312	83	9,4	
POS535_29-1	15.06.2019 17:46	CSEM	profile end	66° 36,150' N	17° 38,322' W	411	0,0	101	0	0,0	
POS535_29-1	15.06.2019 15:34	CSEM	profile start	66° 36,168' N	17° 40,760' W	411	0,0	82	0	0,0	
POS535_29-1	15.06.2019 15:14	CSEM	max depth/on ground	66° 36,184' N	17° 41,071' W	411	0,0	120	0	0,0	SL_{max} = 380m
POS535_29-1	15.06.2019 14:53	CSEM	in the water	66° 36,200' N	17° 41,234' W	411	0,0	252	0	0,0	
POS535_29-1	15.06.2019 14:36	CSEM	on deck	66° 36,159' N	17° 40,859' W	411	0,0	111	0	0,0	
POS535_29-1	15.06.2019 13:42	CSEM	in the water	66° 36,139' N	17° 41,505' W	410	0,0	32	0	0,0	
POS535_28-1	15.06.2019 11:28	OBEM	on deck	66° 36,240' N	17° 39,304' W	383	0,0	16	0	0,0	
POS535_28-1	15.06.2019 11:19	OBEM	at surface	66° 36,187' N	17° 39,352' W	403	0,0	211	0	0,0	
POS535_28-1	15.06.2019 11:13	OBEM	information	66° 36,239' N	17° 39,297' W	384	0,0	213	0	0,0	released
POS535_27-1	15.06.2019 10:39	OBEM	on deck	66° 36,524' N	17° 39,115' W	407	0,0	336	0	0,0	
POS535_27-1	15.06.2019 10:26	OBEM	at surface	66° 36,437' N	17° 39,152' W	403	0,0	57	0	0,0	
POS535_27-1	15.06.2019 10:20	OBEM	information	66° 36,429' N	17° 39,156' W	399	0,0	11	0	0,0	released
POS535_26-1	15.06.2019 09:47	OBEM	on deck	66° 36,725' N	17° 39,189' W	407	0,0	308	0	0,0	
POS535_26-1	15.06.2019 09:32	OBEM	at surface	66° 36,591' N	17° 39,229' W	403	0,0	0,8	0	0,0	
POS535_26-1	15.06.2019 09:26	OBEM	information	66° 36,584' N	17° 39,251' W	403	0,0	55	0	0,0	released
POS535_25-1	15.06.2019 08:52	Gravity corer	on deck	66° 36,439' N	17° 39,623' W	373	0,0	108	0	0,0	
POS535_25-1	15.06.2019 08:44	Gravity corer	max depth/on ground	66° 36,437' N	17° 39,637' W	372	0,0	210	0	0,0	364m max
POS535_25-1	15.06.2019 08:39	Gravity corer	in the water	66° 36,436' N	17° 39,611' W	372	0,0	321	0	0,0	
POS535_24-1	15.06.2019 08:14	Gravity corer	on deck	66° 36,404' N	17° 40,215' W	373	0,0	203	0	0,0	
POS535_24-1	15.06.2019 08:07	Gravity corer	max depth/on ground	66° 36,413' N	17° 40,255' W	370	0,0	112	0	0,0	364m max
POS535_24-1	15.06.2019 08:01	Gravity corer	in the water	66° 36,412' N	17° 40,211' W	373	0,0	345	0	0,0	
POS535_23-1	14.06.2019 17:25	Heatflow Probe	on deck	66° 36,265' N	17° 38,800' W	415	0,0	263	0	0,0	
POS535_23-1	14.06.2019 17:15	Heatflow Probe	hoisting	66° 36,247' N	17° 38,784' W	383	0,0	122	0	0,0	
POS535_23-1	14.06.2019 17:00	Heatflow Probe	max depth/on ground	66° 36,244' N	17° 38,784' W	421	0,0	123	0	0,0	SL_{max} = 411m

Activity	Timestamp	Device	Action	Latitude	Longitude	Depth (m)	Speed (kn)	Course	Wind Dir	Wind Velocity	Comment
POS535_23-1	14.06.2019 16:41	Heatflow Probe	hoisting	66° 36,048' N	17° 39,202' W	393	0,0	74	0	0,0	
POS535_23-1	14.06.2019 16:26	Heatflow Probe	max depth/on ground	66° 36,047' N	17° 39,217' W	402	0,0	76	0	0,0	SL_{max} = 396m
POS535_23-1	14.06.2019 15:58	Heatflow Probe	hoisting	66° 36,263' N	17° 39,624' W	1	0,0	69	0	0,0	
POS535_23-1	14.06.2019 15:43	Heatflow Probe	max depth/on ground	66° 36,261' N	17° 39,646' W	3	0,0	183	0	0,0	SL_{max} = 374m
POS535_23-1	14.06.2019 15:21	Heatflow Probe	hoisting	66° 36,420' N	17° 39,668' W	371	0,0	76	0	0,0	
POS535_23-1	14.06.2019 15:06	Heatflow Probe	max depth/on ground	66° 36,442' N	17° 39,660' W	1	0,0	177	0	0,0	SL_{max} = 366m
POS535_23-1	14.06.2019 14:58	Heatflow Probe	hoisting	66° 36,425' N	17° 39,677' W	1	0,0	173	0	0,0	
POS535_23-1	14.06.2019 14:44	Heatflow Probe	max depth/on ground	66° 36,434' N	17° 39,663' W	374	0,0	32	0	0,0	SL_{max} = 366m
POS535_23-1	14.06.2019 14:15	Heatflow Probe	hoisting	66° 36,182' N	17° 40,268' W	156	0,0	146	0	0,0	
POS535_23-1	14.06.2019 14:00	Heatflow Probe	max depth/on ground	66° 36,195' N	17° 40,268' W	1	0,0	128	0	0,0	SL_{max} = 380m
POS535_23-1	14.06.2019 13:53	Heatflow Probe	in the water	66° 36,202' N	17° 40,245' W	383	0,0	320	0	0,0	
POS535_22-1	14.06.2019 13:17	Martemis	on deck	66° 36,680' N	17° 37,913' W	424	0,0	74	0	0,0	
POS535_22-1	14.06.2019 12:57	Martemis	profile end	66° 36,678' N	17° 38,097' W	424	0,0	88	0	0,0	
POS535_22-1	13.06.2019 14:38	Martemis	profile start	66° 36,143' N	17° 41,502' W	424	0,0	65	75	9,3	
POS535_22-1	13.06.2019 14:28	Martemis	max depth/on ground	66° 36,147' N	17° 41,686' W	424	0,0	105	82	8,4	SL_{max} = 385m
POS535_22-1	13.06.2019 13:02	Martemis	in the water	66° 36,061' N	17° 42,524' W	431	0,0	57	87	8,1	
POS535_21-1	13.06.2019 11:34	Heatflow Probe	on deck	66° 37,619' N	17° 39,030' W	391	0,0	263	88	7,5	
POS535_21-1	13.06.2019 11:25	Heatflow Probe	hoisting	66° 37,597' N	17° 38,973' W	391	0,0	136	91	6,3	
POS535_21-1	13.06.2019 11:09	Heatflow Probe	max depth/on ground	66° 37,601' N	17° 38,949' W	388	0,0	279	93	5,7	388m max
POS535_21-1	13.06.2019 10:53	Heatflow Probe	hoisting	66° 37,482' N	17° 38,601' W	391	0,0	109	84	6,4	
POS535_21-1	13.06.2019 10:37	Heatflow Probe	max depth/on ground	66° 37,480' N	17° 38,586' W	392	0,0	261	71	5,5	386m max
POS535_21-1	13.06.2019 09:50	Heatflow Probe	hoisting	66° 36,706' N	17° 39,592' W	402	0,0	347	33	4,1	
POS535_21-1	13.06.2019 09:36	Heatflow Probe	max depth/on ground	66° 36,714' N	17° 39,599' W	394	0,0	253	40	3,1	391m max
POS535_21-1	13.06.2019 09:08	Heatflow Probe	hoisting	66° 36,631' N	17° 38,535' W	417	0,0	334	49	3,7	
POS535_21-1	13.06.2019 08:53	Heatflow Probe	max depth/on ground	66° 36,628' N	17° 38,588' W	416	0,0	208	16	5,4	414m max
POS535_21-1	13.06.2019 08:25	Heatflow Probe	hoisting	66° 36,409' N	17° 38,367' W	426	0,0	302	23	4,0	
POS535_21-1	13.06.2019 08:10	Heatflow Probe	max depth/on ground	66° 36,411' N	17° 38,385' W	420	0,0	298	358	3,2	416m max

Activity	Timestamp	Device	Action	Latitude	Longitude	Depth (m)	Speed (kn)	Course	Wind Dir	Wind Velocity	Comment
POS535_21-1	13.06.2019 08:02	Heatflow Probe	in the water	66° 36,423' N	17° 38,395' W	419	0,0	159	355	3,4	
POS535_20-1	13.06.2019 06:35	Martemis	on deck	66° 36,449' N	17° 39,624' W	420	0,0	205	10	4,4	
POS535_20-1	12.06.2019 22:22	Martemis	profile end	66° 36,252' N	17° 39,301' W	420	0,0	303	290	8,8	Device failed
POS535_20-1	12.06.2019 13:08	Martemis	profile start	66° 36,002' N	17° 37,603' W	390	0,0	285	294	9,6	
POS535_20-1	12.06.2019 10:26	Martemis	max depth/on ground	66° 35,925' N	17° 43,736' W	463	0,0	231	286	8,7	420m
POS535_20-1	12.06.2019 10:24	Martemis	max depth/on ground	66° 35,935' N	17° 43,705' W	462	0,0	216	280	8,8	380m
POS535_20-1	12.06.2019 08:52	Martemis	in the water	66° 36,008' N	17° 42,545' W	433	1,0	238	282	6,7	
POS535_19-1	11.06.2019 17:33	OBEM	deployed	66° 36,579' N	17° 38,915' W	412	0,0	184	306	2,2	
POS535_18-1	11.06.2019 17:09	OBEM	deployed	66° 36,580' N	17° 39,417' W	393	0,0	8	303	2,3	
POS535_17-1	11.06.2019 16:45	OBEM	deployed	66° 36,549' N	17° 40,190' W	378	0,0	201	315	0,0	
POS535_16-1	11.06.2019 16:20	OBEM	deployed	66° 36,581' N	17° 40,754' W	402	0,0	189	347	1,6	
POS535_15-1	11.06.2019 15:42	OBEM	deployed	66° 36,397' N	17° 38,878' W	414	0,0	79	324	0,0	
POS535_14-1	11.06.2019 15:04	POSIDONIA	on deck	66° 36,955' N	17° 41,133' W	406	0,0	115	309	1,8	
POS535_14-1	11.06.2019 14:49	POSIDONIA	information	66° 36,960' N	17° 41,081' W	403	2,0	143	283	1,6	End of calibration
POS535_14-1	11.06.2019 12:57	POSIDONIA	information	66° 36,990' N	17° 41,100' W	402	2,0	218	359	0,0	start of calibration
POS535_14-1	11.06.2019 12:34	POSIDONIA	in the water	66° 36,992' N	17° 41,005' W	403	0,0	288	351	0,0	
POS535_14-1	11.06.2019 12:16	POSIDONIA	on deck	66° 36,951' N	17° 41,066' W	403	0,0	219	11	1,0	
POS535_14-1	11.06.2019 12:07	POSIDONIA	in the water	66° 36,998' N	17° 40,996' W	404	0,0	134	346	2,7	
POS535_13-1	11.06.2019 11:34	Release Test	on deck	66° 36,445' N	17° 39,127' W	403	0,0	141	328	2,3	
POS535_13-1	11.06.2019 11:28	Release Test	max depth/on ground	66° 36,466' N	17° 39,166' W	397	0,0	146	321	2,8	200m max
POS535_13-1	11.06.2019 11:21	Release Test	in the water	66° 36,491' N	17° 39,210' W	396	0,0	136	309	3,2	
POS535_12-1	11.06.2019 10:59	Heatflow Probe	on deck	66° 36,568' N	17° 39,555' W	388	0,0	92	317	4,7	
POS535_12-1	11.06.2019 10:49	Heatflow Probe	hoisting	66° 36,559' N	17° 39,645' W	379	0,0	200	296	2,9	
POS535_12-1	11.06.2019 10:33	Heatflow Probe	max depth/on ground	66° 36,578' N	17° 39,645' W	378	0,0	129	323	4,2	376m max
POS535_12-1	11.06.2019 10:07	Heatflow Probe	hoisting	66° 36,433' N	17° 39,621' W	365	0,0	249	302	5,5	
POS535_12-1	11.06.2019 09:51	Heatflow Probe	max depth/on ground	66° 36,436' N	17° 39,615' W	7	0,0	244	308	5,7	371m max
POS535_12-1	11.06.2019 09:26	Heatflow Probe	hoisting	66° 36,443' N	17° 40,301' W	368	0,0	340	315	8,2	

Activity	Timestamp	Device	Action	Latitude	Longitude	Depth (m)	Speed (kn)	Course	Wind Dir	Wind Velocity	Comment
POS535_12-1	11.06.2019 09:11	Heatflow Probe	max depth/on ground	66° 36,449' N	17° 40,283' W	372	0,0	325	286	6,3	366m max
POS535_12-1	11.06.2019 08:45	Heatflow Probe	hoisting	66° 36,637' N	17° 40,375' W	380	0,0	168	301	4,1	
POS535_12-1	11.06.2019 08:28	Heatflow Probe	max depth/on ground	66° 36,634' N	17° 40,340' W	377	0,0	358	298	5,2	377m max
POS535_12-1	11.06.2019 08:14	Heatflow Probe	in the water	66° 36,625' N	17° 40,335' W	375	0,0	102	283	6,0	
POS535_11-1	10.06.2019 17:20	OBEM	deployed	66° 36,357' N	17° 39,606' W	378	0,0	2	95	7,4	
POS535_10-1	10.06.2019 16:49	OBEM	deployed	66° 36,356' N	17° 40,223' W	372	0,0	188	96	7,1	
POS535_9-1	10.06.2019 16:21	OBEM	deployed	66° 36,350' N	17° 40,746' W	409	0,0	171	86	5,4	
POS535_8-1	10.06.2019 15:48	OBEM	deployed	66° 36,137' N	17° 38,993' W	410	0,0	9	86	6,3	
POS535_7-1	10.06.2019 14:58	OBEM	deployed	66° 36,145' N	17° 39,605' W	385	0,0	88	100	6,9	
POS535_6-1	10.06.2019 14:32	OBEM	deployed	66° 36,142' N	17° 40,216' W	383	0,0	2	90	7,6	
POS535_5-1	10.06.2019 13:57	OBEM	deployed	66° 36,143' N	17° 40,760' W	412	0,0	210	89	6,2	
POS535_4-1	10.06.2019 10:28	Gravity corer	on deck	66° 37,539' N	17° 38,511' W	386	0,0	283	101	7,4	
POS535_4-1	10.06.2019 10:19	Gravity corer	max depth/on ground	66° 37,541' N	17° 38,478' W	383	0,0	187	100	7,5	384m max
POS535_4-1	10.06.2019 10:13	Gravity corer	in the water	66° 37,528' N	17° 38,447' W	382	0,0	262	102	8,1	
POS535_3-1	10.06.2019 09:26	Gravity corer	on deck	66° 36,512' N	17° 39,628' W	375	0,0	177	100	7,6	
POS535_3-1	10.06.2019 09:17	Gravity corer	max depth/on ground	66° 36,512' N	17° 39,638' W	375	0,0	343	101	6,9	374m max
POS535_3-1	10.06.2019 09:10	Gravity corer	in the water	66° 36,513' N	17° 39,615' W	376	0,0	128	100	6,5	
POS535_2-1	10.06.2019 08:35	Gravity corer	on deck	66° 36,429' N	17° 40,303' W	369	0,0	356	105	6,7	
POS535_2-1	10.06.2019 08:26	Gravity corer	max depth/on ground	66° 36,424' N	17° 40,321' W	368	0,0	78	113	7,0	366m max
POS535_2-1	10.06.2019 08:15	Gravity corer	in the water	66° 36,404' N	17° 40,322' W	369	0,0	303	108	6,7	
POS535_1-1	09.06.2019 18:09	Release Test	on deck	66° 36,983' N	17° 41,532' W	403	0,0	264	77	8,6	
POS535_1-1	09.06.2019 17:05	Release Test	max depth/on ground	66° 36,997' N	17° 41,532' W	402	0,0	3	84	7,9	SL_{max} = 300m
POS535_1-1	09.06.2019 16:48	Release Test	in the water	66° 36,979' N	17° 41,528' W	402	0,0	161	77	7,3	Start research operations POS535

10.2. Station Protocol Heat Flow

HF	Date	Time	Position		Depth [m]	Penetration [cm]	Heat Pulse	Max. tension [kN]	T_{max} [°C]	dT/dz [K / m]
			Latitude	Longitude						
01	11.06	08:28 – 08:43	66°36.64	-17°40.37	377	120	Yes	23	4.6	1.51
02		09:11 – 09:26	66°36.44	-17°40.29	369	x	Yes	24	-	-
03		09:51 – 10:06	66°36.45	-17°39.61	370	90	Yes	23	17.0	7.51
04		10:33 – 10:49	66°36.58	-17°39.64	379	220	Yes	30	15.5	5.06
05	13.06	8:10 – 8:25	66°36.43	-17°38.40	416	200	Yes	27	6.2	1.61
06		8:52 – 9:08	66°36.63	-17°38.58	412	220	Yes	23	8.5	2.49
07		9:35 – 9:50	66°36.72	-17°39.56	387	140	Yes	24	4.8	1.03
08		10:37 – 10:45	66°37.48	-17°38.59	382	120	Yes	26	6.2	1.32
09		11:09 – 11:17	66°37.59	-17°38.94	388	x	Yes	30	-	-
10	14.6	14:00 – 14:15	66°36.20	-17°40.24	380	x	Yes	24	-	-
11		14:43 – 14:58	66°36.43	-17°39.67	360	150	No	<20	7.5	2.29
12		15:05 – 15:20	66°36.43	-17°39.67	360	40	Yes	20	7.5	7.40
13		15:43 – 15:58	66°36.27	-17°39.66	360	150	Yes	25	8.5	2.90
14		16:26 – 16:41	66°36.05	-17°39.24	410	170	Yes	30	5.6	1.25
15		17:00 – 17:15	66°36.25	-17°38.80	420	190	Yes	34	6.5	1.75

- After ground contact an extra 5m of winch cable was given as slack, there was no change in tension for measurements without penetration.
- All measurements were taken at the Grimsey Vent Field

10.3. Core Descriptions

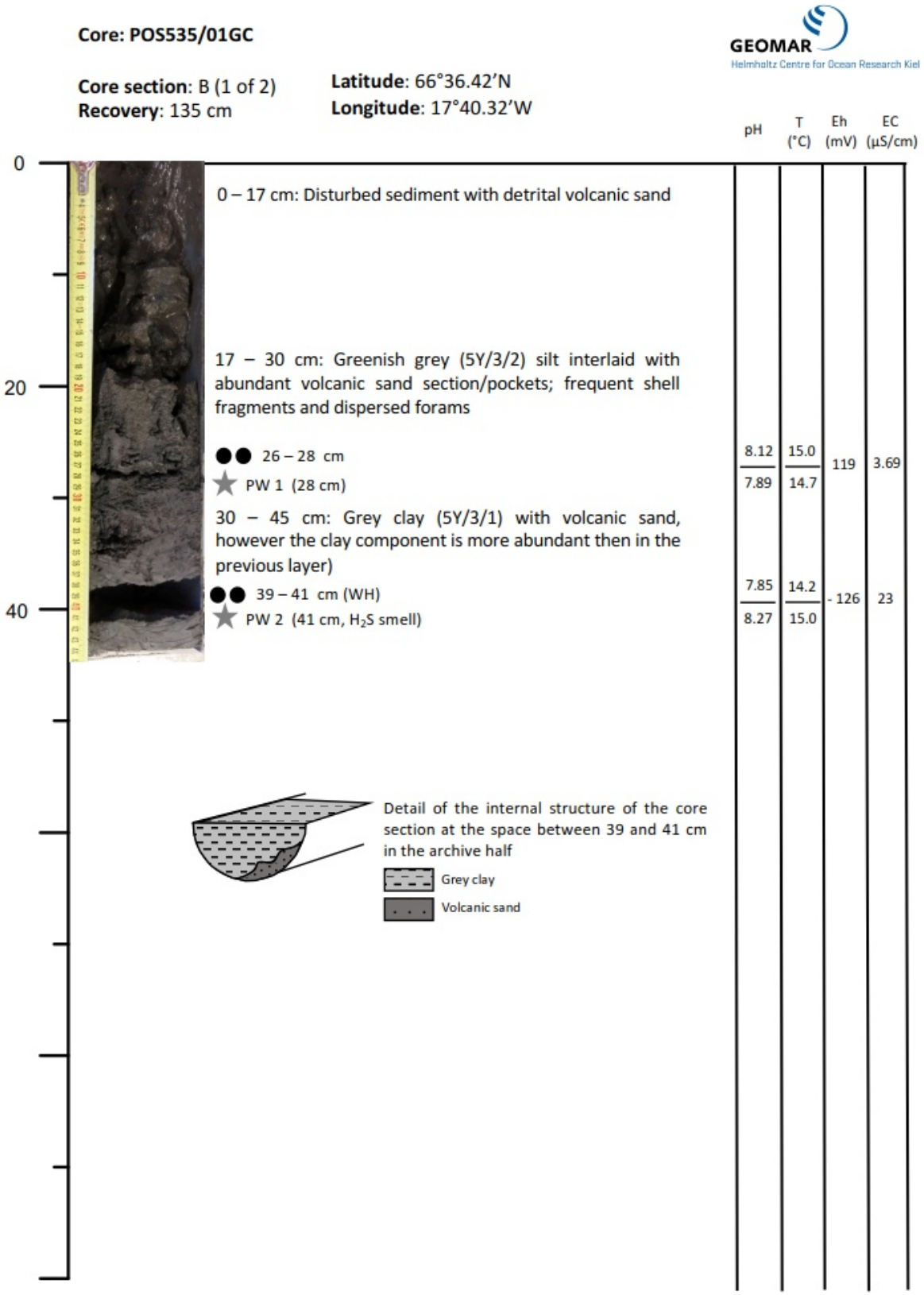

Core: POS535/01GC

GEOMAR
Helmholtz Centre for Ocean Research Kiel

Core section: A (2 of 2)
Recovery: 135 cm

Latitude: 66°36.42'N
Longitude: 17°40.32'W

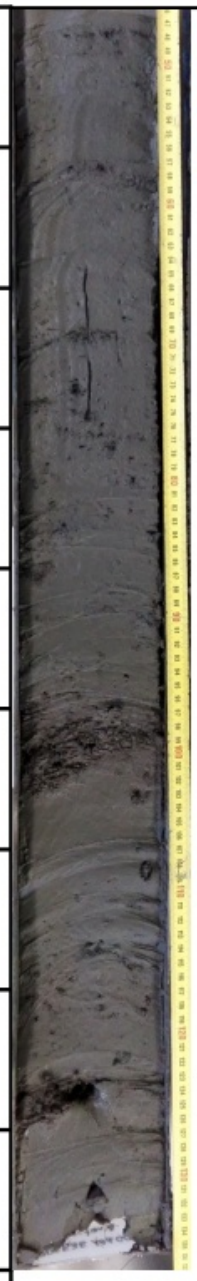

45 - 46.5 cm: Homogeneous grey clay (5Y/3/1)

46.5 – 97 cm: Grey silt (5Y/3/1) with several lenses of sand size volcanic material with frequent pebble size volcanic clasts; some shells are present in the detrital domains. At 95 to 97 cm its visible some black patches

●● 74 –76 cm
★ PW_03 (75 cm)

● 92 –93 cm (volcanic fragment with 2 cm)

●● 99 –101 cm
★ PW_04 (100 cm)

97 – 101 cm: Dehydrated silt/sand sediment with anhydrite/barite (white specks) (10YR/3/1)

101 – 135 cm: Grey silt with granule to pebble size volcanic clasts and rare volcanic sand size lenses (glass fragments). Some forams/shells occur in these lenses

●● 123 –125 cm
★ PW_05 (124 cm)

123 – 125 cm: Lense of finely disseminated sulfides/oxides

	pH	T (°C)	Eh (mV)	EC (µS/cm)
74 –76 cm	8.03 / 7.93	13.8 / 14.8	-169	Er1
99 –101 cm	8.45 / 8.40	14.8 / 14.1	-89	437
123 –125 cm	7.46 / 8.31	15.4 / 14.3	105	2.16

Core: POS535/02GC

GEOMAR
Helmholtz Centre for Ocean Research Kiel

Core section: C (1 of 3)
Recovery: 233 cm

Latitude: 66°36.51'N
Longitude: 17°39.64'W

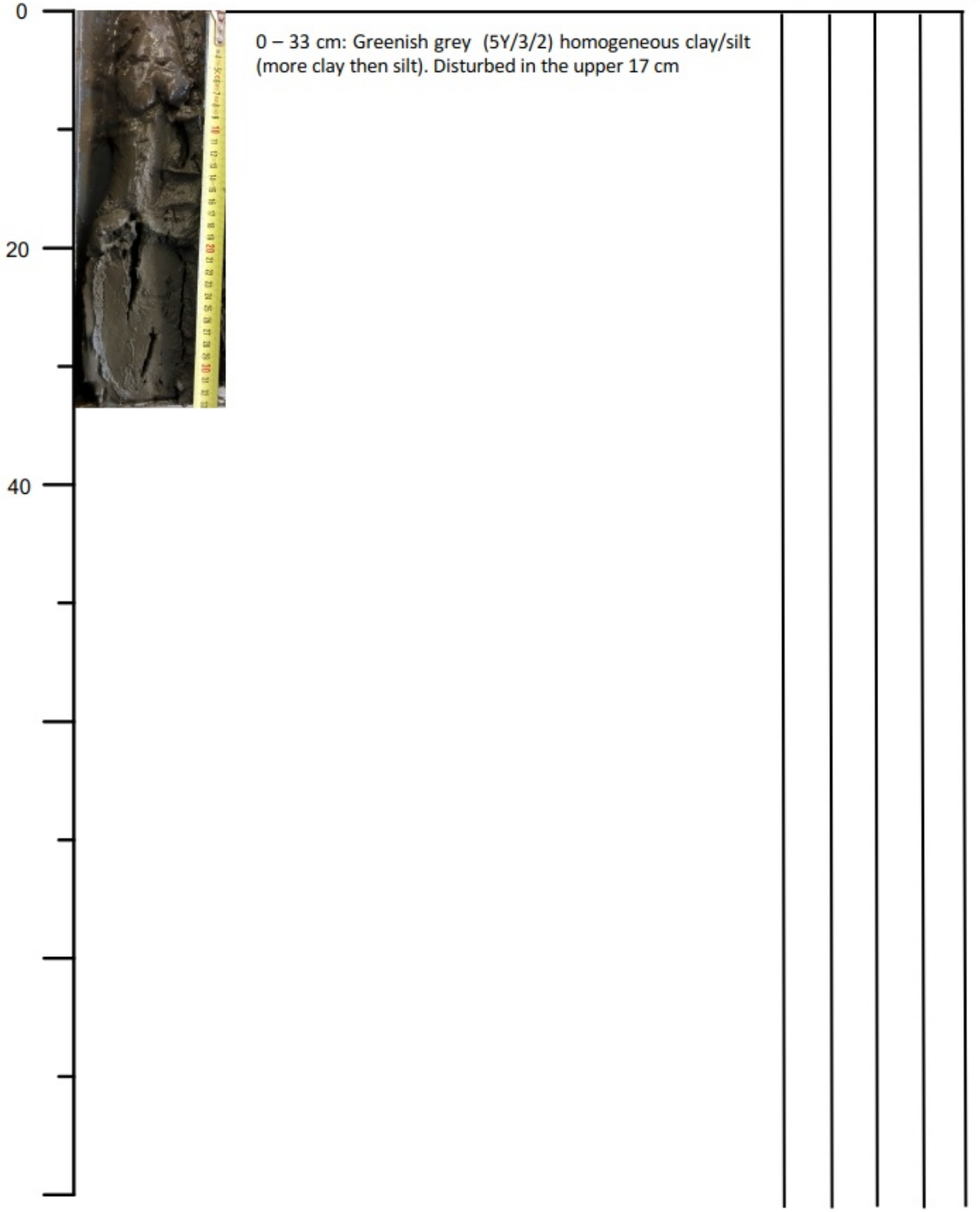

Core: POS535/02GC

GEOMAR
Helmholtz Centre for Ocean Research Kiel

Core section: B (2 of 3)
Recovery: 233 cm

Latitude: 66°36.51'N
Longitude: 17°39.64'W

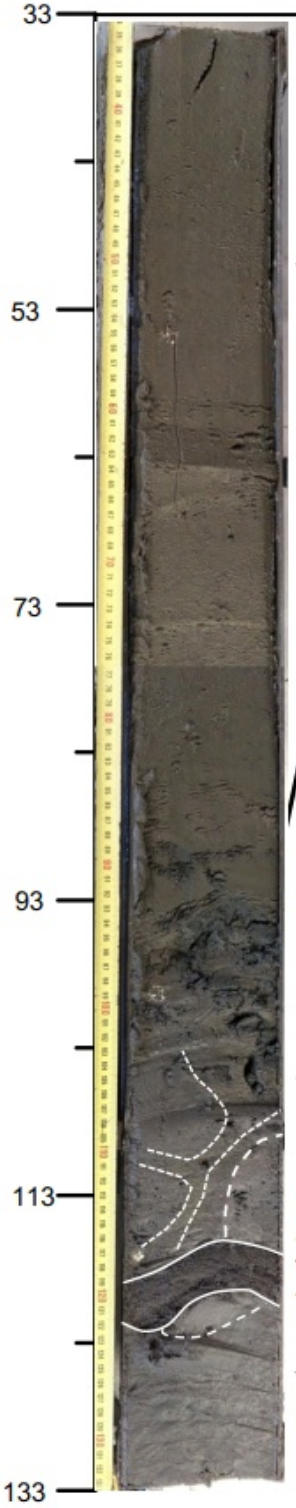

33 - 89 cm: Dark greenish (5Y/3/2) clay, homogeneous with scarce shell/shell fragments

●● 49 –51 cm
★ PW_06 (50 cm)

89 - 90 cm: Layer of volcanic sand (5Y/2.5/2)

●● 92 –94 cm (baked mud)
★ PW_07 (95 cm) + PW_08 (blank)
⬬ 94 –96 cm (volcanic pebble)

90 - 100 cm: Baked greyish (5Y/3/1) clay mixed with volcanic pebbles and volcanic sand (the pebbles are rounded and with an weathered appearance)

100 - 116 cm: Heterogeneous greenish grey clay with volcanic sand pockets/lenses and pebbles (up to 1 cm) and fragments of hardened clay. There is a yellowish green (5Y/4/2) clay forming a channel and a light grey section

●● 110 –113 cm (channel)
★ PW_09 (113 cm channel)
★ PW_10 (113 cm – grey patch)
●● 112 –114 cm (grey patch)

116 – 124 cm: Heterogeneous layer of volcanic material with alternating layers of sand size material and silt size material. There is a vesicular basalt pebble at 124 cm. Above and below this layer there are light grey irregular patches of clay (5Y/5/1)

●● 117 –119 cm (channel)
★ PW_11 (118 cm channel)

124 - 133 cm: Homogeneous grey clay

	pH	T (°C)	Eh (mV)	EC (µS/cm)
49 –51 cm	7.77 / 8.06	18.0 / 18.7	-18	27
92 –94 cm (baked mud)	8.47 / 8.52	18.4 / 18.9	61	25.5
110 –113 cm (channel)	7.95 / 7.71	18.5 / 19.1	- 97	20.6
112 –114 cm (grey patch)	8.16 / 8.26	18.9 / 19.1	- 128	18.9
117 –119 cm (channel)	8.06 / 8.04	18.6 / 19.0	97	2.26

Core: POS535/02GC

GEOMAR
Helmholtz Centre for Ocean Research Kiel

Core section: A (3 of 3)
Recovery: 233 cm

Latitude: 66°36.51'N
Longitude: 17°39.64'W

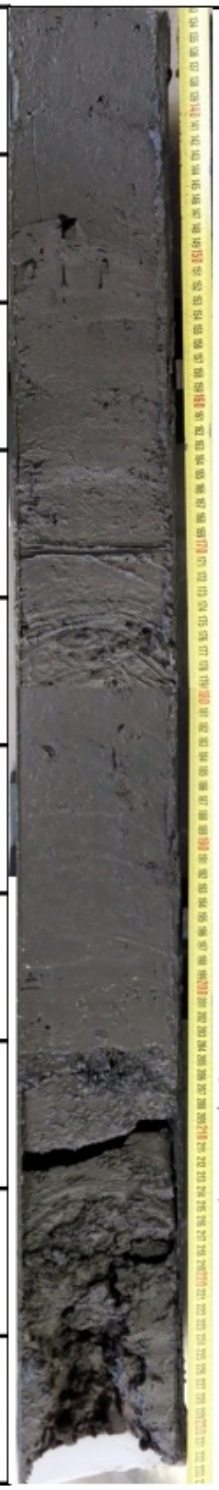

133 – 204 cm: Homogeneous dark grey clay (5Y/4/1) with frequent intercalations of volcanic sand (in pockets) and volcanic pebbles (rounded and vesicular, black)

●● 139 – 141 cm
★ PW_12 (140 cm)

204 – 207 cm: Detrital layer of volcanic fragments from sand to pebble size; the fragments are angular and greyish

●● 204 – 206 cm
★ PW_13 (204 cm)

●● 213 – 215 cm
★ PW_14 (214 cm)

207 – 233 cm: Dehydrated dark grey clay (with a bit of silt); below 220 cm the sediment gets more hydrated with frequent volcanic pebbles

pH	T (°C)	Eh (mV)	EC (µS/cm)
7.82 / 7.70	16.5 / 15.9	-141	Er1
8.12 / 7.87	16.2 / 15.7	- 62	4.76

Core: POS535/03GC

GEOMAR
Helmholtz Centre for Ocean Research Kiel

Core section: C (1 of 3)
Recovery: 300 cm

Latitude: 66°37.54'N
Longitude: 17°38.48'W

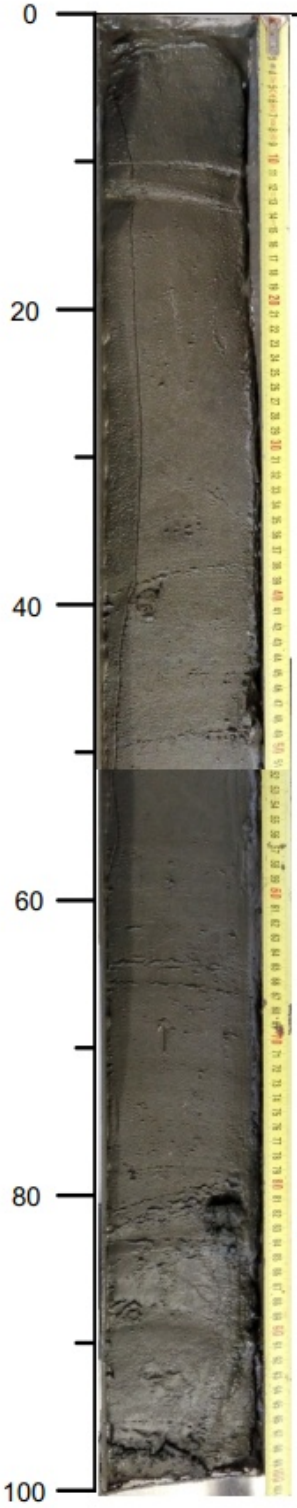

0 – 100 cm: Homogeneous dark greenish grey clay (5Y/3/2) with shells/shell fragments; in the upper 10 cm there are black patches within the sediment; these black patches also occur dispersed along the core but are more scarce

●● 50 –52 cm
★ PW_15 (52 cm) + PW_16 (blank)

82 cm: Hard clay nodule (more greyish then the surrounding clay, 5Y/3/1)

	pH	T (°C)	Eh (mV)	EC (µS/cm)
50 –52 cm	7.85 / 7.91	15.4 / 16.2	43	25.1

Core: POS535/03GC

GEOMAR
Helmholtz Centre for Ocean Research Kiel

Core section: B (2 of 3)
Recovery: 300 cm

Latitude: 66°37.54'N
Longitude: 17°38.48'W

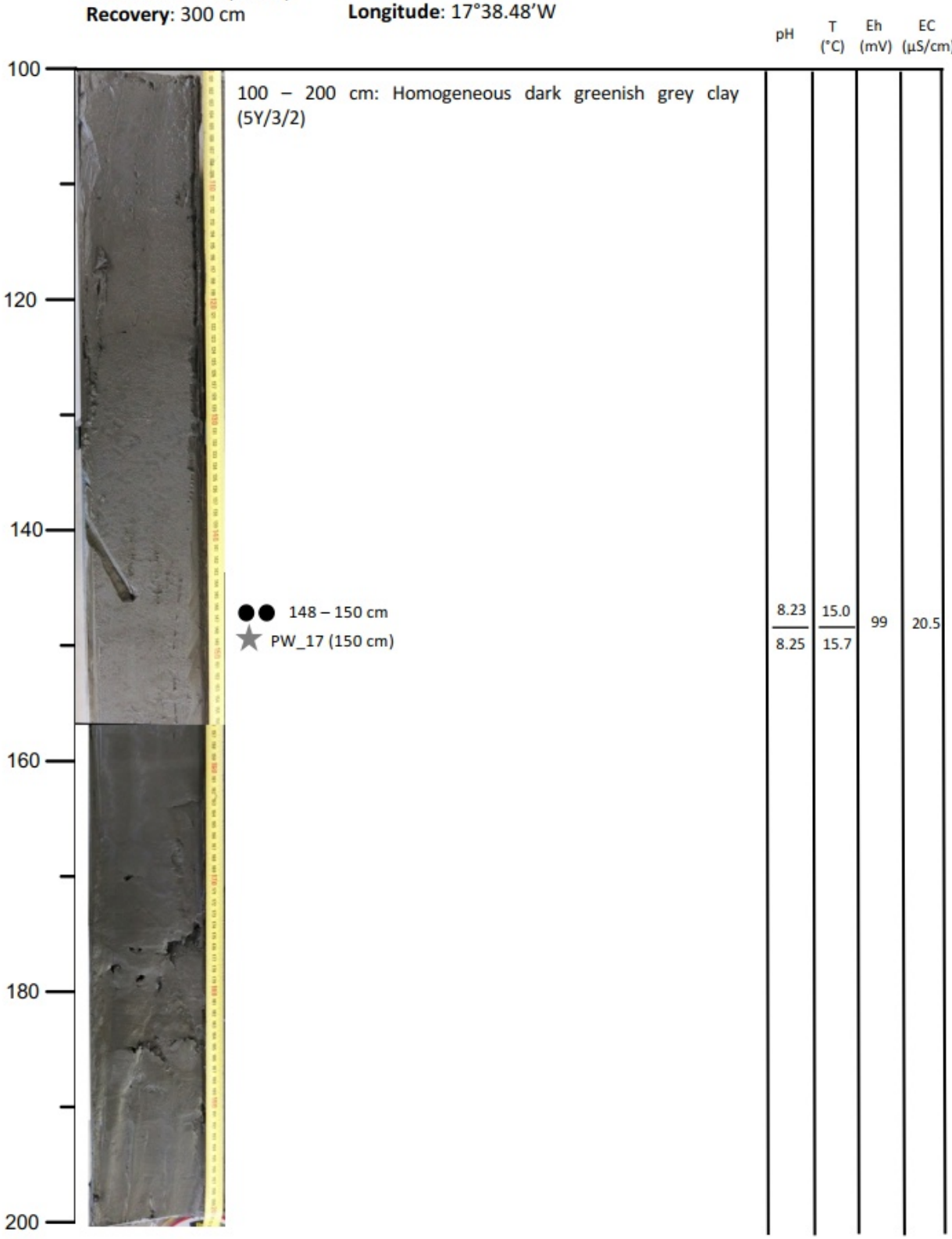

Core: POS535/03GC

GEOMAR
Helmholtz Centre for Ocean Research Kiel

Core section: A (3 of 3)
Recovery: 300 cm

Latitude: 66°37.54'N
Longitude: 17°38.48'W

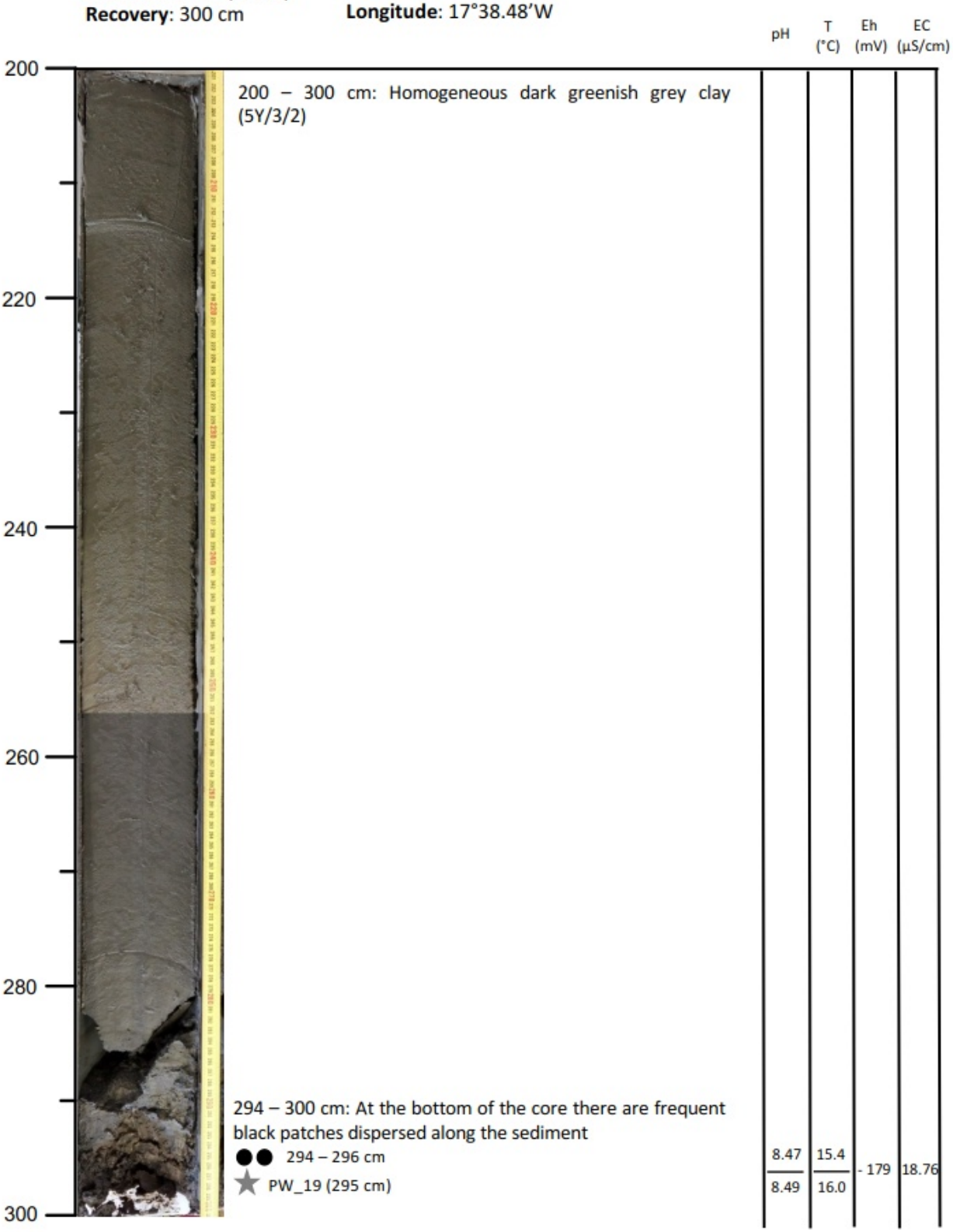

Core: POS535/04GC

GEOMAR
Helmholtz Centre for Ocean Research Kiel

Core section: B (1 of 2)
Recovery: 115 cm

Latitude: 66°36.413'N
Longitude: 17°40.255'W

pH | T (°C) | Eh (mV) | EC (µS/cm)

0 – 16 cm: Disturbed sediment; greenish grey (5Y/3/2) clay/silt interlaid with volcanic detritus (sand to pebble, black and reddish) and shell fragments

16 – 20 cm: Very dehydrated greyish silt (10YR/3/1)

●● 17 –19 cm

★ PW_20 (19 cm)

20 – 27 cm: Homogeneous greyish silt

0

20

40

Core: POS535/04GC

GEOMAR
Helmholtz Centre for Ocean Research Kiel

Core section: A (2 of 2)
Recovery: 115 cm

Latitude: 66°36.413'N
Longitude: 17°40.255'W

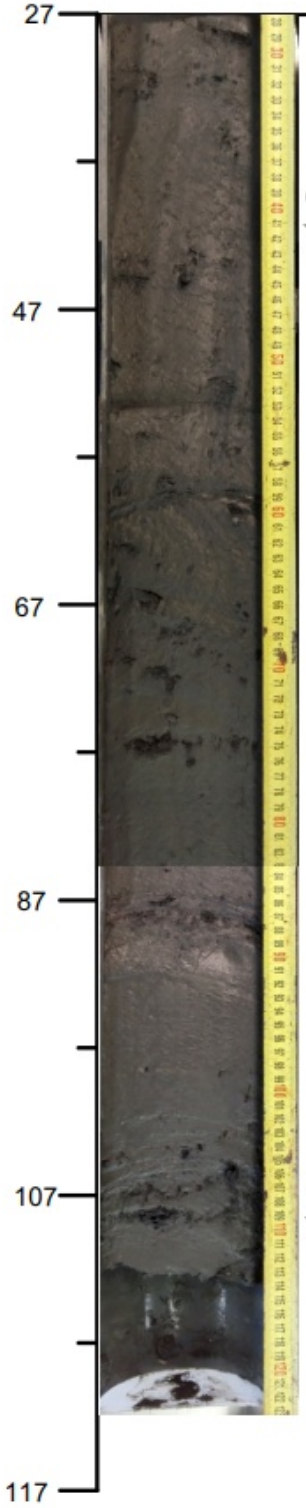

27 - 115 cm: Greenish grey clay (5Y/3/1) with centimetric intercalations of volcanic fragments (sand size) with occasional isolated pebble size volcanic fragments.

●● 39 –41 cm
★ PW_21 (40 cm)

●● 108 – 110 cm
★ PW_22 (108 cm)

	pH	T (°C)	Eh (mV)	EC (µS/cm)
39 –41 cm	8.11 / 7.80	15.1 / 13.6	- 132	Er1
108 – 110 cm	8.07 / 8.22	15.9 / 14.0	- 161	Er1

Core: POS535/05GC

GEOMAR
Helmholtz Centre for Ocean Research Kiel

Core section: C (1 of 3)
Recovery: 265 cm

Latitude: 66°36.437'N
Longitude: 17°39.637'W

0 – 20 cm: Greenish grey clay (5Y/3/2) with scarce anhydrite sand size grains and clumps up to 1 cm in diameter

●● 14 –16 cm
★ PW_23 (15 cm) + PW_24 (blank)

20 - 30 cm: Volcanic and anhydrite sand intermixed with greyish clay (80/20)

30 - 36 cm: Anhydrite sand intermixed with clay (90/10); some clusters of anhydrite can reach 2 cm

●● 34 – 36 cm
★ PW_25 (35 cm)

36 – 65 cm: Heteregonous layer of anhydrite sand in a clay matrix (70/30) (5Y/4/1); frequent areas of volcanic material (sand to pebble size); there are areas/channels of Fe oxidation giving a red colour (2.5YR/2.5/3) to the anhydrite

●● 60 – 62 cm
★ PW_26 (62 cm)

	pH	T (°C)	Eh (mV)	EC (µS/cm)
0				
	7.99 / 8.02	15.9 / 15.4	- 100	21.8
20				
	8.07 / 7.77	16.5 / 15.1	- 60	22.9
40				
60	7.57 / 7.30	18.6 / 15.8	106	15.22

Core: POS535/05GC

GEOMAR
Helmholtz Centre for Ocean Research Kiel

Core section: B (2 of 3)
Recovery: 265 cm

Latitude: 66°36.437'N
Longitude: 17°39.637'W

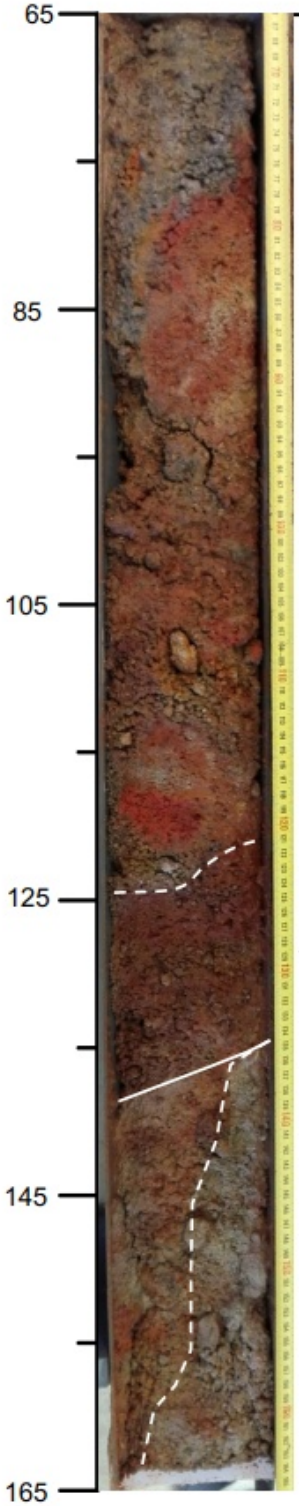

65 – 99 cm: Anhydrite sand with a small % of clay (5Y/4/1) and occasional volcanic sand; there is an area of Fe oxidation staining (2.5YR/3/3)

●● 85 –87 cm
★ PW_27 (86 cm)

99 – 121 cm: Heterogenous anhydrite debris layer with diverse grain size (sand/pebbles) also showing some oxidation staining. Between 118-121 red lens (2.5YR/3/4)

●● 118 –120 cm
★ PW_28 (119 cm)

121 – 135 cm: Anhydrite sand with a brown colour (2.5YR/2.5/3)

●● 125–127 cm
★ PW_29 (128 cm)

135 - 165 cm: Heterogenous layer of anhydrite debris showing a distinct difference in clast size, side by side (a fine area next to a coarse one); in the fine grained anhydrite layer there is oxidation staining

●● 140–142 cm

●● 149–151 cm
★ PW_30 (151 cm)

	pH	T (°C)	Eh (mV)	EC (µS/cm)
●● 85 –87 cm ★ PW_27 (86 cm)	7.50 7.24	18.3 15.3	117	2.34
●● 118 –120 cm ★ PW_28 (119 cm)	7.51 7.33	18.5 15.4	127	Er1
●● 125–127 cm ★ PW_29 (128 cm)	7.38 7.45	18.6 15.8	135	0.82
●● 140–142 cm	7.53 7.42	18.5 15.8	141	Er1
●● 149–151 cm ★ PW_30 (151 cm)	7.59 7.34	18.3 15.6	137	2.61

Core: POS535/05GC

Core section: A (3 of 3)
Recovery: 265 cm

Latitude: 66°36.437'N
Longitude: 17°39.637'W

GEOMAR
Helmholtz Centre for Ocean Research Kiel

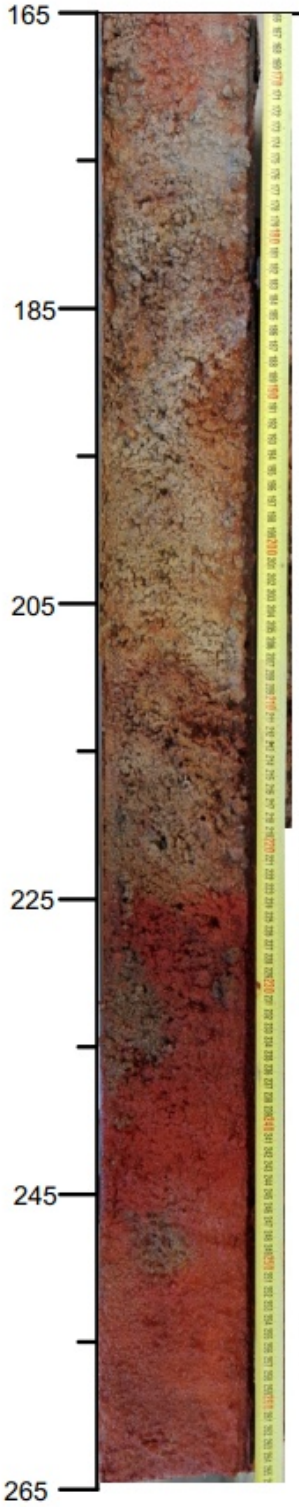

165 - 223 cm: Greyish (5Y/5/1) anhydrite sand/pebbles with frequent red, orange, brown tin

220 – 221 cm
PW_31 (221 cm) + PW_32 (blank)

223 - 265 cm: Reddish stained anhydrite (2.5YR/3/4) with sand to pebble size; there are some greyish areas. The red stain can indicate hematite and so alteration of sulfides

255 – 257 cm
PW_33 (256 cm)

2.5YR/3/3 – dark red

pH	T (°C)	Eh (mV)	EC (µS/cm)
7.74 / 7.49	16.9 / 15.5	167	4.76
7.64 / 7.55	16.0 / 15.7	165	0.78

Core: POS535/06GC

GEOMAR
Helmholtz Centre for Ocean Research Kiel

Core section: A (1 of 1)
Recovery: 91 cm

Latitude: 66°21.53'N
Longitude: 16°55.45'W

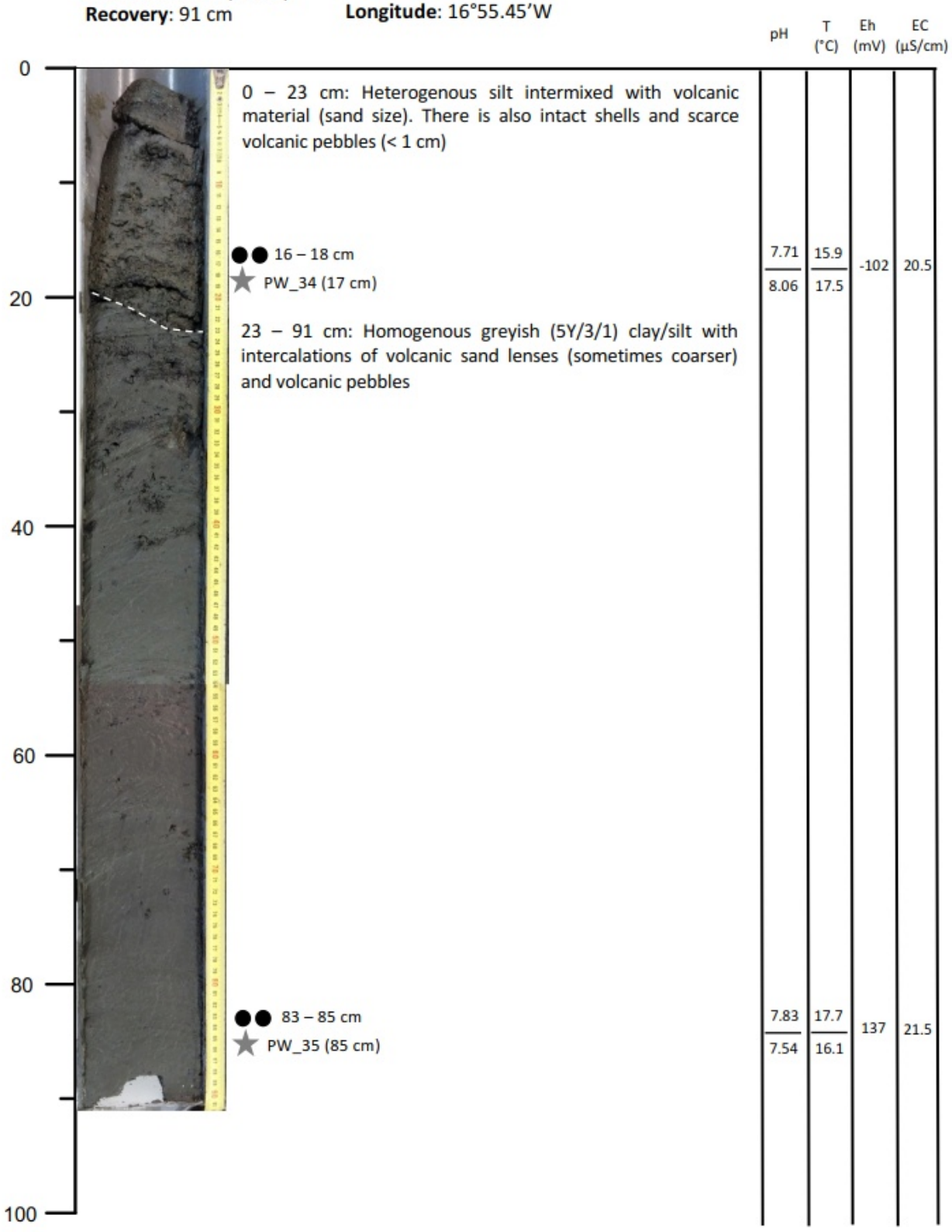

Core: POS535/07GC

GEOMAR
Helmholtz Centre for Ocean Research Kiel

Core section: A (1 of 1)
Recovery: 51 cm

Latitude: 66°21.423'N
Longitude: 16°55.431'W

0 – 16 cm: Disturbed sediment (5Y/3/2) with a subrounded volcanic cobble, most probably basalt (9x6 cm)

16 – 23 cm: Volcanic sand debris with volcanic pebbles and shells

●● 19 – 21 cm
★ PW_36 (19 cm)

23 – 51 cm: Homogeneous greyish (5Y/3/1) silt intermixed with volcanic pebbles and scarce volcanic sand pockets

●● 39 – 41 cm
★ PW_37 (41 cm)

	pH	T (°C)	Eh (mV)	EC (µS/cm)
19 – 21 cm	7.38 / 7.93	17.7 / 15.9	42	240
39 – 41 cm	7.85 / 8.37	16.9 / 16.0	150	2.88

Core: POS535/08GC

GEOMAR
Helmholtz Centre for Ocean Research Kiel

Core section: A (1 of 1)
Recovery: 66 cm

Latitude: 66°21.53'N
Longitude: 16°55.424'W

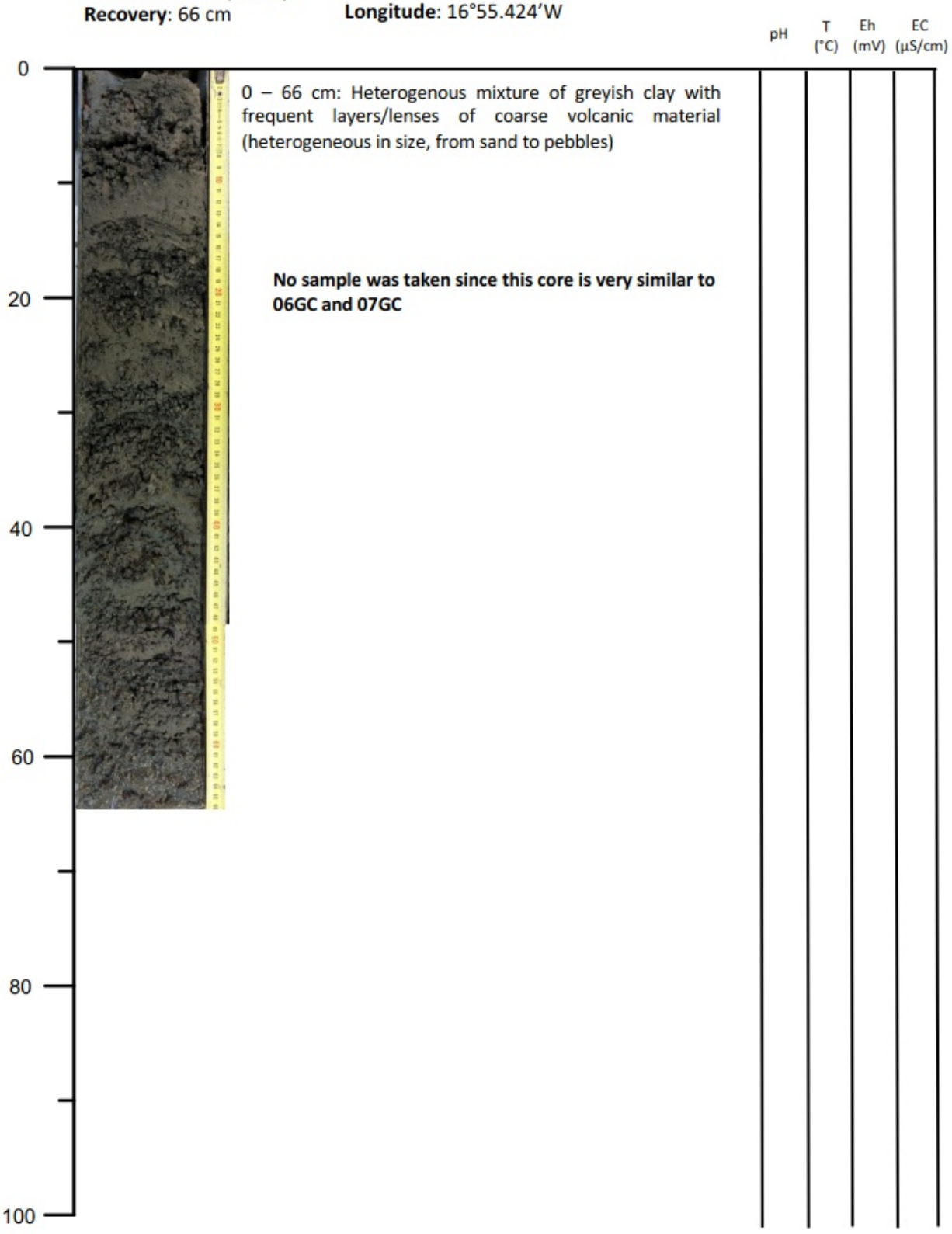

Core: POS535/09GC

GEOMAR
Helmholtz Centre for Ocean Research Kiel

Core section: A (1 of 1)
Recovery: 80 cm

Latitude: 66°26.489'N
Longitude: 17°24.168'W

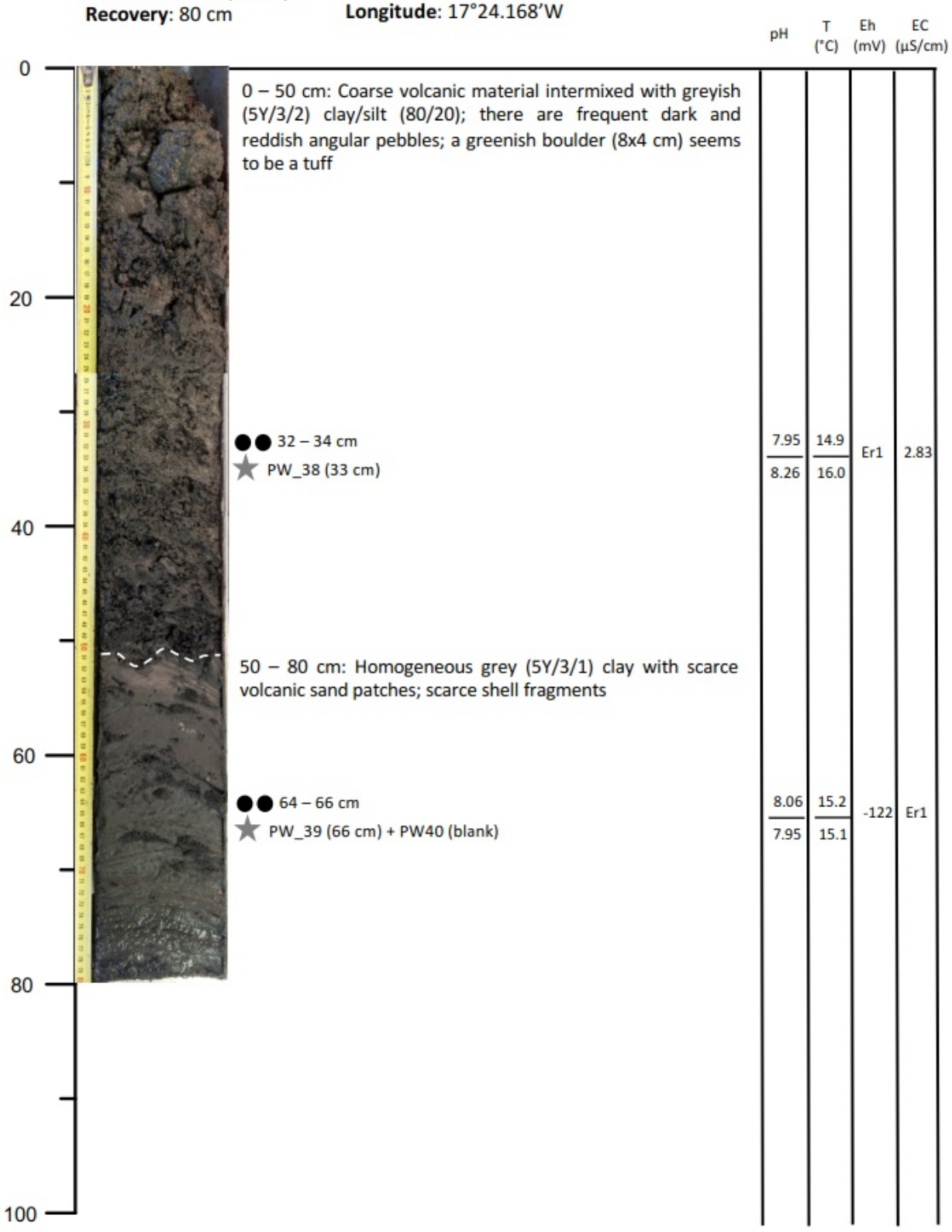

Core: POS535/10GC

GEOMAR
Helmholtz Centre for Ocean Research Kiel

Core section: A (1 of 1)
Recovery: 61 cm

Latitude: 66°26.549'N
Longitude: 17°24.139'W

0 – 26 cm: Very coarse and angular volcanic material; there are several reddish clasts (volcano-sedimentary? pyroclasts? lapilli?); 5Y/3/2

●● 13 – 15 cm
★ PW_41 (14 cm)

26 – 61 cm: Grey (5Y/3/1) clay/silt with anhydrite sand domains (5Y/5/1). In the clay domains there are some patches with a rounded light grey halo surrounding a yellowish center.

●● 37 – 39 cm
★ PW_42 (38 cm)

●● 47 – 49 cm
★ PW_43 (48 cm)

	pH	T (°C)	Eh (mV)	EC (µS/cm)
13 – 15 cm	7.98 / 7.78	17.0 / 15.2	Er1	22.1
37 – 39 cm	7.83 / 7.88	17.2 / 16.5	117	991

Core: POS535/11GC

GEOMAR
Helmholtz Centre for Ocean Research Kiel

Core section: C (1 of 3)
Recovery: 267 cm

Latitude: 73°33.988'N
Longitude: 8°09.467'E

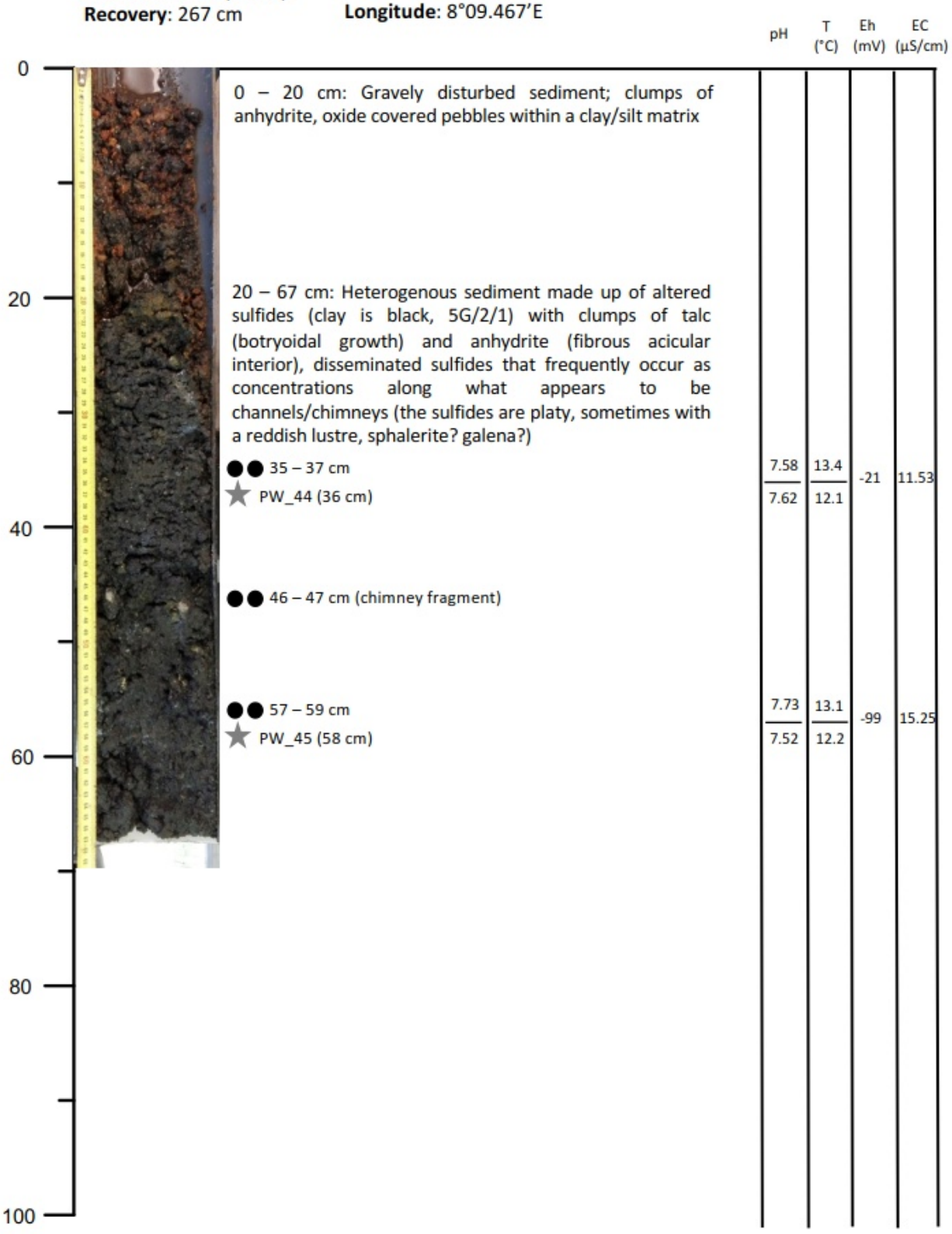

Core: POS535/11GC

GEOMAR
Helmholtz Centre for Ocean Research Kiel

Core section: B (2 of 3)
Recovery: 267 cm

Latitude: 73°33.988'N
Longitude: 8°09.467'E

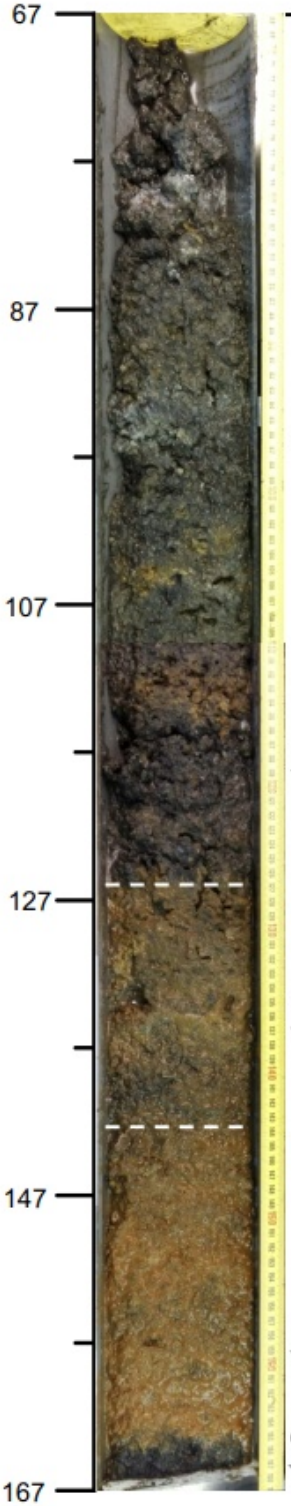

67 – 126 cm: Heterogenous clay layer with anhydrite clumps, anhydrite sand, talc (botryoidal), pink talc, oxidation patches, disseminated sulfides and sulfides in plates/chimney fragments

81 – 83 cm (pinkish talc?)

96 – 77 cm (sulfide sample)

117 – 119 cm
PW_46 (119 cm)

126 – 144 cm: Heterogenous greenish clay layer showing a gradation in colour from greenish (5Y/4/3) to greenish dark brown (10YR/3/2) with talc/anhydrite clasts

135 – 137 cm
PW_47 (136 cm) + PW_48 (blank)

144 – 166 cm: Heterogenous brown orange clay with anhydrite/talc sand; from brownish (10YR/4/4) to orange (10YR/4/5)

157 – 159 cm
PW_49 (158 cm)

166 – 167 cm
PW_50 (167 cm)

166 - 167 cm: Black clay layer with disseminated sulfides and anhydrite sand

	pH	T (°C)	Eh (mV)	EC (µS/cm)
117 – 119 cm / PW_46 (119 cm)	7.73 / 7.57	13.4 / 13.1	-119	23.9
135 – 137 cm / PW_47 (136 cm) + PW_48 (blank)	7.52 / 7.68	14.0 / 12.8	-66	20.8
157 – 159 cm / PW_49 (158 cm)	7.59 / 7.73	14.1 / 13.5	6	20.3
166 – 167 cm / PW_50 (167 cm)	8.01 / 7.69	14.7 / 14.4	-299	0.76

Core: POS535/11GC

GEOMAR
Helmholtz Centre for Ocean Research Kiel

Core section: A (3 of 3)
Recovery: 267 cm

Latitude: 73°33.988'N
Longitude: 8°09.467'E

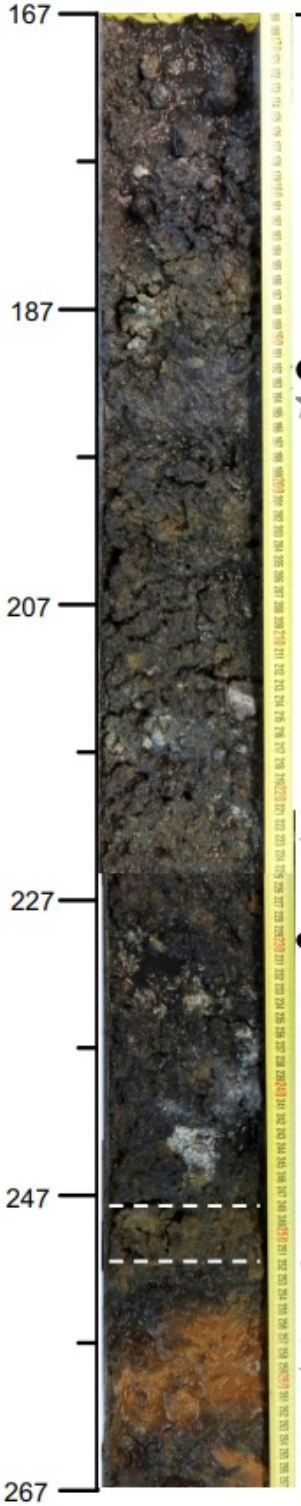

	pH	T (°C)	Eh (mV)	EC (µS/cm)
167 – 246 cm: Heterogenous greenish clay layer with anhydrite sand/clumps, talc (white botryoidal, pink) and disseminated sulfides				
192 – 194 cm / PW_51 (193 cm)	7.71 / 7.66	14.7 / 14.2	-104	24.2
221 – 223 cm / PW_52 (222 cm)	7.72 / 7.68	14.8 / 14.2	-99	17.18
230cm (small chimney fragment; sulfides)				
246 - 251 cm: Greenish (5Y/4/3) silt layer with anhydrite clumps				
(sulfide in beehive chimney) 251 – 254 cm: Black layer with chimney fragments				
257 – 259 cm / PW_53 (258 cm) 254 – 261 cm: Clay/silt orange layer (10YR/4/5) with black patches	7.64 / 7.53	14.8 / 14.3	-115	24.3
261 - 267 cm: Black/orange layer with chimney fragments; some fragments had on the surface native copper)				
264 – 267 cm (chimney fragments with oxidized surface with dispersed native copper crystal with dendritic growth)				

Core: POS535/14GC

GEOMAR
Helmholtz Centre for Ocean Research Kiel

Core section: C (1 of 3)
Recovery: 300 cm

Latitude: 73°33.997'N
Longitude: 8°09.493'E

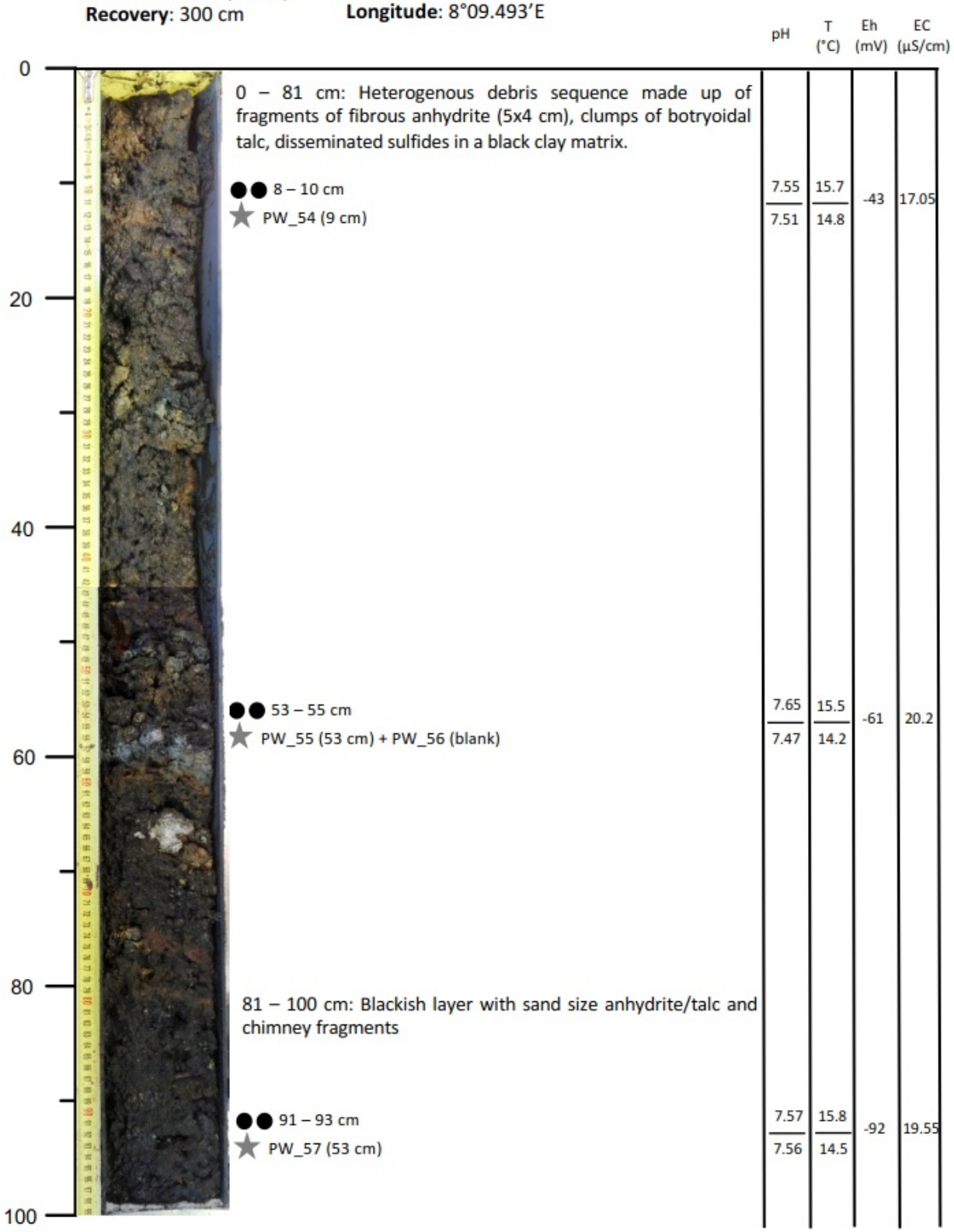

Core: POS535/14GC

GEOMAR
Helmholtz Centre for Ocean Research Kiel

Core section: B (2 of 3)
Recovery: 300 cm

Latitude: 73°33.997'N
Longitude: 8°09.493'E

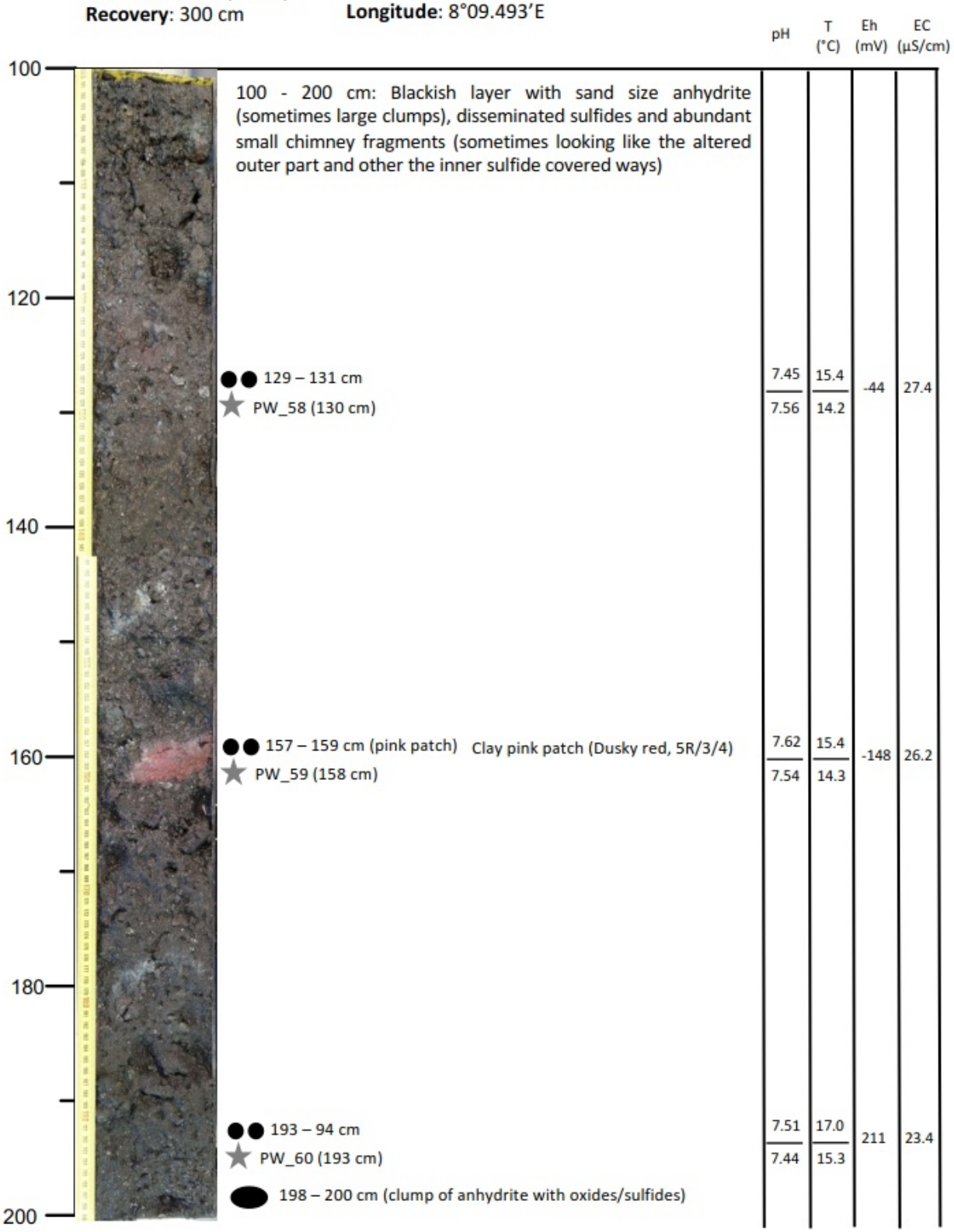

Core: POS535/14GC

Core section: A (3 of 3)
Recovery: 300 cm

Latitude: 73°33.997'N
Longitude: 8°09.493'E

GEOMAR
Helmholtz Centre for Ocean Research Kiel

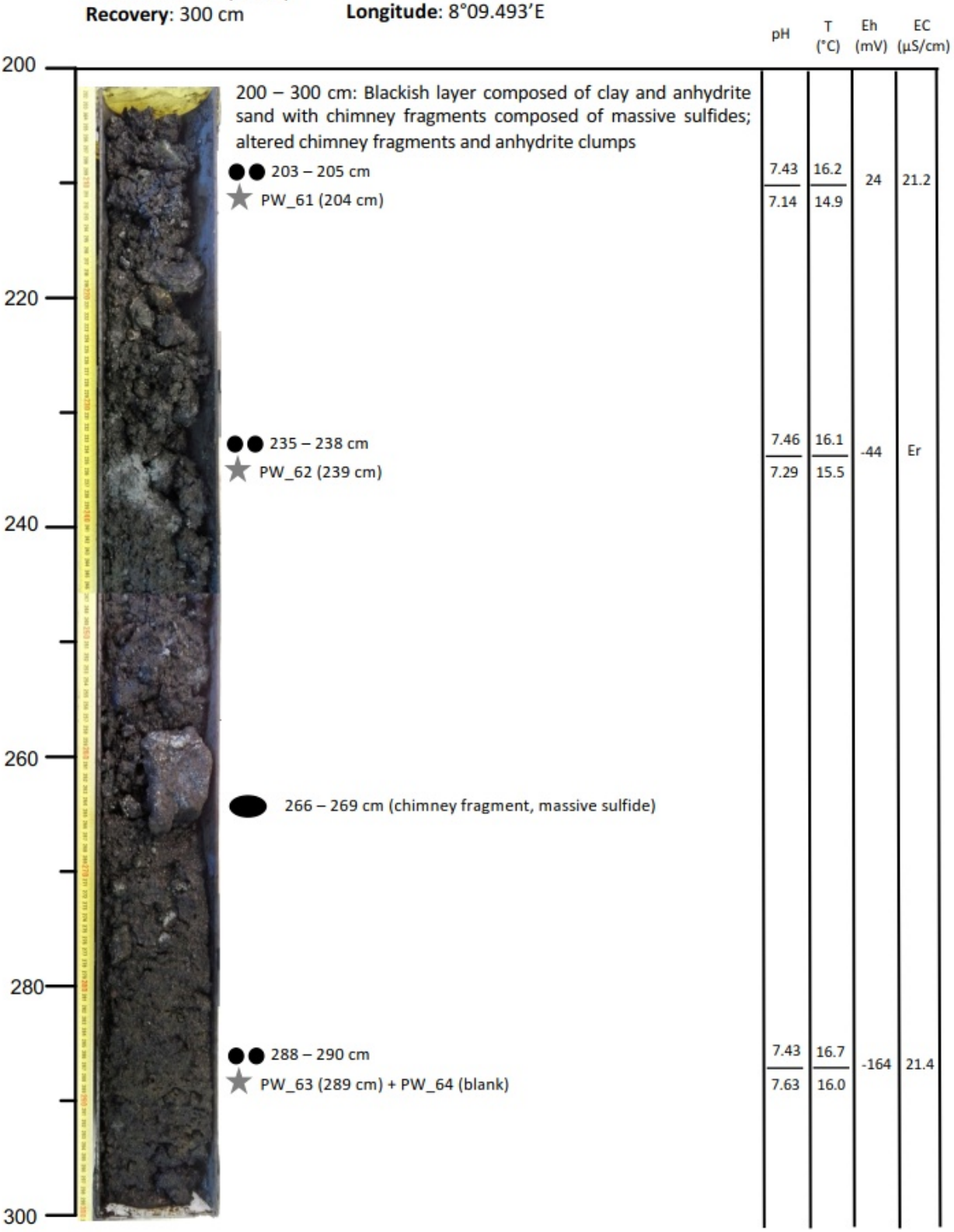

10.4. Pore Fluid Samples

Sample	Core	Depth	Sample	Core	Depth
POS535_PoreWater_001	01GC	28cm	POS535_PoreWater_034	06GC	17cm
POS535_PoreWater_002	01GC	41cm	POS535_PoreWater_035	06GC	85cm
POS535_PoreWater_003	01GC	75cm	POS535_PoreWater_036	07GC	19cm
POS535_PoreWater_004	01GC	100cm	POS535_PoreWater_037	07GC	41cm
POS535_PoreWater_005	01GC	124cm	POS535_PoreWater_038	09GC	33cm
POS535_PoreWater_006	02GC	50cm	POS535_PoreWater_039	09GC	66cm
POS535_PoreWater_007	02GC	95cm	POS535_PoreWater_040	**blank**	
POS535_PoreWater_008	**blank**		POS535_PoreWater_041	10GC	14cm
POS535_PoreWater_009	02GC	113cm	POS535_PoreWater_042	10GC	38cm
POS535_PoreWater_010	02GC	113cm	POS535_PoreWater_043	10GC	48cm
POS535_PoreWater_011	02GC	118cm	POS535_PoreWater_044	11GC	36cm
POS535_PoreWater_012	02GC	140cm	POS535_PoreWater_045	11GC	58cm
POS535_PoreWater_013	02GC	204cm	POS535_PoreWater_046	11GC	119cm
POS535_PoreWater_014	02GC	214cm	POS535_PoreWater_047	11GC	136cm
POS535_PoreWater_015	03GC	52cm	POS535_PoreWater_048	**blank**	
POS535_PoreWater_016	**blank**		POS535_PoreWater_049	11GC	158cm
POS535_PoreWater_017	03GC	150cm	POS535_PoreWater_050	11GC	167cm
POS535_PoreWater_018	03GC	239cm	POS535_PoreWater_051	11GC	193cm
POS535_PoreWater_019	03GC	295cm	POS535_PoreWater_052	11GC	222cm
POS535_PoreWater_020	04GC	19cm	POS535_PoreWater_053	11GC	258cm
POS535_PoreWater_021	04GC	40cm	POS535_PoreWater_054	14GC	9cm
POS535_PoreWater_022	04GC	108cm	POS535_PoreWater_055	14GC	53cm
POS535_PoreWater_023	05GC	15cm	POS535_PoreWater_056	**blank**	
POS535_PoreWater_024	**blank**		POS535_PoreWater_057	14GC	93cm
POS535_PoreWater_025	05GC	35cm	POS535_PoreWater_058	14GC	130cm
POS535_PoreWater_026	05GC	62cm	POS535_PoreWater_059	14GC	158cm
POS535_PoreWater_027	05GC	86cm	POS535_PoreWater_060	14GC	193cm
POS535_PoreWater_028	05GC	119cm	POS535_PoreWater_061	14GC	204cm
POS535_PoreWater_029	05GC	128cm	POS535_PoreWater_062	14GC	239cm
POS535_PoreWater_030	05GC	151cm	POS535_PoreWater_063	14GC	289cm
POS535_PoreWater_031	05GC	221cm	POS535_PoreWater_064	**blank**	
POS535_PoreWater_032	**blank**				
POS535_PoreWater_033	05GC	256cm			

GEOMAR
Helmholtz-Zentrum für Ozeanforschung Kiel

GEOMAR Reports

No.	Title
1	FS POSEIDON Fahrtbericht / Cruise Report POS421, 08. – 18.11.2011, Kiel - Las Palmas, Ed.: T.J. Müller, 26 pp, DOI: 10.3289/GEOMAR_REP_NS_1_2012
2	Nitrous Oxide Time Series Measurements off Peru – A Collaboration between SFB 754 and IMARPE –, Annual Report 2011, Eds.: Baustian, T., M. Graco, H.W. Bange, G. Flores, J. Ledesma, M. Sarmiento, V. Leon, C. Robles, O. Moron, 20 pp, DOI: 10.3289/GEOMAR_REP_NS_2_2012
3	FS POSEIDON Fahrtbericht / Cruise Report POS427 – Fluid emissions from mud volcanoes, cold seeps and fluid circulation at the Don-_Kuban deep sea fan (Kerch peninsula, Crimea, Black Sea) – 23.02. – 19.03.2012, Burgas, Bulgaria - Heraklion, Greece, Ed.: J. Bialas, 32 pp, DOI: 10.3289/GEOMAR_REP_NS_3_2012
4	RV CELTIC EXPLORER EUROFLEETS Cruise Report, CE12010 – ECO2@NorthSea, 20.07. – 06.08.2012, Bremerhaven – Hamburg, Eds.: P. Linke et al., 65 pp, DOI: 10.3289/GEOMAR_REP_NS_4_2012
5	RV PELAGIA Fahrtbericht / Cruise Report 64PE350/64PE351 – JEDDAH-TRANSECT -, 08.03. – 05.04.2012, Jeddah – Jeddah, 06.04 - 22.04.2012, Jeddah – Duba, Eds.: M. Schmidt, R. Al-Farawati, A. Al-Aidaroos, B. Kürten and the shipboard scientific party, 154 pp, DOI: 10.3289/GEOMAR_REP_NS_5_2013
6	RV SONNE Fahrtbericht / Cruise Report SO225 - MANIHIKI II Leg 2 The Manihiki Plateau - Origin, Structure and Effects of Oceanic Plateaus and Pleistocene Dynamic of the West Pacific Warm Water Pool, 19.11.2012 - 06.01.2013 Suva / Fiji – Auckland / New Zealand, Eds.: R. Werner, D. Nürnberg, and F. Hauff and the shipboard scientific party, 176 pp, DOI: 10.3289/GEOMAR_REP_NS_6_2013
7	RV SONNE Fahrtbericht / Cruise Report SO226 – CHRIMP CHatham RIse Methane Pockmarks, 07.01. - 06.02.2013 / Auckland – Lyttleton & 07.02. – 01.03.2013 / Lyttleton – Wellington, Eds.: Jörg Bialas / Ingo Klaucke / Jasmin Mögeltönder, 126 pp, DOI: 10.3289/GEOMAR_REP_NS_7_2013
8	The SUGAR Toolbox - A library of numerical algorithms and data for modelling of gas hydrate systems and marine environments, Eds.: Elke Kossel, Nikolaus Bigalke, Elena Piñero, Matthias Haeckel, 168 pp, DOI: 10.3289/GEOMAR_REP_NS_8_2013
9	RV ALKOR Fahrtbericht / Cruise Report AL412, 22.03.-08.04.2013, Kiel – Kiel. Eds: Peter Linke and the shipboard scientific party, 38 pp, DOI: 10.3289/GEOMAR_REP_NS_9_2013
10	Literaturrecherche, Aus- und Bewertung der Datenbasis zur Meerforelle (Salmo trutta trutta L.) Grundlage für ein Projekt zur Optimierung des Meerforellenmanagements in Schleswig-Holstein. Eds.: Christoph Petereit, Thorsten Reusch, Jan Dierking, Albrecht Hahn, 158 pp, DOI: 10.3289/GEOMAR_REP_NS_10_2013
11	RV SONNE Fahrtbericht / Cruise Report SO227 TAIFLUX, 02.04. – 02.05.2013, Kaohsiung – Kaohsiung (Taiwan), Christian Berndt, 105 pp, DOI: 10.3289/GEOMAR_REP_NS_11_2013
12	RV SONNE Fahrtbericht / Cruise Report SO218 SHIVA (Stratospheric Ozone: Halogens in a Varying Atmosphere), 15.-29.11.2011, Singapore - Manila, Philippines, Part 1: SO218- SHIVA Summary Report (in German), Part 2: SO218- SHIVA English reports of participating groups, Eds.: Birgit Quack & Kirstin Krüger, 119 pp, DOI: 10.3289/GEOMAR_REP_NS_12_2013
13	KIEL276 Time Series Data from Moored Current Meters. Madeira Abyssal Plain, 33°N, 22°W, 5285 m water depth, March 1980 – April 2011. Background Information and Data Compilation. Eds.: Thomas J. Müller and Joanna J. Waniek, 239 pp, DOI: 10.3289/GEOMAR_REP_NS_13_2013

GEOMAR
Helmholtz-Zentrum für Ozeanforschung Kiel

GEOMAR Reports

No.	Title
14	RV POSEIDON Fahrtbericht / Cruise Report POS457: ICELAND HAZARDS Volcanic Risks from Iceland and Climate Change:The Late Quaternary to Anthropogene Development Reykjavík / Iceland – Galway / Ireland, 7.-22. August 2013. Eds.: Reinhard Werner, Dirk Nürnberg and the shipboard scientific party, 88 pp, DOI: 10.3289/GEOMAR_REP_NS_14_2014
15	RV MARIA S. MERIAN Fahrtbericht / Cruise Report MSM-34 / 1 & 2, SUGAR Site, Varna – Varna, 06.12.13 – 16.01.14. Eds: Jörg Bialas, Ingo Klaucke, Matthias Haeckel, 111 pp, DOI: 10.3289/GEOMAR_REP_NS_15_2014
16	RV POSEIDON Fahrtbericht / Cruise Report POS 442, "AUVinTYS" High-resolution geological investigations of hydrothermal sites in the Tyrrhenian Sea using the AUV "Abyss", 31.10. – 09.11.12, Messina – Messina, Ed.: Sven Petersen, 32 pp, DOI: 10.3289/GEOMAR_REP_NS_16_2014
17	RV SONNE, Fahrtbericht / Cruise Report, SO 234/1, "SPACES": Science or the Assessment of Complex Earth System Processes, 22.06. – 06.07.2014, Walvis Bay / Namibia - Durban / South Africa, Eds.: Reinhard Werner and Hans-Joachim Wagner and the shipbord scientific party, 44 pp, DOI: 10.3289/GEOMAR_REP_NS_17_2014
18	RV POSEIDON Fahrtbericht / Cruise Report POS 453 & 458, "COMM3D", Crustal Structure and Ocean Mixing observed with 3D Seismic Measurements, 20.05. – 12.06.2013 (POS453), Galway, Ireland – Vigo, Portugal, 24.09. – 17.10.2013 (POS458), Vigo, Portugal – Vigo, Portugal, Eds.: Cord Papenberg and Dirk Klaeschen, 66 pp, DOI: 10.3289/GEOMAR_REP_NS_18_2014
19	RV POSEIDON, Fahrtbericht / Cruise Report, POS469, "PANAREA", 02. – 22.05.2014, (Bari, Italy – Malaga, Spain) & Panarea shallow-water diving campaign, 10. – 19.05.2014, Ed.: Peter Linke, 55 pp, DOI: 10.3289/GEOMAR_REP_NS_19_2014
20	RV SONNE Fahrtbericht / Cruise Report SO234-2, 08.-20.07.2014, Durban, -South Africa - Port Louis, Mauritius, Eds.: Kirstin Krüger, Birgit Quack and Christa Marandino, 95 pp, DOI: 10.3289/GEOMAR_REP_NS_20_2014
21	RV SONNE Fahrtbericht / Cruise Report SO235, 23.07.-07.08.2014, Port Louis, Mauritius to Malé, Maldives, Eds.: Kirstin Krüger, Birgit Quack and Christa Marandino, 76 pp, DOI: 10.3289/GEOMAR_REP_NS_21_2014
22	RV SONNE Fahrtbericht / Cruise Report SO233 WALVIS II, 14.05-21.06.2014, Cape Town, South Africa - Walvis Bay, Namibia, Eds.: Kaj Hoernle, Reinhard Werner, and Carsten Lüter, 153 pp, DOI: 10.3289/GEOMAR_REP_NS_22_2014
23	RV SONNE Fahrtbericht / Cruise Report SO237 Vema-TRANSIT Bathymetry of the Vema-Fracture Zone and Puerto Rico TRench and Abyssal AtlaNtic BiodiverSITy Study, Las Palmas (Spain) - Santo Domingo (Dom. Rep.) 14.12.14 - 26.01.15, Ed.: Colin W. Devey, 130 pp, DOI: 10.3289/GEOMAR_REP_NS_23_2015
24	RV POSEIDON Fahrtbericht / Cruise Report POS430, POS440, POS460 & POS467 Seismic Hazards to the Southwest of Portugal; POS430 - La-Seyne-sur-Mer - Portimao (7.4. - 14.4.2012), POS440 - Lisbon - Faro (12.10. - 19.10.2012), POS460 - Funchal - Portimao (5.10. - 14.10.2013), POS467 - Funchal - Portimao (21.3. - 27.3.2014), Ed.: Ingo Grevemeyer, 43 pp, DOI: 10.3289/GEOMAR_REP_NS_24_2015
25	RV SONNE Fahrtbericht / Cruise Report SO239, EcoResponse Assessing the Ecology, Connectivity and Resilience of Polymetallic Nodule Field Systems, Balboa (Panama) – Manzanillo (Mexico), 11.03. -30.04.2015, Eds.: Pedro Martínez Arbizu and Matthias Haeckel, 204 pp, DOI: 10.3289/GEOMAR_REP_NS_25_2015

GEOMAR
Helmholtz-Zentrum für Ozeanforschung Kiel

GEOMAR Reports

No.	Title
26	RV SONNE Fahrtbericht / Cruise Report SO242-1, JPI OCEANS Ecological Aspects of Deep-Sea Mining, DISCOL Revisited, Guayaquil - Guayaquil (Equador), 29.07.-25.08.2015, Ed.: Jens Greinert, 290 pp, DOI: 10.3289/GEOMAR_REP_NS_26_2015
27	RV SONNE Fahrtbericht / Cruise Report SO242-2, JPI OCEANS Ecological Aspects of Deep-Sea Mining DISCOL Revisited, Guayaquil - Guayaquil (Equador), 28.08.-01.10.2015, Ed.: Antje Boetius, 552 pp, DOI: 10.3289/GEOMAR_REP_NS_27_2015
28	RV POSEIDON Fahrtbericht / Cruise Report POS493, AUV DEDAVE Test Cruise, Las Palmas - Las Palmas (Spain), 26.01.-01.02.2016, Ed.: Klas Lackschewitz, 17 pp, DOI: 10.3289/GEOMAR_REP_NS_28_2016
29	Integrated German Indian Ocean Study (IGIOS) - From the seafloor to the atmosphere - A possible German contribution to the International Indian Ocean Expedition 2 (IIOE-2) programme – A Science Prospectus, Eds.: Bange, H.W. , E.P. Achterberg, W. Bach, C. Beier, C. Berndt, A. Biastoch, G. Bohrmann, R. Czeschel, M. Dengler, B. Gaye, K. Haase, H. Herrmann, J. Lelieveld, M. Mohtadi, T. Rixen, R. Schneider, U. Schwarz-Schampera, J. Segschneider, M. Visbeck, M. Voß, and J. Williams, 77pp, DOI: 10.3289/GEOMAR_REP_NS_29_2016
30	RV SONNE Fahrtbericht / Cruise Report SO249, BERING – Origin and Evolution of the Bering Sea: An Integrated Geochronological, Volcanological, Petrological and Geochemical Approach, Leg 1: Dutch Harbor (U.S.A.) - Petropavlovsk-Kamchatsky (Russia), 05.06.2016-15.07.2016, Leg 2: Petropavlovsk-Kamchatsky (Russia) - Tomakomai (Japan), 16.07.2016-14.08.2016, Eds.: Reinhard Werner, et al., DOI: 10.3289/GEOMAR_REP_NS_30_2016
31	RV POSEIDON Fahrtbericht/ Cruise Report POS494/2, HIERROSEIS Leg 2: Assessment of the Ongoing Magmatic-Hydrothermal Discharge of the El Hierro Submarine Volcano, Canary Islands by the Submersible JAGO, Valverde – Las Palmas (Spain), 07.02.-15.02.2016, Eds.: Hannington, M.D. and Shipboard Scientific Party, DOI: 10.3289/GEOMAR_REP_NS_31_2016
32	RV METEOR Fahrtbericht/ Cruise Report M127, Extended Version, Metal fluxes and Resource Potential at the Slow-spreading TAG Midocean Ridge Segment (26°N, MAR) – Blue Mining@Sea, Bridgetown (Barbados) – Ponta Delgada (Portugal) 25.05.-28.06.2016, Eds.: Petersen, S. and Shipboard Scientific Party, DOI: 10.3289/GEOMAR_REP_NS_32_2016
33	RV SONNE Fahrtbericht/Cruise Report SO244/1, GeoSEA: Geodetic Earthquake Observatory on the Seafloor, Antofagasta (Chile) – Antofagasta (Chile), 31.10.-24.11.2015, Eds.: Jan Behrmann, Ingo Klaucke, Michal Stipp, Jacob Geersen and Scientific Crew SO244/1, DOI: 10.3289/GEOMAR_REP_NS_33_2016
34	RV SONNE Fahrtbericht/Cruise Report SO244/2, GeoSEA: Geodetic Earthquake Observatory on the Seafloor, Antofagasta (Chile) – Antofagasta (Chile), 27.11.-13.12.2015, Eds.: Heidrun Kopp, Dietrich Lange, Katrin Hannemann, Anne Krabbenhoeft, Florian Petersen, Anina Timmermann and Scientific Crew SO244/2, DOI: 10.3289/GEOMAR_REP_NS_34_2016
35	RV SONNE Fahrtbericht/Cruise Report SO255, VITIAZ – The Life Cycle of the Vitiaz-Kermadec Arc / Backarc System: from Arc Initiation to Splitting and Backarc Basin Formation, Auckland (New Zealand) - Auckland (New Zealand), 02.03.-14.04.2017, Eds.: Kaj Hoernle, Folkmar Hauff, and Reinhard Werner with contributions from cruise participants, DOI: 10.3289/GEOMAR_REP_NS_35_2017

GEOMAR
Helmholtz-Zentrum für Ozeanforschung Kiel

GEOMAR Reports

No.	Title
36	RV POSEIDON Fahrtbericht/Cruise Report POS515, CALVADOS - CALabrian arc mud VolcAnoes: Deep Origin and internal Structure, Dubrovnik (Croatia) – Catania (Italy), 18.06.-13.07.2017, Eds.: M. Riedel, J. Bialas, A. Krabbenhoeft, V. Bähre, F. Beeck, O. Candoni, M. Kühn, S. Muff, J. Rindfleisch, N. Stange, DOI: 10.3289/GEOMAR_REP_NS_36_2017
37	RV MARIA S. MERIAN Fahrtbericht/Cruise Report MSM63, PERMO, Southampton – Southampton (U.K.), 29.04.-25.05.2017, Eds.: Christian Berndt and Judith Elger with contributions from cruise participants C. Böttner, R.Gehrmann, J. Karstens, S. Muff, B. Pitcairn, B. Schramm, A. Lichtschlag, A.-M. Völsch, DOI: 10.3289/GEOMAR_REP_NS_37_2017
38	RV SONNE Fahrtbericht/Cruise Report SO258/1, INGON: The Indian - Antarctic Break-up Engima, Fremantle (Australia) - Colombo (Sri Lanka), 07.06.-09.07.2017, 29.04.-25.05.2017, Eds.: Reinhard Werner, Hans-Joachim Wagner, and Folkmar Hauff with contributions from cruise participants, DOI: 10.3289/GEOMAR_REP_NS_38_2017
39	RV POSEIDON Fahrtbericht/Cruise Report POS509, ElectroPal 2: Geophysical investigations of sediment hosted massive sulfide deposits on the Palinuro Volcanic Complex in the Tyrrhenian Sea, Malaga (Spain) – Catania (Italy), 15.02.-03.03.2017, Ed.: Sebastian Hölz, DOI: 10.3289/GEOMAR_REP_NS_39_2017
40	RV POSEIDON Fahrtbericht/Cruise Report POS518, Baseline Study for the Environmental Monitoring of Subseafloor CO_2 Storage Operations, Leg 1: Bremerhaven – Bremerhaven (Germany), 25.09.-11.10.2017, Leg 2: Bremerhaven – Kiel (Germany), 12.10.-28.10.2017, Eds.: Peter Linke and Matthias Haeckel, DOI: 10.3289/GEOMAR_REP_NS_40_2018
41	RV MARIA S. MERIAN Fahrtbericht/Cruise Report MSM71, LOBSTER: Ligurian Ocean Bottom Seismology and Tectonics Research, Las Palmas (Spain) – Heraklion (Greece), 07.02.-27.02.2018, Eds.: H. Kopp, D. Lange, M. Thorwart, A. Paul, A. Dannowski, F. Petersen, C. Aubert, F. Beek, A. Beniest, S. Besançon, A. Brotzer, G. Caielli, W. Crawford, M. Deen, C. Lehmann, K. Marquardt, M. Neckel, L. Papanagnou, B. Schramm, P. Schröder, K.-P. Steffen, F. Wolf, Y. Xia, DOI: 10.3289/GEOMAR_REP_NS_41_2018
42	RV METEOR Fahrtbericht/Cruise Report M143, SLOGARO: Slope failures and active gas expulsion along the Romanian margin – investigating relations to gas hydrate distribution, Varna (Romania) – Heraklion (Greece), 12.12.-22.12.2017, Eds.: M. Riedel, F. Gausepohl, I. Gazis, L. Hähnel, M. Kampmeier, P. Urban, J. Bialas, DOI: 10.3289/GEOMAR_REP_NS_42_2018
43	RV POSEIDON Fahrtbericht/Cruise Report POS510, ANYDROS: Rifting and Hydrothermal Activity in the Cyclades Back-arc Basin, Catania (Italy) – Heraklion (Greece), 06.03.-29.03.2017, Ed.: M.D. Hannington, DOI: 10.3289/GEOMAR_REP_NS_43_2018
44	RV POSEIDON Fahrtbericht/Cruise Report POS524, GrimseyEM: Geophysical and geological investigations in the vicinity of the Grimsey Hydrothermal Field offshore Northern Iceland for the assessment of the geothermal potential and the exploration for potential mineralizations within the seafloor, Reykjavik (Iceland) – Bergen (Norway), 7.6 - 26.6.2018, Eds.: Sebastian Hölz and Sofia Martins, DOI: 10.3289/GEOMAR_REP_NS_44_2018
45	RV POSEIDON Fahrtbericht/Cruise Report POS527, Baseline Study for the Environmental Monitoring of Subseafloor CO_2 Storage Operations, Kiel – Kiel (Germany), 15.8. - 3.9.2018, Eds.: Eric Achterberg and Mario Esposito, DOI: 10.3289/GEOMAR_REP_NS_45_2018

GEOMAR
Helmholtz-Zentrum für Ozeanforschung Kiel

GEOMAR Reports

No.	Title
46	RV SONNE Fahrtbericht/Cruise Report SO264, SONNE-EMPEROR: The Plio/Pleistocene to Holocene development of the pelagic North Pacific from surface to depth – assessing its role for the global carbon budget and Earth´s climate, Suva (Fiji) – Yokohama (Japan), 30.6. – 24.8.2018 Ed.: Dirk Nürnberg, DOI: 10.3289/GEOMAR_REP_NS_46_2018
47	RV SONNE Fahrtbericht/Cruise Report SO265, SHATSKY EVOLUTION: Evolution of the Shatsky Rise Hotspot System, Yokohama (Japan) – Kaohsiung (Taiwan), 26.08. – 11.10.2018, Eds.: Jörg Geldmacher, Reinhard Werner, and Folkmar Hauff with contributions from cruise participants, DOI: 10.3289/GEOMAR_REP_NS_47_2018
48	RV MARIA S. MERIAN Fahrtbericht/Cruise Report MSM78, PERMO 2, Edinburgh – Edinburgh (U.K.), 16.10. – 25.10.2018, Eds.: Jens Karstens, Christoph Böttner, Mike Edwards, Ismael Falcon-Suarez, Anita Flohr, Rachael James, Anna Lichtschlag, Doris Maicher, Iain Pheasant, Ben Roche, Bettina Schramm, Michael Wilson, DOI: 10.3289/GEOMAR_REP_NS_48_2019
49	RV SONNE Fahrtbericht/Cruise Report SO267, ARCHIMEDES I: Arc Rifting, Metallogeny and Micro-plate Evolution – an Integrated Geodynamic, Magmatic and Hydrothermal Study of the Fonualei Rift System, NE Lau Basin, Suva (Fiji) – Suva (Fiji), 11.12.2018 – 26.01.2019, Eds.: Mark Hannington, Heidrun Kopp, Michael Schnabel, DOI: 10.3289/GEOMAR_REP_NS_49_2019
50	RV Pelagia Fahrtbericht/Cruise Report 64PE-445, SALTAX: Geomorphology and geophysics of sub-marine salt flows in the Red Sea Rift, Limassol (Cyprus) – Safaga (Egypt), 27.08. – 21.09.2018, Eds.: Nico Augustin, Neil C. Mitchell, Froukje M. van der Zwan & Scientific Shipboard Party, DOI: 10.3289/GEOMAR_REP_NS_50_2019
51	RV POSEIDON Fahrtbericht/Cruise Report POS526, SeASOM: Semi-Autonomous Subsurface Optical Monitoring for methane seepage and cold-water coral studies in the North Sea, Bergen (Norway) – Doggerbank (Netherlands) – Hirtshals (Denmark) – Tisler (Norway) – Kiel (Germany), 23.07. – 11.08.2018, Eds.: Jens Greinert, Tim Schoening, DOI: 10.3289/GEOMAR_REP_NS_51_2019
52	RV POSEIDON Fahrtbericht/Cruise Report POS534, STEMM-CCS: Strategies for Environmental Monitoring of Marine Carbon Capture and Storage, Leg 1: Kiel (Germany) – Aberdeen (United Kingdom), 01.05. – 22.05.2019, Leg 2: Aberdeen (United Kingdom) – Bremerhaven (Germany), 23.05. – 29.05.2019, Ed.: Mark Schmidt, DOI: 10.3289/GEOMAR_REP_NS_52_2019
53	RV POSEIDON Fahrtbericht/Cruise Report POS535, Loki2GrimseyEM: Geophysical and geological investigations of massive sulfides at and in the vicinity of Loki's Castle (Norway) and similar experiments around the Grimsey Hydrothermal Field (Iceland) for the assessment of the geothermal potential and the exploration for potential mineralizations within the seafloor, Akureyri (Iceland) – Bremerhaven (Germany), 09.06 – 03.07.2019, Eds.: Sebastian Hölz, Amir Haroon and Sofia Martins, DOI: 10.3289/GEOMAR_REP_NS_53_2019

For GEOMAR Reports, please visit:
https://oceanrep.geomar.de/view/series/GEOMAR_Report.html

Reports of the former IFM-GEOMAR series can be found under:
https://oceanrep.geomar.de/view/series/IFM-GEOMAR_Report.html

GEOMAR
Helmholtz-Zentrum für Ozeanforschung Kiel

Das GEOMAR Helmholtz-Zentrum für Ozeanforschung Kiel ist Mitglied der Helmholtz-Gemeinschaft Deutscher Forschungszentren e.V.

The GEOMAR Helmholtz Centre for Ocean Research Kiel is a member of the Helmholtz Association of German Research Centres

Helmholtz-Zentrum für Ozeanforschung Kiel / Helmholtz Centre for Ocean Research Kiel
GEOMAR
Dienstgebäude Westufer / West Shore Building
Düsternbrooker Weg 20
D-24105 Kiel
Germany

Helmholtz-Zentrum für Ozeanforschung Kiel / Helmholtz Centre for Ocean Research Kiel
GEOMAR
Dienstgebäude Ostufer / East Shore Building
Wischhofstr. 1-3
D-24148 Kiel
Germany

Tel.: +49 431 600-0
Fax: +49 431 600-2805
www.geomar.de